EFFECTS OF HYPERLIPIDEMIA ON DYSFERLIN- AND DYSTROPHIN-DEFICIENT MUSCULAR DYSTROPHIES IN DOUBLE-DISEASE MOUSE MODELS

by

Nadia Milad

B.Sc., McGill University, 2014

A THESIS SUBMITTED IN PARTIAL FULFILLMENT OF

THE REQUIREMENTS FOR THE DEGREE OF

MASTER OF SCIENCE

in

THE FACULTY OF GRADUATE AND POSTDOCTORAL STUDIES

(Anesthesiology, Pharmacology and Therapeutics)

THE UNIVERSITY OF BRITISH COLUMBIA

(Vancouver)

March 2017

Abstract

Muscular dystrophy (MD) is a class of diseases marked by progressive muscle wasting and impaired ambulatory function. Dysferlin- and dystrophin-deficiencies lead to MD and both are expressed in myofibers as well as smooth muscle and endothelial cells lining the vasculature, suggesting vascular function may be a contributing factor to muscle pathology seen in MD. However, murine models of MD develop only mild pathology compared to patients, making therapeutic drug development challenging. Since mice are known to have endogenously low lipid levels and superior vascular health, disrupted vascular function may be aggravating MD progression in humans. We seek to investigate the effect of impaired vascular function on MD pathology through the generation and characterization of double-disease murine models affected by both hyperlipidemia and MD. Firstly, the dysferlin-null (Dysf-KO) model of limb-girdle type 2B MD (LGMD2B) and the dystrophin-null (*mdx*) model of Duchenne MD (DMD) were crossed with apolipoprotein E-KO (ApoE-KO) hyperlipidemia model to generate Dysf-ApoE and Mdx-ApoE double-knockout mice (DKO). To further confirm the effects vascular disease on MD using a more human-relevant model, the Dysf-KO model was also crossed with the milder low-density-lipoprotein receptor-knockout (LDLR-KO) model of hyperlipidemia. Significant worsening of ambulatory function and muscle pathology was observed in the Dysf-ApoE DKO model, displaying reduced stride length, sometimes complete loss of ambulation, and increased muscle wasting, necrosis, fibrosis and fat infiltration. Although the Mdx-ApoE model showed no exacerbation of ambulation decline, significant worsening of muscle necrosis and fibrofatty replacement was observed in Mdx-ApoE DKO mice. However, few Dysf-LDLR DKOs were produced; all were maloccluded

runts with abnormal gait, though without observable muscle pathology upon histological analysis. In all, the Dysf-ApoE and Mdx-ApoE mice demonstrate that hyperlipidemia and associated vascular disease can dramatically aggravate muscle pathology in MD. These double-disease models mimic more closely the severity of human MD and may be useful for evaluating therapeutic interventions. In addition, these data suggest that lipid-lowering and vascular-targeted therapies may be beneficial in LGMD2B and DMD.

Preface

Chapter 4 is based on work conducted in collaboration with Stephanie Sellers under the supervision of Dr. Pascal Bernatchez. I contributed significantly to all aspects of project design, colony upkeep, tissue collection, and data analysis. All experiments and data analysis from Chapters 5 and 6 were conducted by me, except aortic staining which was done with help of Dr. Zoe White.

These projects were approved by the Animal Ethics Board of UBC, under the protocol A14-0070 and A14-0072.

Table of Contents

List of Images

List of Figures

List of Abbreviations

°C	Degree Celcius
µL	Microlitre
µm	Micrometer
µW	Microwatt
ACEI	Angiotensin-converting enzyme inhibitor
ANOVA	Analysis of variance
Apo	Apolipoprotein
BMD	Becker muscular dystrophy
Ca^{2+}	Calcium ion
$CaCl_2$	Calcium chloride
CK	Creatine kinase
cm	Centimeter
cm^2	Square centimeter
CMD	Congenital muscular dystrophy
CO_2	Carbon dioxide
DCM	Dilated cardiomyopathy
DKO	Double knockout
DGC	Dystrophin-associated glycoprotein complex
DMD	Duchenne muscular dystrophy
DNA	Deoxyribonucleic acid
ECM	Extracellular matrix
EDL	Extensor digitorum longus
eNOS	Endothelial nitric oxide synthase
h	Hour(s)
H+E	Hematoxylin and eosin
HDL	High-density lipoprotein
HFD	High-fat diet

IU	International unit
KCl	Potassium chloride
kDa	Kilodalton
KH_2PO_4	Monopotassium phosphate
KO	Knockout
L	Litre
L_0	Optimal length
LDL	Low-density lipoprotein
LDLR	Low-density lipoprotein receptor
LGMD2B	Limb-girdle muscular dystrophy 2B
m	Month(s)
mAb	Monoclonal antibody
MD	Muscular dystrophy
$MgCl_2$	Magnesium chloride
mL	Millilitre
mm	Millimeter
MMD	Miyoshi muscular dystrophy or Miyoshi myopathy
mmol	Millimolar
mN	Millinewton
min	Minute(s)
mRNA	Messenger ribonucleic acid
NaCl	Sodium chloride
NADH	Nicotinamide adenine dinucleotide
$NaHCO_3$	Sodium bicarbonate
NaOH	Sodium hydroxide
nNOS	Neuronal nitric oxide synthase
NO	Nitric oxide
O_2	Oxygen
OCT	Optimal cutting temperature

ORO	Oil red O
PAS	Periodic acid-Schiff
PCR	Polymerase chain reaction
PCSK9	Proprotein convertase subtilisin/kexin type 9
PDGFRα	Platelet-derived growth factor receptor-α
RPM	Revolutions per minute
s	Second(s)
SEM	Standard error of the mean
TA	Tibialis anterior
TG	Triglyceride
Tris-HCl	Tris hydrochloride
VEGF	Vascular endothelial growth factor
VLDL	Very-low-density lipoprotein
VSMC	Vascular smooth muscle cell

Acknowledgements

I would like to thank my supervisory committee, Dr. Fabio Rossi and Dr. Chun Seow, and my supervisor Dr. Pascal Bernatchez for all the helpful insight and guidance. Also, I am extremely grateful to Stephanie Sellers, Dmitri Pavlov and Zoe White for getting me through difficult times and for all the coffee.

Chapter 1: Introduction

1.1 Muscular Dystrophy

Muscular dystrophy (MD) represents a class of over 30 genetic diseases marked by progressive muscle wasting and atrophy, impaired walking ability (often leading to need for wheelchair use) as well as other clinical features specific to the mutation and subtype of MD (Emery, 2002; NINDS, 2011). Disease severity varies greatly between types of MD, ranging from loss of ambulatory function in childhood and significantly reduced life expectancy, to only mild walking impairment beginning in adulthood, which slowly progresses over a normal lifespan. The clinical presentation and the severity of the disease depend on which gene is affected, the type of mutation (frameshift, premature termination, etc.), the patient's genotype/copy number and the penetrance of that specific mutation (Emery, 2002). Many forms of MD are caused by recessive mutations in genes encoding dystrophin-associated glycoprotein complex (DGC) and other sarcolemmal proteins, which play a crucial role in muscle sarcolemma structure, function and integrity (Figure 1.1). Dysferlinopathies and dystrophinopathies are two subgroups of MD marked by distinct clinical features and caused by mutations in dysferlin and dystrophin genes, respectively. A brief description of dysferlin and dystrophin protein expression and function as well as an exploration of the pathophysiological features, treatments and animal models available for dysferlinopathies and dystrophinopathies will follow.

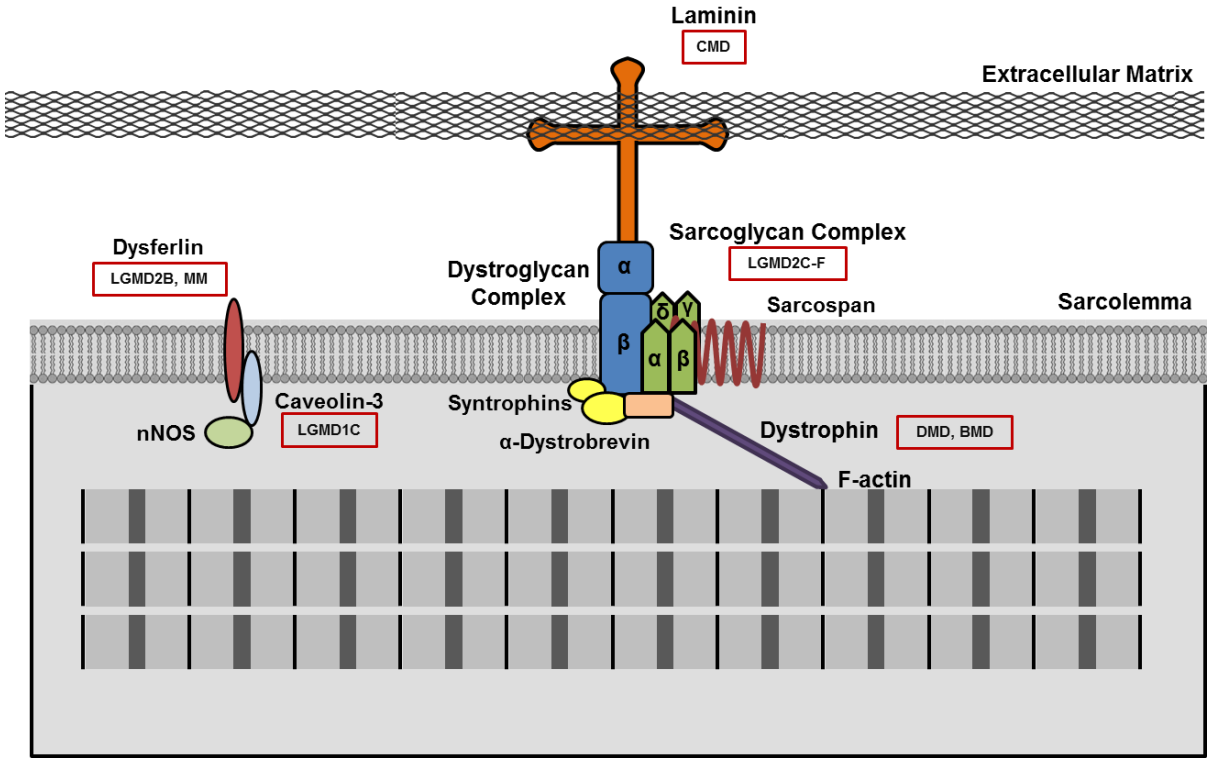

Figure 1.1 Dystrophin-associated glycoprotein complex and associated proteins in muscle. Dystrophin is critical for the maintenance of membrane stability in muscle cells by anchoring actin in the cytoplasm to β-dystroglycan in the sarcolemma. The sarcoglycan complex and sarcospan reinforce this dystrophin and dystroglycan complex interaction. Extracellularly, α-dystroglycan is strongly linked to laminin in the extracellular matrix (ECM). Dysferlin and caveolin-3, though not part of the DGC, associate with it in the sarcolemma and facilitate the interaction with nNOS. Red boxes indicate MD associated with protein loss of function. LGMD: limb-girdle MD, MMD: Miyoshi myopathy, DMD: Duchenne MD, BMD: Becker MD, CMD: congenital MD. Figure adapted from Durbeej and Campbell (2002) and Kobayashi, Izawa, Kuwamura, and Yamate (2012).

1.1.1 Dysferlinopathies

1.1.1.1 Dysferlin Function and Expression

Dysferlinopathies include limb-girdle 2B MD (LGMD2B) and Miyoshi MD (MMD) and are a group of autosomal recessive MDs marked by slow but progressive muscle degeneration caused by mutation of the dysferlin gene (*DYSF*) (Bashir et al., 1998; Bejaoui et al., 1995; Liu et al., 1998). Dysferlin is a 237kDa protein encoded on chromosome 2p12-14 and contains several C2 calcium binding domains (Bansal et al., 2003). It is a member of the ferlin family of transmembrane proteins which are known to be involved in vesicle fusion, intracellular trafficking, membrane resealing, endocytosis and exocytosis (Lek, Evesson, Sutton, North, & Cooper, 2012). Dysferlin is expressed not only at the sarcolemma in association with caveolin-3 and nNOS (Figure 1.1), but also in the membrane of intracellular vesicle (Bansal et al., 2003) where it is critical for membrane repair by facilitating the fusion of these vesicles to the plasma membrane in response to elevated Ca^{2+} (Cai et al., 2009; Glover & Brown, 2007; Washington & Ward, 2006). This patch-like system of membrane repair is important in tissues undergoing constant stress and injury, such as skeletal muscle myofibers (Han et al., 2007). Therefore, *DYSF* mutations leading to little or no functional expression result in impaired sarcolemmal resealing, accumulation of myofiber damage over time and progressive muscle degeneration and inflammation (Bansal et al., 2003; Cai et al., 2009; Cenacchi, Fanin, De Giorgi, & Angelini, 2005), all of which are observed in LGMD2B and MMD patients. Though dysferlin is the only ferlin protein associated with MD, myoferlin is known to be required for muscle myoblast fusion during muscle development (Doherty et al., 2005) and normal response to growth factors like insulin-like growth factor receptor 1

(Demonbreun et al., 2010). Nevertheless, loss of myoferlin expression does not result in muscle degeneration.

The expression and activity of dysferlin in non-muscle tissues have also been investigated to better understand the phenotype observed in dysferlin-deficiency. For instance, dysferlin mRNA and protein are strongly expressed in monocytes (De Luna et al., 2007; Gallardo et al., 2011) and loss of dysferlin expression has been shown to alter immune response (Chiu et al., 2009). Dysferlin-deficient monocytes display inflammatory marker upregulation (Rawat et al., 2010), impaired cell adhesion (de Morree et al., 2013) as well as increased cell motility and phagocytosis activity (Nagaraju et al., 2008). It has been proposed that the loss of dysferlin in macrophages may lead to an "inappropriately aggressive" response to muscle cell damage and release of sarcoplasmic proteins (Nagaraju et al., 2008), further aggravating muscle pathology. In addition, dysferlin expression has been found in endothelial cells and vascular smooth muscle cells (VSMCs) which line the blood vessels and loss of expression led to blunted angiogenesis and adhesion molecule expression (Sharma et al., 2010). Dysferlin protein is also expressed in cardiomyocytes, mainly localized to intracellular vesicles and intercalated disks connecting cardiomyocytes (Chase, Cox, Burzenski, Foreman, & Shultz, 2009; Han et al., 2007), however its function in the heart is not fully understood. As you can see, the non-muscle tissues expressing dysferlin are also affected by the absence of dysferlin expression and exploration of dysferlin function in these tissues may reveal additional pathogenic mechanisms in LGMD2B and MMD.

1.1.1.2 Miyoshi and Limb-girdle 2B Muscular Dystrophies

Miyoshi MD, also known as Miyoshi myopathy, is an autosomal recessive form of MD enriched in Japan and mainly affects distal limb muscles, such as those in the lower leg, forearm, hand and foot (Kobayashi, Izawa, Kuwamura, & Yamate, 2012). Early in the disease, there is distal muscle hypertrophy and weakness followed by slow but progressive wasting, especially in the posterior lower leg, resulting in problems tip-toe walking (Dimachkie & Barohn, 2014). A major clinical and diagnostic feature is the presence of elevated circulating creatine kinase (CK), often 30-100 times higher than normal (Galassi, Rowland, Hays, Hopkins, & DiMauro, 1987). In some patients, the steady progression results in proximal leg muscle weakness, affecting the patient's ability to climb stairs, walk and even stand (Aoki, 2015), while others can remain relatively stable and never develop proximal muscle pathology (Dimachkie & Barohn, 2014). Although the upper body muscles are usually spared, the most severely affected MMD patients can exhibit shoulder and upper arm muscle weakness (Aoki, 2015; Mahjneh et al., 2001).

On the other hand, limb-girdle MDs (LGMDs) are a rare subgroup of MD caused by mutations in over 15 genes and affect approximately 1 in 15,000-120,000 people (Urtasun et al., 1998; van der Kooi et al., 1996). Within LGMD, type 2B is caused by a loss of function mutation in dysferlin and accounts for approximately 3-19% of all LGMD cases (Tagawa et al., 2003), being more prominent in some populations such as southern Europe (Guglieri, Straub, Bushby, & Lochmuller, 2008). CK levels in LGDM2B patients can vary widely, from normal to 20-60 times normal concentrations (Rosales et al., 2010). Like MMD, LGMD2B leads to mild muscle weakness and atrophy with onset in adolescence or early adulthood and

progresses slowly over a normal lifespan; however, this can vary significantly between families and individuals (Guglieri, Straub, Bushby, & Lochmuller, 2008). LGMD2B differs from MMD in that early stages are marked by weakness and atrophy of pelvic and shoulder girdle muscles. Proximal lower-limb muscles can show signs of weakness as early as late adolescence while involvement of distal muscles is usually minimal and noticeable only by "careful examination or ancillary investigations such as muscle CT scan" (Aoki, 2015). Affected skeletal muscles display signs of myofiber degeneration and regeneration: increased myofiber necrosis, significant muscle inflammation, variable myofiber cross-sectional area, increased percentage of centralized nuclei, and increased fibrosis (Gallardo, Rojas-Garcia, de Luna, Pou, & Brown, 2001; McNally et al., 2000; Rosales et al., 2010). Significant fibrofatty remodelling can be observed in some skeletal muscles, especially lumbar, thigh and calf muscles, with adipocytes replacing up to 70% of muscle area in some cases (Angelini, Peterle, Gaiani, Bortolussi, & Borsato, 2001; Seror, Krahn, Laforet, Leturcq, & Maisonobe, 2008). Histological analysis of patient muscles found high lipid content in muscle adipocytes as well as within myofibers, which was not observed in normal, healthy muscle tissue (Grounds et al., 2014). Despite dysferlin expression in cardiomyocytes, cardiac dysfunction is not considered a major clinical feature of dysferlinopathies (Chase, Cox, Burzenski, Foreman, & Shultz, 2009). While most LGMD2B patients maintain normal cardiac function, a few cases of mild to moderate dilated cardiomyopathy (DCM) have been recorded, displaying decreased ejection fraction and increased left ventricular diastolic diameter (Guglieri, Straub, Bushby, & Lochmuller, 2008; Kuru et al., 2004; Wenzel et al., 2007).

1.1.1.3 Dysferlinopathy Treatments

Though the molecular cause of LGMD2B and MMD has been known for many years, there are still no effective pharmacological treatments for dysferlinopathies. Despite corticosteroid effectiveness in slowing disease progression and prolonging independent walking time in some forms of MD, dysferlinopathy patients do not respond favourably to corticosteroids. A double-blind, placebo-controlled study of glucocorticoids in LGMD2B patients found no beneficial effect of corticosteroid treatment on muscle strength score compared to placebo; in fact, a trend towards worsened muscle weakness in the treatment group was observed by the end of the trial (Walter et al., 2013). This potentially detrimental effect is important since dysferlinopathy muscle histology closely resembles polymyositis and misdiagnosis can lead to prescription of contraindicated corticosteroids in LGMD2B patients (Walter et al., 2013). Therefore, management of LGMD2B symptoms is challenging and no specific treatments are available.

After several pharmacological treatments were found to have no beneficial effect in LGMD2B and MMD patients, curative approaches such as gene therapy are being investigated. In gene therapy, a functional copy of dysferlin under a muscle-specific promoter can be inserted into the genome using an adeno-associated virus vector transfer system leading to restored dysferlin expression in skeletal muscle (Barthélémy, Wein, Krahn, Lévy, & Bartoli, 2011). Animal studies of gene therapy have succeeded in re-establishing dysferlin expression in muscle, resulting in improved membrane repair function, reduce muscle pathology and ameliorate ambulatory function (Lostal et al., 2010). However, there are some issues surrounding the safety and efficacy of gene therapy in human dysferlin-deficiency that must

be addressed (Barthélémy, Wein, Krahn, Lévy, & Bartoli, 2011). Other treatments targeting the fundamental loss of functional dysferlin expression, for instance exon skipping and transplicing agents, are also being explored but these therapies must be tailored to the specific dysferlin mutation and remain in the early stages of development in animal models (Aartsma-Rus et al., 2009).

1.1.1.4 Animal Models of Dysferlinopathies

The most commonly used animal models of dysferlinopathy are the two naturally occurring murine models: A/J and SJL/J mice. In addition, the A/J strain has been introgressed to a C57BL/6 background, also known as the BLA/J strain, and displays a similar phenotype to the A/J strain (Hornsey, Laval, Barresi, Lochmuller, & Bushby, 2013). These strains contain different mutations: A/J mice have a retrotransposon insertion (Ho et al., 2004) while SJL/J mice carry a splice-site mutation (Bittner et al., 1999) in the dysferlin gene, both of which result in little to no dysferlin protein expression and function. These models develop similar late onset, progressive MD with a muscle pattern resembling LGMD2B although displaying only mild muscle weakness, peaking at around 6-8 months of age (Kobayashi, Izawa, Kuwamura, & Yamate, 2010; Weller, Magliato, Bell, & Rosenberg, 1997). There is also a targeted knockout model of dysferlinopathy, the dysferlin-null mouse (Dysf-KO), that was developed by Dr. Kevin Campbell at the University of Iowa (Bansal et al., 2003). The pathological features of the Dysf-KO mice resemble SJL/J and A/J mice, only earlier in onset: some necrotic fibers and early signs of muscle damage can be seen by 2 months of age (Ho et al., 2004).

Like dysferlinopathy patients, all three dysferlin-deficient models also display elevated and variable CK levels (Ho et al., 2004). Although altogether milder than human dysferlinopathy muscle biopsies show, affected muscles in these mouse models display similar "degeneration/necrosis of muscle fibers, variations in the size of muscle fibers, atrophy of muscle fibers, inflammatory cell infiltration, centronuclear fibers, fatty infiltration and fibrosis in the limb girdle (mainly rectus femoris and lateral longissimus muscles)" (Kobayashi, Izawa, Kuwamura, & Yamate, 2012; Roche, Ru, & Bloch, 2012). Quantification of muscle degeneration revealed that less than 1% of muscle cross-sectional area was undergoing necrosis, even in mice as old as 19 months (Terrill et al., 2013). It has been suggested that type 2 fast-twitch muscle fibers are being targeted since mostly slow-twitch fibers were remaining in affected muscles; however, muscles such as iliocostalis, composed mainly of fast-twitch fibers, were largely untouched (Kobayashi, Izawa, Kuwamura, & Yamate, 2010). Significant replacement of muscle area with adipocytes, reaching 20-40% in psoas major and 10-20% in quadriceps femoris, has been demonstrated in old A/J mice (Terrill et al., 2013). Further investigation revealed that lipids were accumulating in adipocytes as well as within muscle fibers, as seen using oil red O (ORO) staining and electron microscopy images (Grounds et al., 2014). The major issue with these models is that although skeletal muscle damage can be observed histologically, it is only significant in older mice (>12 months) and does not result in apparent muscle weakness: SJL/J and A/J mice demonstrate little to no change in muscle strength and typically do not lose the ability to walk (Kobayashi, Izawa, Kuwamura, & Yamate, 2012; Weller, Magliato, Bell, & Rosenberg, 1997). This makes drug development

trials in mouse models inefficient since there is little room for therapeutic amelioration until 8-10 months and *in vivo* functional benefits cannot be explored.

1.1.2 Dystrophinopathies

1.1.2.1 Dystrophin Function and Expression

The dystrophin gene (*DMD*) is located on the X chromosome short arm between 21.1 and 21.2 and encodes dystrophin protein, an important member of the DGC (Figure 1.1). The DGC spans the plasma membrane, creating a critical link between the extracellular matrix and the intracellular cytoskeleton (Ervasti & Campbell, 1993). In skeletal muscle myofibers, dystrophin binds to actin filaments and to β-dystroglycan (another DGC protein) in the plasma membrane leading to stabilization of the membrane and anchorage of muscle contractile units to the sarcolemma (Straub, Bittner, Léger, & Voit, 1992). This attachment point is required for maintenance of sarcolemmal structure and protection from mechanical stress and injury during muscle contraction (Petrof, Shrager, Stedman, Kelly, & Sweeney, 1993). Although muscle development seems normal, loss of dystrophin expression leads to impaired force generation, DGC disassembly and mislocalization, increased sarcolemma fragility and increased susceptibility myofiber injury (Petrof, Shrager, Stedman, Kelly, & Sweeney, 1993; Rybakova, Patel, & Ervasti, 2000; Straub, Rafael, Chamberlain, & Campbell, 1997). Significant muscle damage and release of sarcolemmal contents then activates inflammatory cell recruitment and cytokine release, which in turn triggers fibroblast differentiation and collagen deposition (Ieronimakis et al., 2016). In addition, dystrophin is highly expressed in cardiomyocytes and

loss of expression leads to increased susceptibility to mechanical stress-induced injury and progressive cardiac dysfunction (Danialou et al., 2001).

Besides cardiac and skeletal muscle, dystrophin can also be found in VSMCs and endothelial cells lining the vasculature (Loufrani et al., 2001) as well as in the brain, liver, spleen and placenta (Chelly, Kaplan, Maire, Gautron, & Kahn, 1988). In the central nervous system, it is though that the DGC is involved in signal transduction and calcium homeostasis which may be impaired in the absence of dystrophin expression (Mehler, 2000). Nevertheless, the precise function of dystrophin in these non-muscle tissues is not fully understood. Dystrophin activity in skeletal and cardiac muscle has been the focus of most dystrophinopathy research since loss of expression leads to such severe muscle and heart pathology in Duchenne MD (DMD) and Becker MD (BMD).

1.1.2.2 Duchenne and Becker Muscular Dystrophies

Mutation to the dystrophin gene is the cause of DMD and BMD. Since the dystrophin gene located on the X chromosome, recessive mutations primarily affect boys who only have one copy of the X chromosome. Yet several studies have shown that female heterozygous carriers of dystrophin mutations can present with mild MD symptoms such as elevated circulating CK, intolerance to exercise, abnormal gait, and cardiac dysfunction (Mavrogeni et al., 2013; Papa et al., 2016; Schade van Westrum et al., 2011). Skeletal muscle phenotypes in female carriers are sporadic whereas progressive cardiac function decline affects most carriers, sometimes developing end-stage DCM and requiring heart transplantation (Melacini et al., 1998; Politano et al., 1996).

Duchenne MD is the most common type of MD occurring in nearly 1 in 3600-6000 male births worldwide and accounts for approximately 80% of all MD cases (Bushby et al., 2010; Emery, 1991). DMD is marked by extremely severe muscle wasting and atrophy as well as dramatic respiratory and cardiac decline. Although the age of onset and diagnosis in DMD boys varies between individuals, disease progression is invariably rapid, leaving approximately 90% of boys confined to a wheelchair by the age of 12 (Emery, Muntoni, & Quinlivan, 2015). Children usually present with impaired ability to stand from sitting on the floor (also known as Gower's sign), abnormal gait, muscle weakness, calf pseudohypertrophy, and elevated serum CK levels (Emery, Muntoni, & Quinlivan, 2015). At birth, circulating CK levels can reach 1000 times that of unaffected individuals and gradually decrease as the disease progresses and muscle mass decreases (Emery, Muntoni, & Quinlivan, 2015; Zatz et al., 1991). Muscle biopsies are used to assess the presence and level of dystrophin expression which helps distinguish DMD from other MDs or inflammatory muscle diseases and gives an indication of disease severity, where less dystrophin expression indicates worse skeletal and cardiac disease prognosis (Emery, Muntoni, & Quinlivan, 2015).

Upon histological analysis, the gross pseudohypertrophy observed is in fact a combination of muscle hypertrophy and significant necrosis and fibrofatty replacement (N. Deconinck & Dan, 2007; Kornegay et al., 2012; Tyler, 1003). In particular, the gastrocnemius and quadriceps femoris muscles are severely affected by fibro-fatty infiltration (Cros, Harnden, Pellissier, & Serratrice, 1989; Jones, Round, Edwards, Grindwood, & Tofts, 1983). As the disease progresses, severe wasting and weakening of weight bearing muscles in the legs and torso lead to loss of ambulatory function in childhood to early adolescence followed by

progressive cardiac and pulmonary decline. Without intervention, respiratory failure usually occurs around 16-18 years of age in DMD patients (Stromberg, Darin, Kroksmark, & Tulinius, 2012). The use of mechanical ventilation and respiratory physiotherapy since the late 1980s has led to a huge drop in respiratory deaths (Matsumura, Saito, Fujimura, Shinno, & Sakoda, 2011; Passamanno et al., 2012). Cardiac complications account for a large fraction of DMD mortality (Eagle et al., 2002) usually manifesting as DCM, ventricular arrhythmia and eventually heart failure (Chénard, Bécane, Tertrain, De Kermadec, & Weiss, 1993; de Kermadec, Bécane, Chénard, Tertrain, & Weiss, 1994). Nearly 80% of DMD patients develop significant cardiomyopathy by 18 years of age which has been attributed to increased cardiomyocyte damage and heart fibrosis (Townsend, Yasuda, & Metzger, 2007).

Becker MD is a variant of DMD, displaying many of the same pathophysiological features except later in onset, slower in progression and with larger heterogeneity in severity and presentation between patients: on average patients retain walking ability until middle age and live a normal lifespan (Bushby et al., 1993). Boys affected with BMD display calf enlargement, weakness of the proximal muscles in the pelvis, shoulders and thighs (Bushby et al., 1993) and elevated serum CK in the early stage of disease, peaking around 15 years of age (Zatz et al., 1991). Therefore, treatment and management of DMD and BMD symptoms involve similar therapeutic interventions.

1.1.2.3 Dystrophinopathy Treatments

In terms of pharmacological therapies for DMD, glucocorticosteroids (i.e. deflazacort and prednisone) are commonly prescribed and have been shown to slow the decline in muscle

strength and motor function. Clinical trials have demonstrated that short- and long-term daily corticosteroid treatment can prolong ambulatory function: patients on prednisolone showed longer 9-minute walk distances, shorter 4-stair climbing and sitting on floor to standing times, as well as delayed loss of ambulatory function (Griggs et al., 1991; Manzur, Kuntzer, Pike, & Swan, 2008; Mendell et al., 1989). In addition, steroid therapy appears to stabilize pulmonary function and potentially slow cardiac function decline (Biggar, Gingras, Fehlings, Harris, & Steele, 2001; Markham et al., 2005). In an observational study of DMD patients on renin-angiotensin system antagonists with or without steroid treatment, addition of corticosteroid therapy was shown to lower all-cause mortality, likely due to reduced rate of DCM and heart failure compared to DMD patients on renin-angiotensin blockers alone (Schram et al., 2013). Unfortunately, steroid therapy is accompanied by significant side effects, such as weight gain, Cushingoid appearance (moon face, thin skin, abdominal striae, etc.), behavioural changes, excessive hair growth, acne, osteoporosis, hyperglycemia, and gastrointestinal side effects (Manzur, Kuntzer, Pike, & Swan, 2008). As previously mentioned, therapies targeting respiratory function, such as mechanical ventilation, cough-assist devices and respiratory physiotherapy, have also proved beneficial. Ventilated patients show a huge improvement in overall survival compared to non-ventilated patients (Eagle et al., 2002). Since the administration of corticosteroids and respiratory physiotherapy, longitudinal studies have found a significant improvement in average lifespan: from 19 years of age from 1977-1984 to 31 years 2004-2010 (Matsumura, Saito, Fujimura, Shinno, & Sakoda, 2011). Similarly, another retrospective study observed increased rate of survival to age 25 after initiation of steroid therapy and ventilation: “13.5% in DMD patients born in the 1960s, 31.6% in those

born in the 1970s, and 49.2% in those born in the 1980s" (Passamanno et al., 2012). Therefore, it seems that improvement of respiratory function can have a significant effect on the preservation of motor function and survival. However, these treatments cannot cure nor stop the progression of the disease; inevitably, DMD patients experience ambulatory, pulmonary and cardiac function decline.

Therapies targeting the lack of dystrophin, such as gene therapy and exon skipping agents, are increasingly being explored. Exon-skipping therapy acts through the administration of anti-sense oligonucleotides which bind to the mutated exon region on the dystrophin pre-mRNA and block the translation of the error-containing exon (Aartsma-Rus et al., 2009). Although several exon-skipping agent clinical trials in the past decade have failed, recently a phosphorodiamidate morpholino oligomer exon-skipping therapy, called Exondys51 or eteplirsen, was approved in the United States for use in DMD patients. Clinical trials looking at weekly intravenous injection of eteplirsen in patients with an exon 51 mutation showed restored dystrophin expression, significant improvement in 6-minute walk distance, delayed decline in walking ability and in pulmonary function compared to controls, without any severe adverse events (Mendell et al., 2016; Mendell et al., 2013). However, eteplirsen is only useful for patients with exon 51 mutations, which accounts for approximately 20% of the all DMD patients (Tayeb, 2010). Therefore, additional methods of DMD treatment are still needed.

1.1.2.4 Animal Models of Dystrophinopathies

The most utilized model for DMD research is the *mdx* mouse model: a C57BL/10 background strain containing a naturally occurring point mutation in *Dmd* gene, which results

in dystrophin protein truncation (Sicinski et al., 1989) and little to no dystrophin expression (Bulfield, Sillers, Wight, & Moore, 1984; Chamberlain et al., 1988; Hoffman, Brown, & Kunkel, 1987). These mice were initially characterized for their elevated serum CK compared to wild-type mice which normalizes over time, as in DMD (Bulfield, Sillers, Wight, & Moore, 1984; Coulton, Morgan, Partridge, & Sloper, 1988). New strains of *mdx* mice, called *mdx2*^{cv}, *mdx3*^{cv}, *mdx4*^{cv}and *mdx5*^{cv}, have been developed from female offspring of C57BL/6 background males treated with a potent mutagen (Chapman, Miller, Armstrong, & Caskey, 1989). These strains have been shown to display similar skeletal muscle and cardiac pathologies to the original *mdx* mouse while showing fewer dystrophin-positive "revertant" cells (Danko, Chapman, & Wolff, 1992).

Despite the lack of dystrophin expression, *mdx* mice display only a mild phenotype compared to what is observed in human DMD patients. Between 2 to 8 weeks of age, *mdx* skeletal muscles undergo severe cycles of damage – marked by myofiber necrosis (up to 80% in some muscles) and inflammatory cell infiltration – followed by robust regeneration of muscle tissue (J. E. Anderson, Bressler, & Ovalle, 1988; Coulton, Morgan, Partridge, & Sloper, 1988; Tanabe, Esaki, & Nomura, 1986). By adulthood, *mdx* skeletal muscle histology shows almost complete regeneration with minimal fatty infiltration, fibrosis or myofiber necrosis (<5% of muscle area) with high percentage of centrally nucleated cells (J. E. Anderson, Bressler, & Ovalle, 1988; Bulfield, Sillers, Wight, & Moore, 1984). Although this robust regeneration occurs in most skeletal muscles, the diaphragm remains affected in *mdx* mice, showing progressive myofiber necrosis and fibrosis, with collagen content reaching up to seven times that of wild-type mice by 16 months of age (Stedman et al., 1991). Eventually,

old *mdx* mice display moderate pathology in some skeletal muscles (i.e. tongue, diaphragm and gastrocnemius) while leaving others relatively unaffected, such as quadriceps femoris and tibialis anterior (TA) muscles (Chamberlain, Metzger, Reyes, Townsend, & Faulkner, 2007; Collins & Morgan, 2003; Muller et al., 2001). Moderate exercise has been shown to exacerbate muscle damage in susceptible muscles, such as TA (Muller et al., 2001). Although diaphragm and tongue muscles are most severely affected, diaphragm is mostly slow-type muscle fibers and tongue muscle is mainly fast-twitch, indicating that the pattern of muscles affected in *mdx* is not determined solely by myofiber type (Chamberlain, Metzger, Reyes, Townsend, & Faulkner, 2007). Studies looking at muscle weakness in young *mdx* muscles found a progressive decrease in diaphragm specific force (Moorwood, Liu, Tian, & Barton, 2013) and showed a 20% drop in specific force in some limb muscles, such as extensor digitorum longus (EDL) and soleus, when normalized to the pseudohypertrophied muscle cross-sectional area (Faulkner, Brooks, Dennis, & Lynch, 1997; Lynch, Hinkle, Chamberlain, Brooks, & Faulkner, 2001). However, evaluation of muscle force in adult *mdx* mice, after complete muscle regeneration, showed higher isometric force in the soleus, leading researchers to posit that "when *mdx* mice lose muscle fibers by necrosis, they do not just replace them with equally efficient new muscle, but with heavier, stronger, muscles than wild-type" (Coulton, Curtin, Morgan, & Partridge, 1988).

Although less severe and later in onset than human patients, cardiac muscle is affected in *mdx* mice, displaying myocardial lesions, muscle fibrosis and inflammatory cell infiltration (Coulton, Morgan, Partridge, & Sloper, 1988). Mild myocardial fibrosis can be observed as early as 4-6 months of age in *mdx* mice and progresses over time; however functional

deficiencies of the heart can only be seen much later or when young mice are challenged with a dobutamine stress echocardiogram (Fayssoil et al., 2013; Meyers & Townsend, 2015). After 21 months of age, *mdx* mice undergo significant myocardial remodelling and can develop end-stage cardiomyopathy and heart failure (Bostick et al., 2012). The lifespan of these mice is only mildly reduced, from an average lifespan of 26 months in wild-type to 22 months in *mdx*, usually due to increased cardiac failure and muscle tumors development, known as rhabdomyosarcoma, in elderly *mdx* mice (Chamberlain, Metzger, Reyes, Townsend, & Faulkner, 2007).

There are also several dog and cat breeds that have been shown to develop skeletal and cardiac muscle pathology due to spontaneous dystrophin mutations. The Golden Retriever muscular dystrophy (GRMD) breed is the preferred canine model and develops symptoms similar to those seen in DMD patients (Cooper, Valentine, Wilson, Patterson, & Concannon, 1988). The most affected GRMD dogs do not survive past the first weeks of life while those who reach adulthood display severe “bunny-hopping” gait due to limb and pelvic muscle damage (Valentine, Cooper, de Lahunta, O'Quinnm, & Blue, 1988). Nevertheless, use of canine and feline models of DMD for clinical testing is not ideal due to their size, cost, and ethical controversy. The resemblance between GRMD and human DMD pathology, compared to mouse models, suggest that some important aggravating factors are present in the canine model and human disease but not present in the *mdx* mouse model.

1.2 Hyperlipidemia and Vascular Disease

Hyperlipidemia is widespread in the Western world, affecting approximately 40% of Americans and growing in prevalence across the globe (CDC, 2009, 2014; Mozaffarian et al., 2015). High circulating lipid levels, mainly low-density lipoprotein (LDL), are known to be associated with the development of vascular disease, also known as atherosclerosis (R. H. Nelson, 2013; Tomkin & Owens, 2012; Wilson et al., 1998), making cardiovascular disease a leading cause of death and disability in the United States, accounting for 23.7% of deaths in 2011 (CDC, 2014). A combination of high-lipid food intake, lack of exercise and genetic predisposition lead to a significant increase in cholesterol and triglyceride (TG) levels in the blood. Hyperlipidemia is defined as cholesterol levels over 6.21mmol/L (Rosenson, 2016) and was considered to be mainly a life-style disease. However, the Whitehall II study conducted in the United Kingdom has shown that dietary intervention or increased physical activity only modestly reduces total plasma cholesterol (Bouillon et al., 2011). There is increasing evidence that a major contributor to high cholesterol is genetic and hereditary in origin.

In fact, familial hypercholesterolemia (FH), a congenital form of hypercholesterolemia affecting cholesterol and/or lipid transport, is the most commonly inherited disease (A. C. Goldberg & Gidding, 2016). FH-causing mutations are often found in the low-density lipoprotein receptor (LDLR) or in apolipoprotein genes, both of which are involved in the efflux of lipoproteins from the circulation, as shown in Figure 1.2 (Soutar & Naoumova, 2007). Even though it is thought to be significantly underdiagnosed, FH affects approximately 1 in 250 people in the United States and, depending on the specific mutation, the risk of cardiac events is significantly raised and life-expectancy is reduced (A. C. Goldberg & Gidding, 2016).

For instance, patients with heterozygous mutations in LDLR display slightly raised plasma cholesterol and remain asymptomatic until adulthood; however exposure to modestly increased circulating lipids since birth leads to a much higher cumulative risk of cardiovascular disease compared to people who develop similar hyperlipidemia in adulthood (A. C. Goldberg & Gidding, 2016). Likewise, homozygous LDLR mutant patients born with extremely elevated plasma lipid levels can suffer from cardiac events in childhood (A. C. Goldberg & Gidding, 2016).

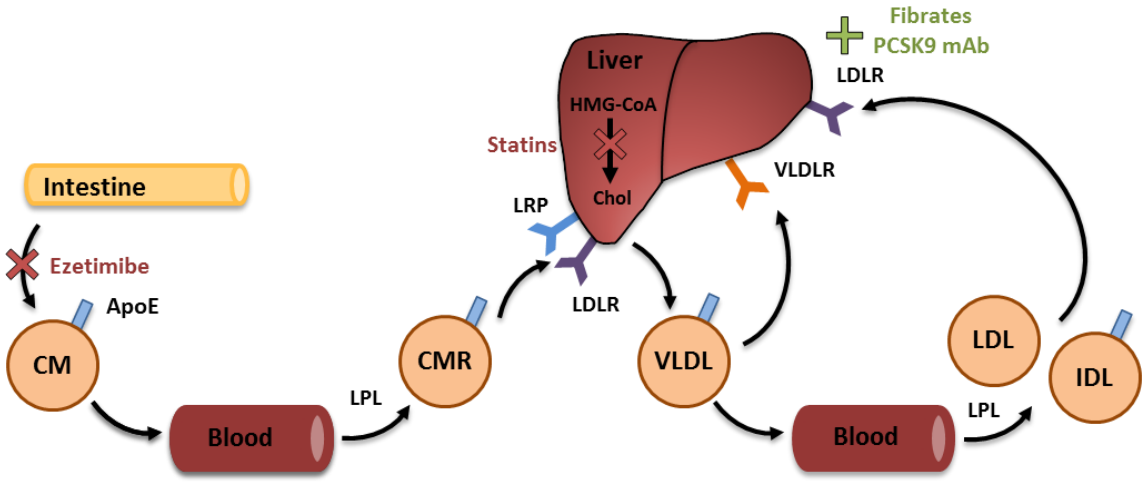

Figure 1.2 Simplified schematic of cholesterol absorption, transport and clearance. Intestinal uptake of dietary lipids is facilitated by NPCL1L (not shown), which can be inhibited by ezetimibe. Gut cells package the cholesterol and triglycerides (TGs) into chylomicrons which are released into the blood. In the circulation, chylomicrons are transformed by LPL into chylomicron remnants, which can be absorbed by the liver via LDLR and LRP binding of lipoprotein-bound ApoE. In the liver, HMG-CoA reductase produces endogenous cholesterol and can be inhibited by statins. VLDL, containing endogenous or exogenous lipids, is released from the liver and can be transformed by LPL into LDL/IDL in the blood or can be absorbed by the liver through VLDLR binding. Circulating IDL and LDL are cleared through interaction

with the LDLR in the liver. LDLR expression in the liver can be enhanced by treatment with both fibrates and PCSK9 mAb, although through different mechanisms. Red X indicates inhibition, green plus sign indicates activation. CM: chylomicron, CMR: chylomicron remnant, LPL: lipoprotein lipase, LRP: LDLR-related protein, VLDL: very low density lipoprotein, VLDLR: VLDL receptor. Figure adapted from Kwiterovich (2000) and Daniels, Killinger, Michal, Wright, and Jiang (2009).

1.2.1 Pathophysiology and Clinical Outcomes

Vascular disease is a major cause of mortality worldwide and a lot of research has explored its pathophysiology and attempted to halt the progression of the disease. The pathogenesis is marked by increased in circulating lipids which infiltrate the vessel wall, dysfunction of endothelial cells, atherosclerotic lesion development, plaque maturation, and eventual plaque rupture. Endothelial dysfunction has been shown to precede lesion development in early atherosclerosis (T. J. Anderson et al., 1995; Reddy, Nair, Sheehan, & Hodgson, 1994) and is caused by increased oxidative stress secondary to hyperlipidemia and/or hyperglycemia (Boulanger et al., 1992). Disrupted endothelial function is marked by reduced vasodilator (i.e. NO and prostacyclin) and increased vasoconstrictor (i.e. endothelin-1) bioavailability leading to impaired flow-mediated dilation (Lerman & Burnett, 1992), increased leukocyte adhesion (Kubes, Suzuki, & Granger, 1991), and abnormal platelet function (Radomski, Palmer, & Moncada, 1987). This endothelial dysfunction also leads to impaired endothelial barrier function, facilitating the accumulation of oxidized lipids in the blood vessel wall which then undergoes remodelling and fibrosis, resulting in atherosclerotic plaque formation (Bonetti, 2002).

The infiltration of lipids into the vessel wall and endothelial cell activation leads to the recruitment of macrophage and VSMC migration to the intimal layer. These cells attempt to clear the lipid and cellular debris in the intima and become lipid-loaded foam cells in the atherosclerotic plaque (Moore & Tabas, 2011). Large plaques can significantly alter vessel distensibility and reduce the lumen of blood vessels leading to impaired blood flow and poor tissue perfusion. In late atherosclerosis, the fibrous cap surrounding the necrotic, lipid-filled core can become thin and lead to plaque rupture and occlusion of the vessel (Moore & Tabas, 2011). Complete occlusion in the coronary arteries or in cerebral vessels results in myocardial infarction and stroke respectively and has become a major cause of death worldwide (CDC, 2014). Therefore, effective prevention and treatment of vascular disease and atherosclerosis can benefit much of the population.

1.2.2 Hyperlipidemia Treatments

Lipid-lowering medications are prescribed to reduce the risk of atherosclerosis and cardiovascular disease by targeting cholesterol and TG absorption, transport, metabolism or efflux, as shown in Figure 1.2. Between 2007 and 2011, approximately 1 in 10 Canadian adults were prescribed lipid-lowering statins, a 3-hydroxy-3-methyl-glutaryl-coenzyme A (HMG-CoA) reductase enzyme antagonist, which blocks endogenous production of cholesterol in the liver (Hennessy et al., 2016). However, the effects of statins spread well beyond HMG-CoA reductase blockade, such as “improvement of endothelial function, increased NO bioavailability, antioxidant properties, inhibition of inflammatory responses, and stabilization of atherosclerotic plaques” (Davignon, 2004). Unfortunately, a rare side effect of

statin treatment is rhabdomyolysis: a condition marked by muscle damage and pain with subsequent increased plasma CK levels (Thompson, Clarkson, Rosenson, & National Lipid Association Statin Safety Task Force Muscle Safety Expert, 2006). Other lipid-lowering therapies target the absorption of cholesterol from the gut, such as ezetimibe (Figure 1.2), which can be used in combination with statins as they target different pathways in cholesterol homeostasis. Ezetimibe blocks the Niemann-Pick C1-like 1 (NPC1L1), a protein involved in endocytosis of cholesterol into cells lining the gastrointestinal tract leading to significant lowering of plasma cholesterol (Phan, Dayspring, & Toth, 2012). However, fibrates function by activating peroxisome proliferator-activated receptor α (PPARα) which increases LDLR expression, increases clearance of LDL and decreases endogenous production of cholesterol and TGs (Staels et al., 1998). Although these drugs have shown modest efficacy, the recently approved alirocumab, a PCSK9 monoclonal antibody (mAb), is able to dramatically decrease plasma LDL with or without statin co-therapy (approximately 40-70%), leading to a significant reduction in cardiovascular risk for FH and high-risk hyperlipidemic patients (Gouni-Berthold & Berthold, 2014; Robinson et al., 2015). Alirocumab acts by reducing the activity of PCSK9, an LDLR recycling inhibitor, leading to increased LDL removal by LDLR in the liver (Robinson et al., 2015). Despite the effectiveness and overall tolerability of currently available lipid-lowering therapies in human hyperlipidemia, these treatments are often ineffective in animal models of hyperlipidemia.

1.2.3 Animal Models of Hyperlipidemia and Vascular Disease

Unlike humans, mice have endogenously low lipid levels in the blood, even when fed high-fat diet (HFD). Likewise, vascular disease and atherosclerosis in wild-type mice is exceptionally rare due to natively high levels of high density lipoprotein (HDL; antiatherogenic) and low baseline levels of LDL and VLDL (proatherogenic) (Zadelaar et al., 2007). Therefore, studies of atherosclerosis in mice must be done in genetically-manipulated mouse models. There are several strains of hyperlipidemic mice but the most commonly used variants are the ApoE-KO and the LDLR-KO, which target cholesterol clearance pathways (Figure 1.2). Apolipoprotein E is a protein found in VLDL, HDL and chylomicron remnants and facilitates the uptake and clearance of these lipoproteins from the circulation (Li, Kypreos, Zanni, & Zannis, 2003). In the liver, lipoprotein receptors such as LDLR and LDLR-related proteins (LRP) mediate the uptake of ApoE-containing lipoproteins (Getz & Reardon, 2009). Therefore, loss of ApoE expression leads to impaired binding and clearance by the liver and subsequent increased plasma VLDL and chylomicron levels (Mahley, 1988). Since LDLR is mostly involved in LDL uptake, LDLR-null mice display impaired LDL clearance and increased in circulating cholesterol (Ishibashi et al., 1993).

Although both models develop atherosclerosis when placed on high-fat diet (HFD) ApoE-KO display higher total cholesterol: 5 times higher than wild-type mice on chow (500mg/dL) and 10 times wild-type levels on HFD (>1000mg/dL) and is mainly comprised of chylomicron remnants and VLDL (Sehayek et al., 2000). In addition, ApoE-KO mice are known to develop atherosclerotic lesions and plaques on HFD and on regular chow (Nakashima, Plump, Raines, Breslow, & Ross, 1994). On the other hand, LDLR-KO mice do

not develop lesions on chow (Ma et al., 2012) and show a milder elevation in total cholesterol, composed mainly of LDL: approximately 2 times the wild-type level on chow (250mg/dL) and 4 times on HFD (450mg/dL) (Ishibashi et al., 1993; Zabalawi et al., 2007). This lipid profile is much more representative of the human hyperlipidemia profile, which is higher in LDL instead of VLDL and chylomicrons.

1.2.4 Vascular Disease and Lipids in MD

As previously published by our lab and others, dysferlin was found to be highly expressed, both mRNA and protein, in vascular endothelial cells, smooth muscle cells and atherosclerotic plaques of humans and mice (Hochmeiseter et al., 2006; Sharma et al., 2010). It was discovered that dysferlin plays a key role endothelial cell adhesion, proliferation and angiogenesis, where dysferlin-null mice demonstrated impaired angiogenesis in response to VEGF incubation, a growth factor known to induce capillary growth (Sharma et al., 2010). Therefore, the contribution of dysferlin activity to normal vascular density and function in muscle is not entirely clear. Similarly, dystrophin can be found in endothelial cells and smooth muscle cells lining the vasculature. Close examination of blood vessels from dystrophin-deficient patients showed significant endothelial cell swelling, basement membrane thickening, increased platelet adhesion and capillary degeneration, even in the earlier stages of disease (Miike, Sugino, Ohtani, Taku, & Yoshioka, 1987). In addition, dystrophin-deficient patients have significantly increased circulating VEGF, whose expression is known to be induced by hypoxia and ischemia (Saito, Yamamoto, Matsumura, Fujimura, & Shinno, 2009). Loss of dystrophin in VSMCs has also been shown to lead to impaired vasodilation, nNOS

dysfunction, reduced NO release (Loufrani et al., 2001; Rauch et al., 2012; Sander et al., 2000; Thomas et al., 1998), reduced vascular density, and increased vessel wall thickness (Loufrani et al., 2004; Loufrani, Levy, & Henrion, 2002). Further studies looking at carotid arteries in dystrophin-deficient animal models found increased vessel wall stiffness and stress as well as increased neointimal thickening in response to collar-injury induced atherosclerosis (Dye, Gleason, Wilson, & Humphrey, 2007).

Few studies have explored lipid levels or vascular function in dysferlinopathy patients or the effect of lipid modulation on disease progression. Nevertheless, one study found that the circulating lipid levels of 10 dysferlinopathy patients were within the normal range (Grounds et al., 2014). Some studies looking at dystrophin-deficiency have shown that DMD patients and *mdx* mice have significantly increased lipid levels in the plasma (Srivastava, Pradhan, Mittal, & Gowda, 2010; Temin & Islamova, 1983) and in the skeletal muscle (Hughes, 1972). High-resolution NMR analysis of DMD patient serum showed a significant increase in total cholesterol, free cholesterol, cholesterol esters, TGs and certain phospholipids compared to unaffected age- and gender-matched controls: i.e. mean TG level of 1.27mmol/L in DMD patients compared to 0.40mmol/L in unaffected individuals while mean total cholesterol levels were 2.08mmol/L and 0.65mmol/L, respectively (Srivastava, Pradhan, Mittal, & Gowda, 2010).

A two-hit hypothesis has been proposed to explain muscle pathology in MD, postulating that only the combination of impaired muscle perfusion and myofiber susceptibility to damage can cause the significant myofiber damage observed in patients (Ennen, Verma, & Asakura, 2013). In addition, the clustering of necrotic myofibers seen in

MD supports the theory that concurrent vascular dysfunction – leading to functional ischemia and disrupted endothelial barrier function – and increased myofiber susceptibility to damage are behind the localized muscle damage. Meanwhile, restoration of dystrophin expression in VSMCs of dystrophin-deficient mice has been shown and improve vascular function and to reduce serum CK (Ito et al., 2006; Ito et al., 2005). Many have abandoned the vascular theory of MD since few studies found any significant impairment of vascular function in the muscle and it was shown that functional muscle ischemia caused by the loss of nNOS expression does not lead to muscle disease (Chao et al., 1996). However, it is likely a combination of impaired vascular function and myofiber fragility and susceptibility to stress which causes significant muscle damage in the absence dysferlin and dystrophin. Therefore, the role of vascular function in MD pathogenesis has not been fully elucidated, though there is evidence that vascular function is disrupted and circulating lipid levels may be affected in the absence of dysferlin or dystrophin expression.

Chapter 2: Hypothesis, Specific Aims and Rationale

2.1 Hypothesis

We hypothesise that vascular function plays a significant role in the development and progression of MD and that through the creation and characterization of double-disease murine models of MD and hyperlipidemia-associated vascular disease, we can assess the effect of impaired vascular health on MD.

2.2 Specific Aims

1. Generate Dysf-ApoE double-knockout mouse model and compare MD phenotype and progression to control groups by looking at ambulatory function, skeletal muscle strength, heart function and skeletal muscle histology.
    a. Rationale: As previously described, animal models of dysferlinopathy do not replicate the severity of disease observed in human patients. This project seeks to assess the effect of hyperlipidemia and subsequently disrupted vascular function, which is commonly observed in humans, on dysferlin-deficient mice using a double-disease model.
2. Generate Dysf-LDLR double-knockout mouse model and compare MD pathology and progression by looking at ambulatory function and skeletal muscle histology.
    a. Rationale: This project seeks to confirm that the effect observed in our Dysf-ApoE DKO project is due to hyperlipidemia and subsequently impaired vascular health, not due to loss of ApoE specifically. This will be done using another hyperlipidemia model, LDLR-KO. This experiment was also devised

to note the effects of a milder, more humanized hyperlipidemia model on dysferlinopathy mice.

3. Generate Mdx-ApoE double-knockout mouse model and compare MD pathology and progression with control groups by looking at ambulatory function, skeletal muscle strength, heart function, skeletal muscle histology and aortic atherosclerosis.
    a. Rationale: As previously mentioned, DMD is the most common form of MD and its pathology is significantly more severe than the phenotype displayed in available murine models. This experiment seeks to determine if the effect of hyperlipidemia on muscle pathology seen in our dysferlinopathy model applies to other, more prominent and severe forms of MD.

Chapter 3: Experimental Design

3.1 Animal Model Breeding and Care

All animals were housed in a 12-hour light/12-hour dark cycle, temperature regulated facility and all experiments were approved by the Animal Care Committee. Experimental mice were placed on regular chow (PicoLab R Rodent Diet 20-5053, #0007688) or HFD (Harlan, TD88137; 0.2% total cholesterol, 21% total fat and 34% sucrose by weight). Mice were sacrificed while under 3.5% isoflurane anesthesia via cardiac puncture and perfused with warmed Krebs solution.

3.1.1 Dysferlin-ApoE Model

Experimental mice were generated using Dysferlin -/- (C57BL/6 background) provided by Dr. Kevin Campbell (Bansal et al., 2003) which were crossed with ApoE -/- mice (C57BL/6 background) from Jackson Laboratory (Bar Harbor, ME). Resultant Dysf +/- ApoE +/- littermates were then crossed to generate all experimental groups: wild-type, ApoE-KO, Dysf-KO, and Dysf-ApoE DKO. Ear-clip DNA was extracted using DNeasy extraction kit (Qiagen, 69506) following manufacturer's instructions. Mice were genotyped using protocol for ApoE-KO suggested by Jackson (forward common 5'-GCCTAGCCGAGGGAGAGCCG-3', wild-type reverse 5'-TGTGACTTGGGAGCTCTGCAGC-3' and mutant reverse 5'-GCCGCCCC GACTGCATC-T-3') and Dysf-KO protocol (common primer 5'-GCCAGACAAGCAAGGT TAGTGTGG-3', wild-type primer 5'-GCGGGCTCTCAGGCACAGTATCGC-3' and mutant primer 5'-CAGGGGCGCCCGGTTCTTTTTGTCAA-3') (Han et al., 2011). Mice were fed HFD starting at 8 weeks of age until sacrifice at 7 and 11 months.

3.1.2 Dysferlin-LDLR Model

Experimental mice were generated by crossing previously mentioned Dysf -/- with LDLR -/- mice (C57BL/6 background) from Jackson Laboratory (Bar Harbor, ME). Dysf +/- LDLR +/- littermates were then crossed to generate experimental groups: wild-type, LDLR-KO, Dysf-KO, and Dysf-LDLR DKO. A "forced" breeding strategy was set up to increase DKO production by breeding Dysf -/- LDLR +/- littermates – generating Dysf-KO and Dysf-LDLR DKO groups. Ear-clip DNA was extracted using DNeasy extraction kit (Qiagen, 69506) following manufacturer's instructions. Mice were genotyped using Dysf-KO protocol previously mentioned (Han et al., 2011) while LDLR PCR was divided into two protocols: one for detection of wild-type LDLR gene (wild-type forward 5'-ACCCCAAGACGTGCTC CCAGGATG-3' and wild-type reverse 5'-CGCACTGCTCCTCATCTGACTTGTC-3') and one for detection of LDLR-knockout insertion (neomycin forward 5'-AGGATCTCGTCGTG ACCCATGGCGA-3' and wild-type reverse, as above) (Gaw, Mancini, & Ishibashi, 1995).

3.1.3 Mdx-ApoE Model

Mdx-ApoE breeding was separated into two sets of crosses (Figure 3.1). Breeder pairs were generated using *mdx4*^{cv}-/- mice (simplified as Mdx) crossed with ApoE -/- mice, both strains are C57BL/6 background from Jackson Laboratories (Bar Harbor, ME). From this cross, Mdx +/- ApoE +/- and Mdx -/y ApoE +/- littermates were bred to generate several genotypes including Mdx -/- ApoE +/- females and Mdx -/y ApoE +/- males, which were then crossed to generate two experimental groups: Mdx and Mdx-ApoE DKO. Separately, ApoE-KO mice were crossed with wild-type C57BL/6 mice to generate ApoE +/- littermates. These heterozygous littermates were crossed to produce the other two experimental groups: wild-

type and ApoE-KO. Ear clip DNA was extracted using hot NaOH and Tris-HCl extraction method (Truett et al., 2000). Mice were genotyped using previously mentioned ApoE-KO PCR protocol and Mdx primer competition method: common reverse primer 5'-GCGCGGCTTGC CTCTGACCTGTCCTAT-3', wild-type forward primer 5'-GATACG CTGCTTTAATGCC TTTAAGAACAGCTGCAGAACAGGAGAC-3' and mutant forward primer 5'-CGGCCA GAACAGCTGCAGAACAGGAGAT-3' (Shin, Hakim, Zhang, & Duan, 2011). Mice were fed HFD starting at 8 weeks of age or kept on chow until sacrifice at 4 and 7 months.

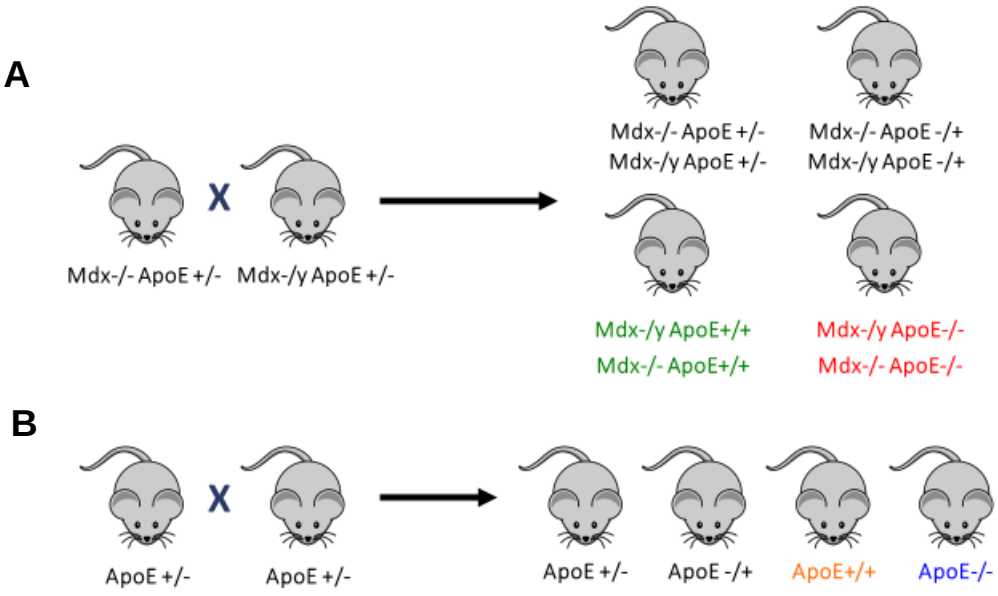

Figure 3.1 Breeding scheme devised for Mdx-ApoE experimental groups. Breeder pair genotypes for generation of (A) Mdx and Mdx-ApoE DKO groups and (B) wild-type and ApoE-KO control groups.

3.2 Ambulatory Function Assessment

Step length was measured by painting the hind-feet of mice and allowing them to run down a small corridor covered with paper, approximately 1.5m in length. Distance between

steps of the same foot were measured and averaged over 3 consecutive runs, excluding areas of stoppage. A value of 0 was given to runs where mice could not move their hindlimbs sufficiently and lost complete ambulatory function, which resulted in a smear across the page.

3.3 *In Vivo* Heart Function

Mice were anesthetised using 0.75% isoflurane and a four-chamber echocardiogram was performed by a blinded technician using the VisualSonics Vevo 2100 system. Heart chamber and ventricle wall tracings were analyzed to determine several cardiac parameters such as cardiac output, fractional shortening, stroke volume, ejection fraction, as well as left ventricular diameter and volume in both diastole and systole.

3.4 *Ex Vivo* Skeletal Muscle Function

Soleus muscle was excised whole and clips were fixed to the tendons at both ends of the muscle. For the diaphragm, a strip of muscle was removed then one clip was attached to the sternum and the other to the central tendon. Soleus and diaphragm muscles were mounted between electrodes in a bath of 37°C Krebs solution [118 mmol/L NaCl, 22.5 mmol/L $NaHCO_3$, 4 mmol/L KCl, 1.2 mmol/L NaH_2PO_4, 2 mmol/L $CaCl_2$, 2 mmol/L $MgCl_2$, 11 mmol/L dextrose] bubbled with 95% O_2/5% CO_2 (pH 7.4) in a circulating bath. Muscle strips were equilibrated at *in situ* muscle length (Lo) to determine maximum force generation. Then, muscles were stimulated at various loads (10%, 20%, 40%, 60% and 80% of maximum force) to assess contraction velocity, which was normalized to muscle length. Power curves were plotted as the product of force and velocity. Next, muscles were fatigued via repeated

stimulation every 4s over 2min at a constant load and declining force during fatigue was expressed as a fraction of the pre-fatigue force. Finally, muscle was stimulated 8 times with 30s recovery periods between stimulations to observe force recovery after fatigue. Muscle force recovery was expressed as a fraction of the pre-fatigue force.

3.5 Gross Hindlimb Size and Skin Lesion Scoring

Hindlimb muscle size was measured from gross photographs of legs after skinning. Whole body photographs taken at the time of sacrifice were used to assess presence and severity of skin lesions using a 0-3 scale: 0 – no lesions, 1 – presence of one or two un-erupted xanthomas, 2 – presence of several un-erupted xanthomas and/or mild erupted lesions, and 3 – presence of several erupted, severe lesions that are past a humane endpoint, requiring immediate sacrifice.

3.6 Skeletal Muscle Histology

Diaphragm, soleus, TA, EDL, gastrocnemius, quadriceps femoris, psoas major and triceps brachii muscles were collected. Muscle tissue was fixed in 10% formalin for 24 hours then transferred to 70% ethanol. A technician paraffin embedded and sectioned muscles into slides 8μm in thickness, which were then stained with hematoxylin and eosin (H+E) or Masson's trichrome stains. Percentage of fat was calculated by tracing adipocyte regions in Aperio ImageScope software and dividing the area by the total area of the muscle. To determine percentage of muscle area occupied by healthy myofiber, areas of non-viable myofiber (e.g. inflammatory cell infiltrations, areas of fibrosis, areas of necrosis etc.) as well

as fat area were subtracted from total muscle area. Collagen content was measured using a positive pixel count algorithm in Aperio ImageScope software of Masson's trichrome stained slides using the following parameters: hue value of 0.66 and hue width of 0.25. Percentage of centralized nuclei was determined using 4 fields of view at 15x zoom of H+E stained slides, including only muscle fibers completely within the frame. Alizarin red stain was also performed on select skeletal muscle slides.

3.7 Aortic Atherosclerosis

Hearts were cut along the atrioventricular plane, frozen in optimal cutting temperature (OCT) compound and aortic root sections were stained with ORO (Mehlem, Hagberg, Muhl, Eriksson, & Falkevall, 2013). Aortas were fixed in 10% formalin, rinsed with 70% ethanol and soaked in filtered Sudan IV solution (5g Sudan IV in 500mL 70% ethanol and 500mL acetone) for 20min. After aortas were rinsed in 80% ethanol, they were soaked in 80% ethanol for 20min then rinsed in running water for 1h and stored in 10% formalin. Photographs of pinned open aortas were taken for analysis and percentage of plaque coverage was determined by dividing plaque area by total vessel wall area.

3.8 Plasma Analysis

Plasma was collected in heparinized tubes via facial bleeding of unfasted mice at 5 months of age on chow, spun down at 4,000RPM for 10min at 4°C and stored at -80°C. Creatine kinase levels were measured using Creatine Kinase Activity Assay Kit (Sigma, MAK116) following manufacturer's instructions.

3.9 Statistical Analysis

Statistical analyses were performed using GraphPad Prism 6. For comparison of all four experimental groups at one time-point, one-way analysis of variance (ANOVA) was used to compare the means of each group. When comparing several curves (i.e. fatigue and recovery curves) or two time-points for all experimental groups, a repeated measures two-way ANOVA was used. Tukey's method was employed to correct for multiple comparisons. A log-rank test was used for the Kaplan-Meir adverse events curve and chi-squared test was used to compare expected and observed offspring numbers in Dysf-LDLR project. A p value of 0.05 or less was considered statistically significant. Figures show data as mean plus standard error of the mean (SEM) and n indicates the number of mice per group.

Chapter 4: Dysferlin-ApoE Double-Knockout Model

4.1 Introduction

Since the discovery of significant dysferlin mRNA and protein expression in endothelial cells (Sharma et al., 2010), the contribution of dysferlin-deficient vascular endothelium to the development of muscle pathology has yet to be determined. Endothelial function was found to be impaired in dysferlin-deficient models, showing a reduction in angiogenesis and dysregulated expression of cell adhesion proteins (Sharma et al., 2010), likely contributing to inflammatory cell infiltration observed in dysferlinopathy mouse models and patients alike. However, the severity of muscle pathology observed in human dysferlinopathy patients is not reproduced in dysferlin-deficient murine models. As previously described, animal models of dysferlinopathy do not lose the ability to walk, only display small changes in muscle strength and show minor increases in muscle damage (Kobayashi, Izawa, Kuwamura, & Yamate, 2012). This discrepancy between model and patient phenotypes makes it difficult to develop and screen potential therapeutics in animal preclinical trials. In addition, the mechanism behind this disparity in disease severity may offer up new targets for future treatment. One possible explanation is that, compared to humans, mice have much lower basal cholesterol levels and do not spontaneously develop atherosclerotic lesions, even when challenged with HFD. It is possible that the comparatively high level of circulating lipids in humans and resultant vascular disease may have a detrimental effect on MD progression and that mice are protected by their superior vascular health. Therefore, study of hyperlipidemia in the context of dysferlinopathy murine models was proposed to investigate the effect of worsened vascular function on the progression of MD pathology.

4.2 Results

4.2.1 Ambulatory Function

When fed a HFD, Dysf-ApoE DKO mice displayed startling impairment of ambulatory function compared to all other groups at 11 months of age. Complete loss of walking ability was observed in 40% of DKOs by 11 months of age (Figure 4.1). Similarly, a significant decrease in average step length was observed at 11 months of age: 2.7cm in DKO vs. 6.2cm, 5.9cm and 5.5cm in WT, ApoE and Dysf groups, respectively (Figure 4.2).

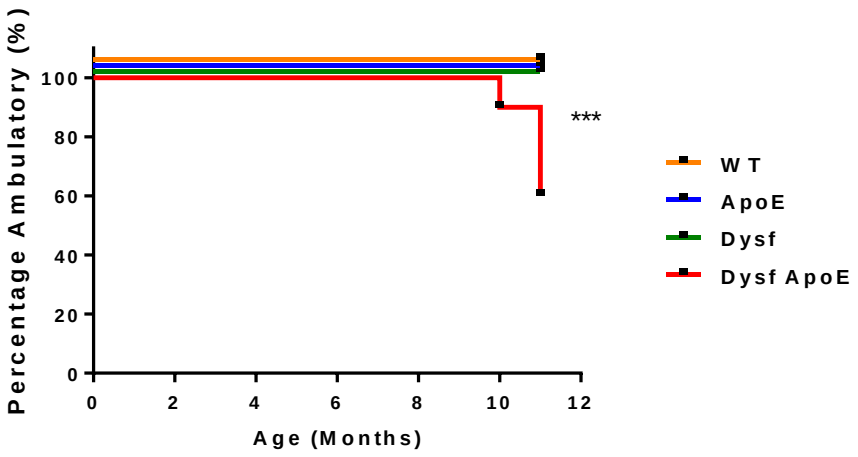

Figure 4.1 Kaplan-Meier curve of ambulatory function in HFD groups. Percentage of group population with maintained ambulatory function over 11-month lifespan. WT (n=12), ApoE (n=12), Dysf (n=18), and Dysf-ApoE (n=10). Log-rank test. ***P<0.001 Dysf-ApoE at 11 months compared to all other groups.

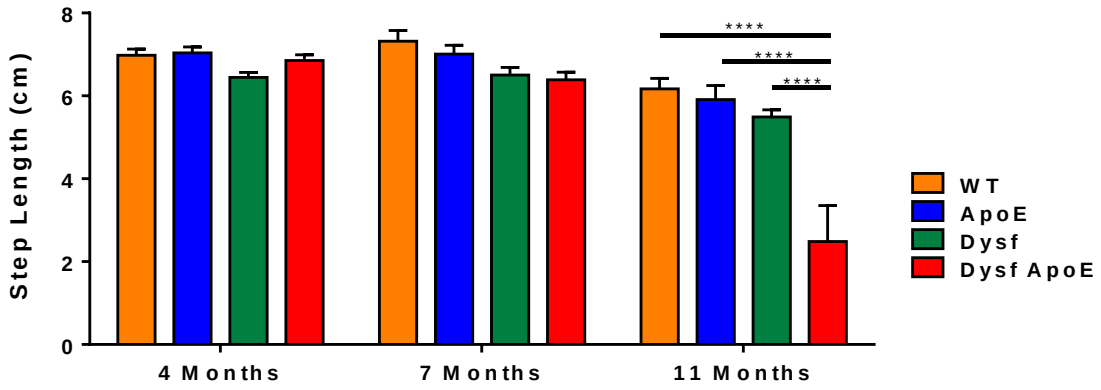

Figure 4.2 Step length at 4, 7 and 11 months of age on HFD. Average step length over 3 runs in cm. WT 4m (n=10), 7m (n=11), 11m (n=5); ApoE 4m (n=14), 7m (n=15), 11m (n=6); Dysf 4m (n=20), 7m (n=17), 11m (n=10); and DKO 4m (n=7), 7m (n=10), 11m (n=10). Mean+SEM, two-way ANOVA. ****P<0.0001

4.2.2 *In Vivo* Heart Function

Assessment of *in vivo* heart function in all four groups of mice at 11 months of age on HFD demonstrated no significant difference in heart function parameters including ejection fraction, fractional shortening or diastolic and systolic volumes (Figure 4.3). Other parameters such as cardiac output, left ventricular diameter (in systole and diastole) and stroke volume were also not significantly different between groups (data not shown).

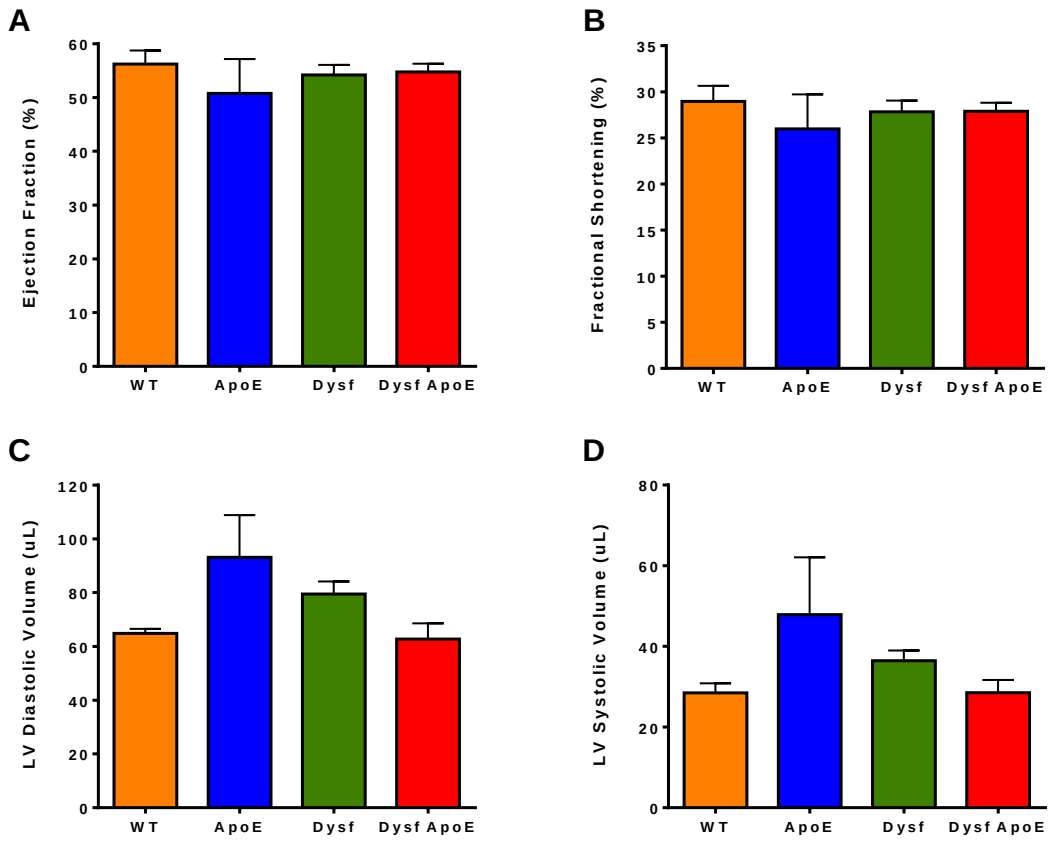

Figure 4.3 *In vivo* heart function parameters at 11 months on HFD. (A) Percent ejection fraction, (B) percent fractional shortening, (C) left ventricular diastolic volume in μL, and (D) left ventricular systolic volume in μL. WT (n=2), ApoE (n=3), Dysf (n=8), and Dysf-ApoE (n=4). Mean+SEM, one-way ANOVA.

4.2.3 *Ex Vivo* Skeletal Muscle Function

The force and functional parameters of excised muscle determined via myography suggest that there is little change in diaphragm power at 7 and 11 months (Figure 4.4A and 4.4B), or rate and ability to recover post-fatigue at 11 months (Figure 4.6A). Surprisingly, no change in fatigue was seen at 7 months of age (Figure 4.5A) while Dysf-ApoE DKO diaphragms fatigued

significantly less than wild-type and ApoE-KO groups at 11 months of age (Figure 4.5B). In the soleus muscle, there seems to be a drop in maximum power of Dysf-ApoE DKO mice at 7 months (Figure 4.4C) and in Dysf-KO mice at 11 months (Figure 4.4D). However, there was no difference in soleus fatigue (Figure 4.5C and 4.5D) or recovery (Figure 4.6B) between groups. Additional skeletal muscle *ex vivo* function data – such as absolute force values, maximum power and load at maximum power – can be found in Appendix A (Table A.1).

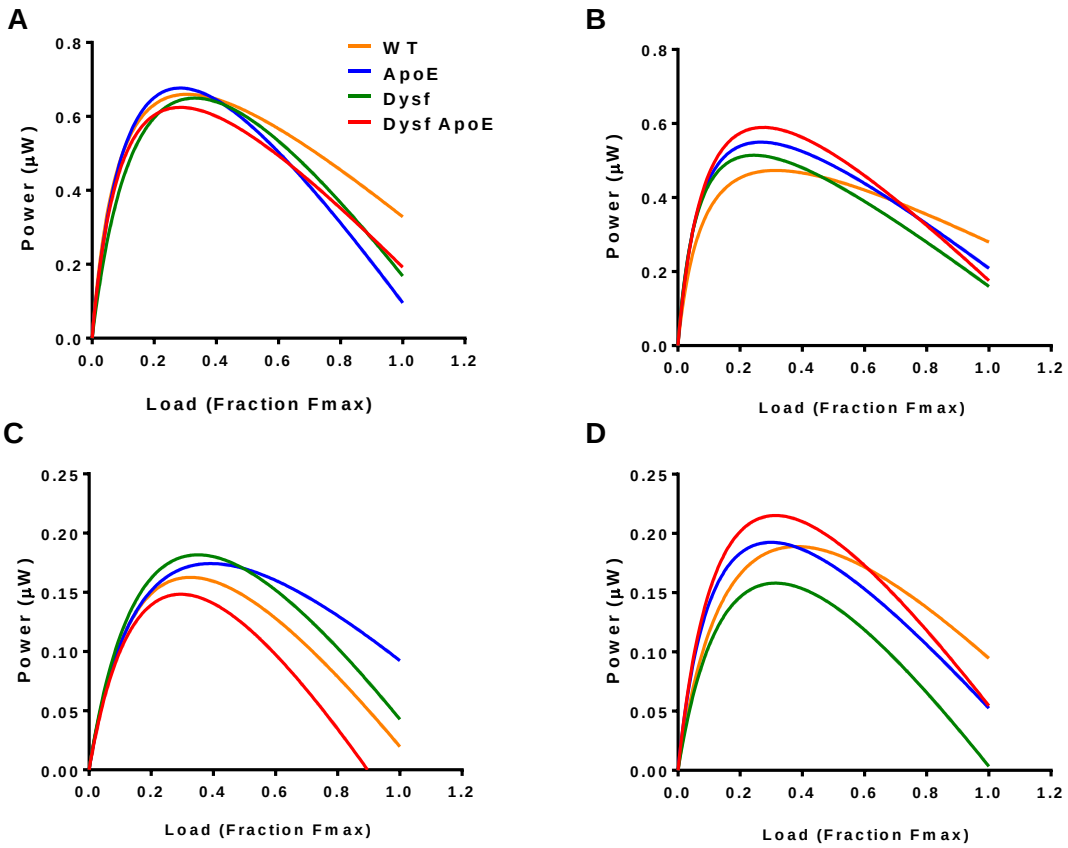

Figure 4.4 Diaphragm and soleus ex vivo power at 7 and 11 months on HFD. Diaphragm power in µW at a given load expressed as fraction of maximum force at (A) 7 and (B) 11 months

and soleus power curves at (C) 7 and (D) 11 months. WT 7m (n=2), 11m (n=10); ApoE 7m (n=7), 11m (n=11); Dysf 7m (n=6), 11m (n=11); and Dysf-ApoE 7m (n=4), 11m (n=8).

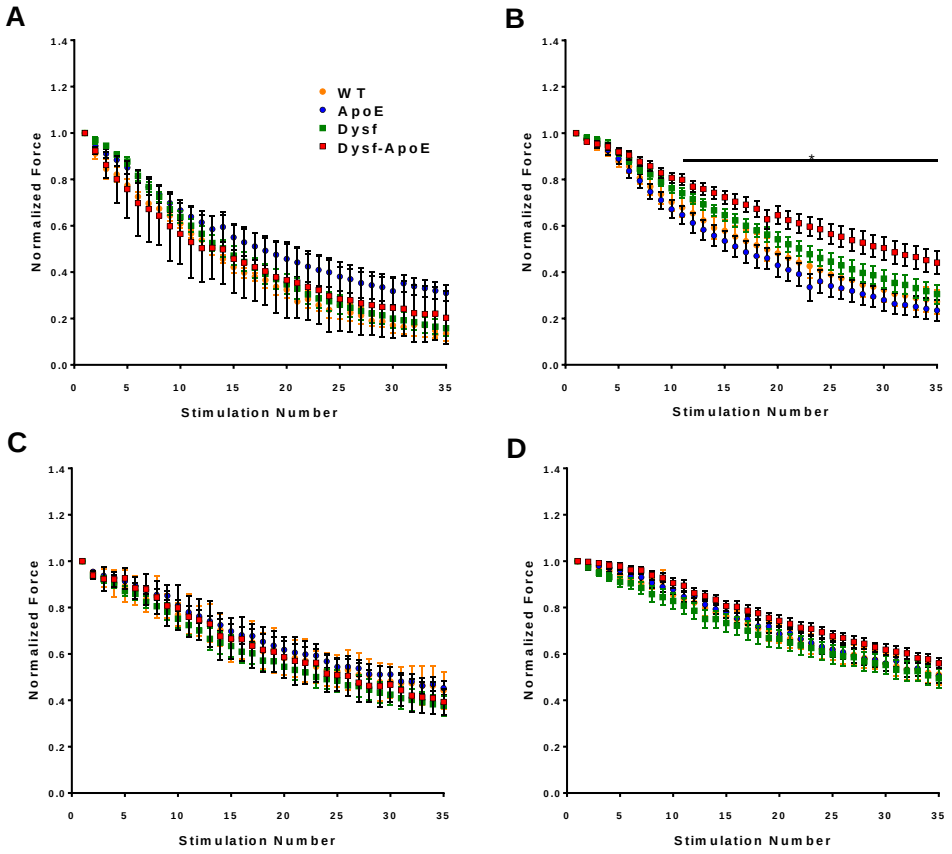

Figure 4.5 Diaphragm and soleus muscle *ex vivo* force fatigue at 7 and 11 months on HFD. Diaphragm normalized force at (A) 7 and (B) 11 months and soleus normalized force at (C) 7 and (D) 11 months, expressed as fraction of initial force. WT 7m (n=2), 11m (n=10); ApoE 7m (n=7), 11m (n=10); Dysf 7m (n=6), 11m (n=10); and Dysf-ApoE 7m (n=3), 11m (n=8). Mean±SEM, two-way ANOVA. *P<0.05 for Dysf-ApoE group compared to WT and ApoE-KO groups.

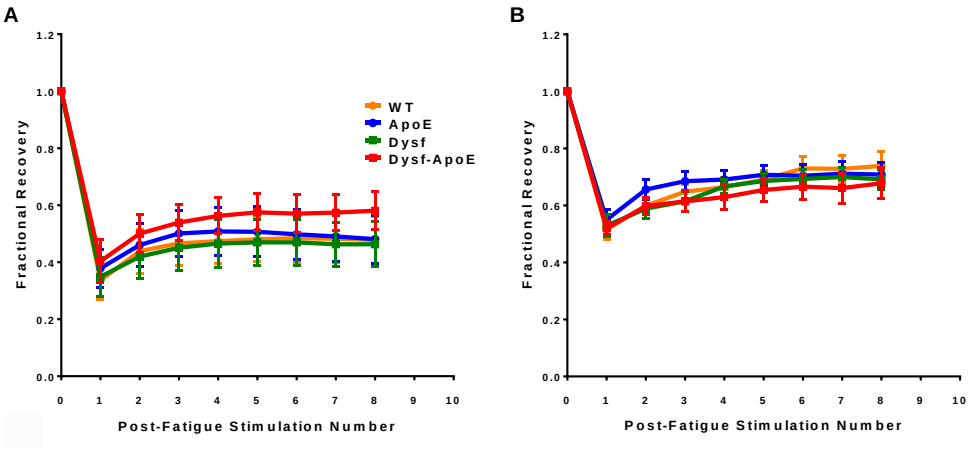

Figure 4.6 Diaphragm and soleus *ex vivo* force recovery at 11 months on HFD. (A) Diaphragm and (B) soleus force recovery at 11 months over 8 stimulations, expressed as a fraction of force generated prior to fatigue. WT (n=10), ApoE (n=9), Dysf (n=9) and Dysf-ApoE (n=7). Mean±SEM, two-way ANOVA.

4.2.4 Gross Hindlimb Size and Skin Lesion Scores

As shown in Image 4.1, hindlimb muscles showed significant wasting where width measurements were significantly reduced in Dysf-ApoE DKOs compared to all other groups at 11 months of age (Figure 4.7). Xanthoma and skin lesion scoring revealed an increased distribution of mild to severe skin lesions in ApoE-KO and Dysf-ApoE DKO groups compared to WT and Dysf-KO (Figure 4.8).

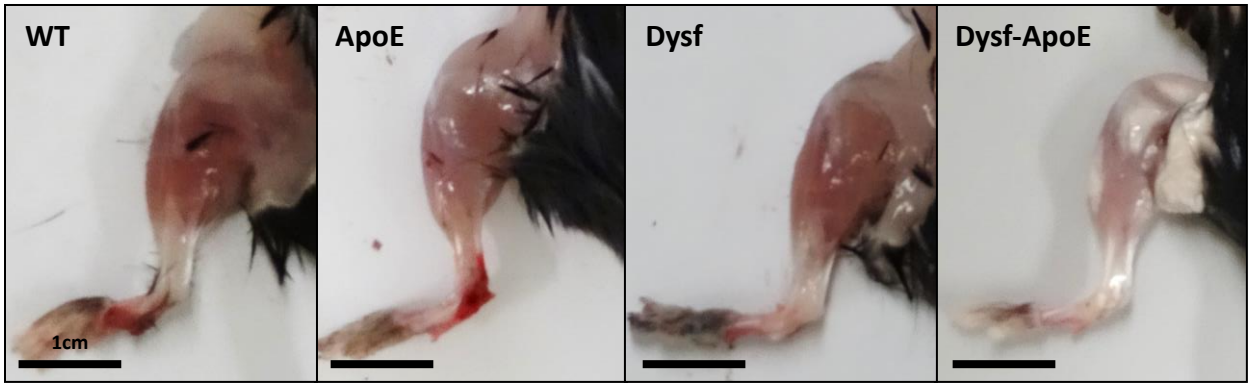

Image 4.1 Representative images of hindlimb at 11 months on HFD. Scale bar=1cm

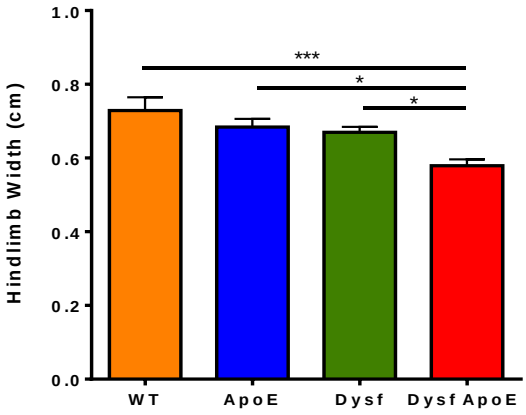

Figure 4.7 Hindlimb size at 11 months on HFD. Hindlimb width measurements in cm. WT (n=10), ApoE (n=13), Dysf (n=20), and Dysf-ApoE (n=9). Mean+SEM, one-way ANOVA. **P<0.01 *P<0.05

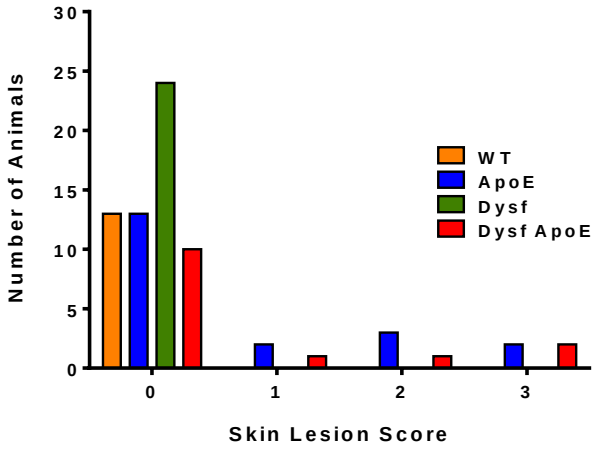

Figure 4.8 Distribution of skin lesion scores at 11 months on HFD. 0 – no skin lesions, 1 – few, mild skin lesions, 2 – severe skin lesions, and 3 – eruptive skin lesions beyond humane endpoint.

4.2.5 Skeletal Muscle Histology

Processing of excised skeletal muscles from all groups revealed severe muscle damage in some Dysf-ApoE DKO muscles, though not all muscles were equally affected. In particular, the quadriceps femoris muscle was found to be severely worsened in DKO mice (Image 4.2). Within quadriceps, total rectus femoris size was reduced to a similar extent in both Dysf-KO and Dysf-ApoE DKO mice at 11 months of age (Figure 4.9A). However, muscle composition was only significantly altered in the Dysf-ApoE DKO group at 7 and 11 months: showing increased fat deposition and reduced percentage of healthy myofibers (Figure 4.9B and 4.9C). In addition, fibrosis was significantly increased in Dysf-ApoE DKO mice compared to all other groups at 7 months but was not significantly different from Dysf-KO mice by 11 months of age (Figure 4.9D). As expected, percentage of centralized nuclei was increased to a similar extent in Dysf-KO and Dysf-ApoE DKO groups at 7 and 11 months of age compared to wild-type and ApoE-KO control groups (Figure 4.10).

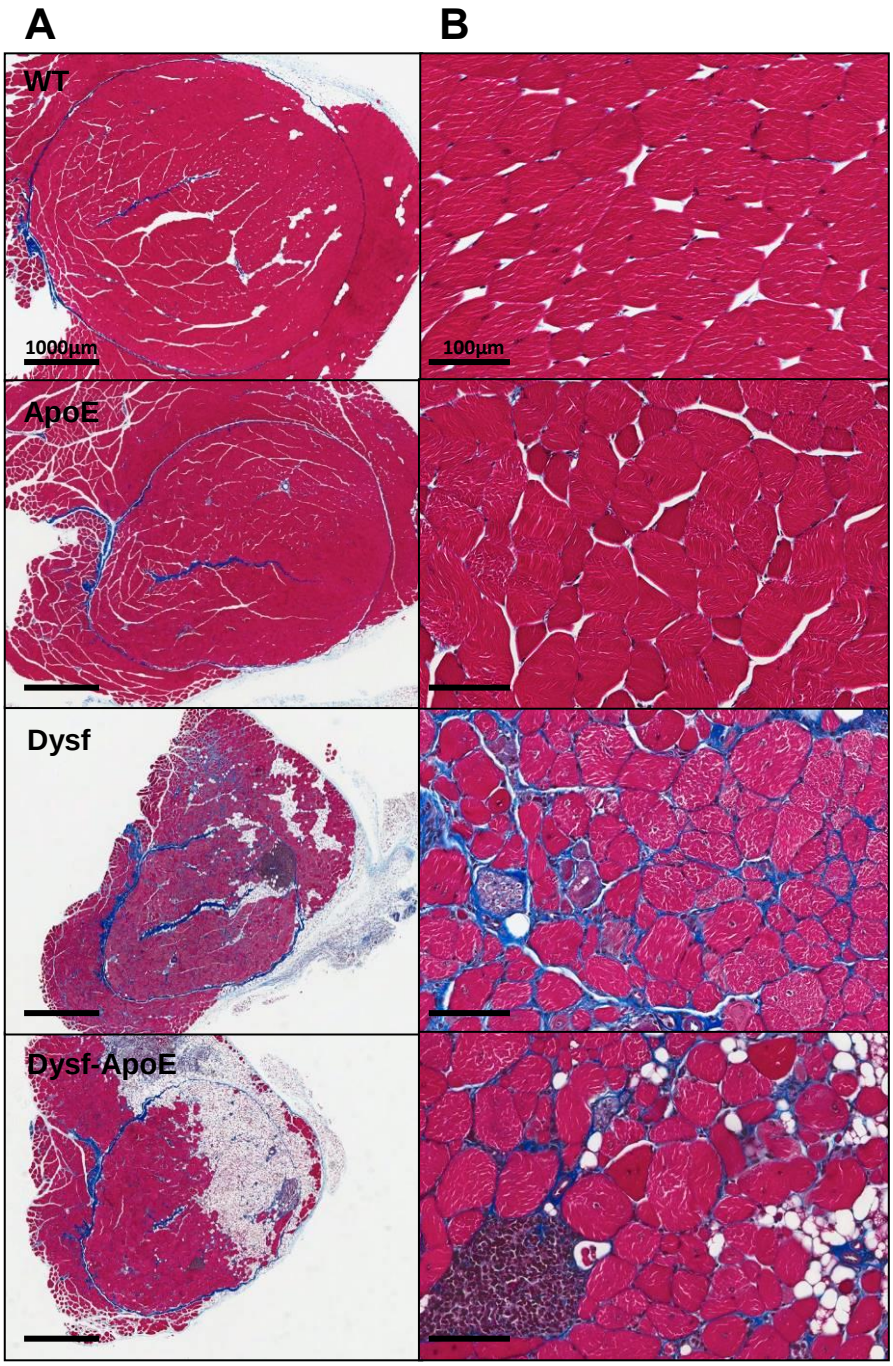

Image 4.2 Representative images of quadriceps femoris at 11 months on HFD. (A) 2x zoom, scale bar=1000µm and (B) 8x zoom, scale bar=100µm of wild-type, ApoE-KO, Dysf-KO and Dysf-ApoE DKO Masson's trichrome stained slides, collagen deposition in blue.

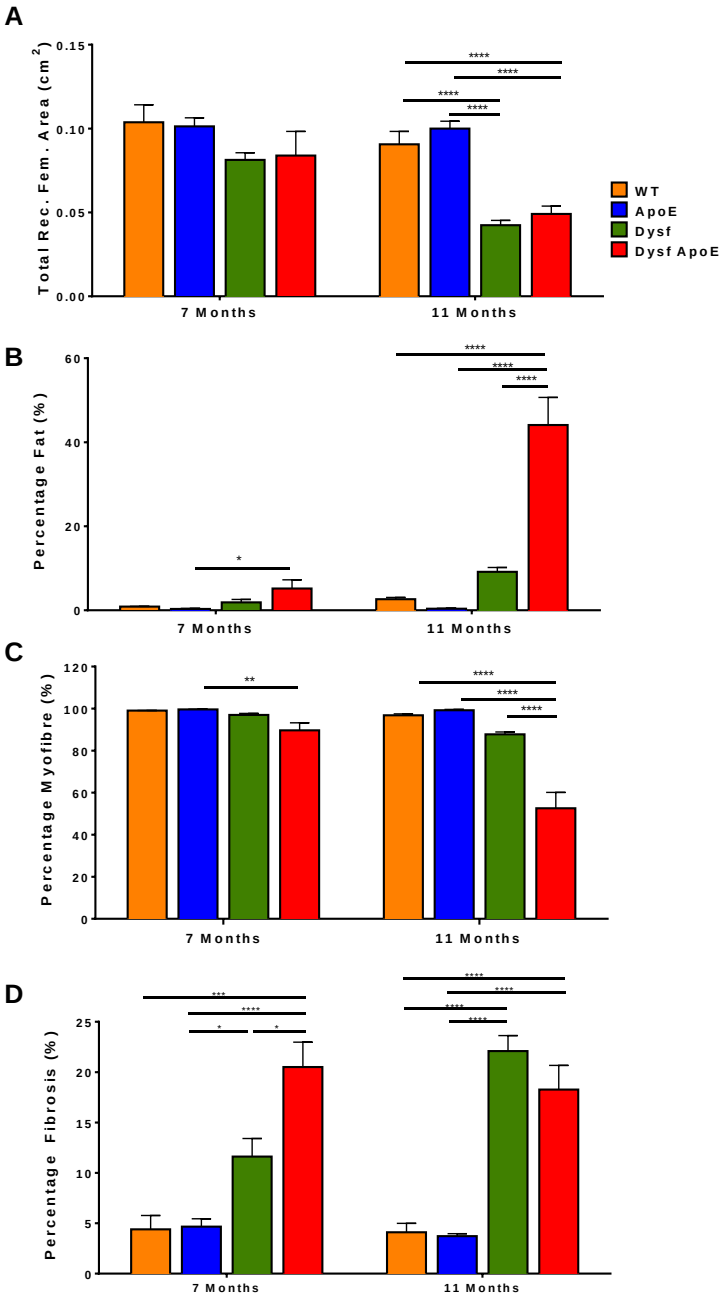

Figure 4.9 Quadriceps femoris muscle size and composition at 7 and 11 months on HFD. (A) Total rectus femoris area in cm^2, percentage of rectus femoris area composed of (B) fat, (C) healthy myofiber, and (D) collagen. WT 7m (n=2), 11m (n=12); ApoE 7m (n=6), 11m (n=12); Dysf 7m

(n=5), 11m (n=18); and Dysf-ApoE 7m (n=3), 11m (n=9). Mean+SEM, two-way ANOVA. *P<0.05 **P<0.01 ***P<0.001 ****P<0.0001

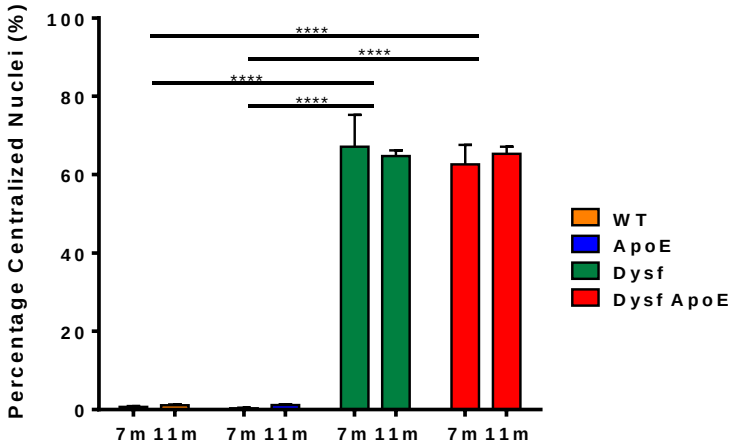

Figure 4.10 Percentage centralized nuclei in quadriceps femoris at 7 and 11 months on HFD. WT 7m (n=2), 11m (n=8); ApoE 7m (n=6), 11m (n=15); Dysf 7m (n=5), 11m (n=20); Dysf-ApoE 7m (n=4), 11m (n=9). Mean+SEM, two-way ANOVA. ****P<0.0001

Similar effects were observed in triceps brachii (Image 4.3) and tibialis anterior muscles (Appendix Image B.1 and Figure B.1); unfortunately, collection of these muscles was only performed for the 11-month old group. In the triceps brachii at 11 months of age on HFD, both Dysf-KO and Dysf-ApoE DKO groups showed reduced total muscle area, while only the Dysf-ApoE DKO group had a significant increase in fat and decrease in healthy myofiber percentage compared to other groups (Figure 4.11). As seen in the quadriceps femoris, percentage fibrosis (Figure 4.11D) and percentage of centralized nuclei (Figure 4.12) in the triceps brachii were significantly increased in Dysf- KO and Dysf-ApoE DKO groups at 11 months compared to the ApoE-KO group, without significant difference between dysferlin-deficient groups. Psoas major

muscles were also collected (Appendix Image B.2); however, due to severe muscle wasting and fat replacement, consistent quantification of fat and damage areas in the muscle was not possible.

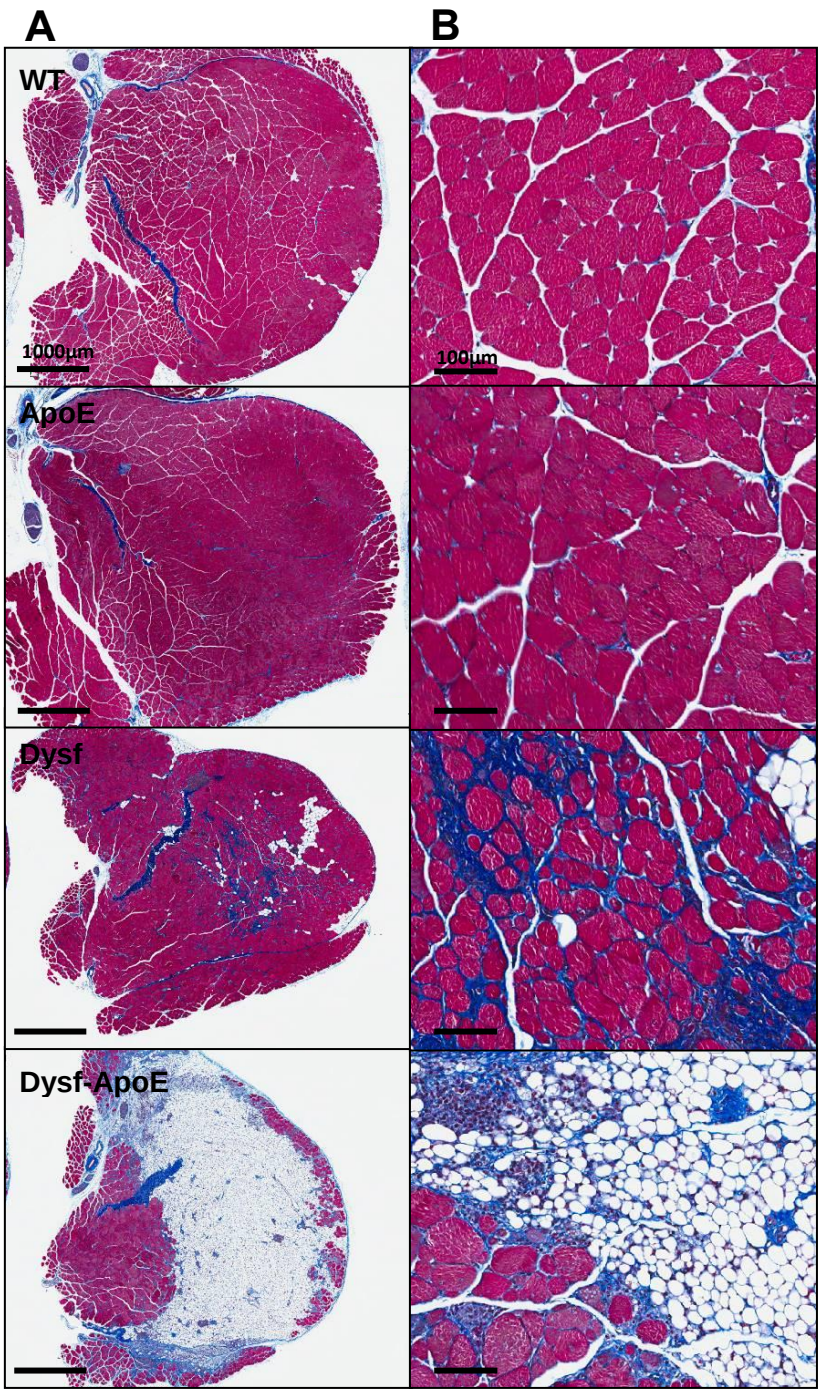

Image 4.3 Representative images of triceps brachii muscle at 11 months on HFD. (A) 2x zoom scale bar=1000µm and (B) 8x zoom scale bar=100µm of wild-type, ApoE-KO, Dysf-KO and Dysf-ApoE DKO Masson's trichrome stained slides, collagen deposition in blue.

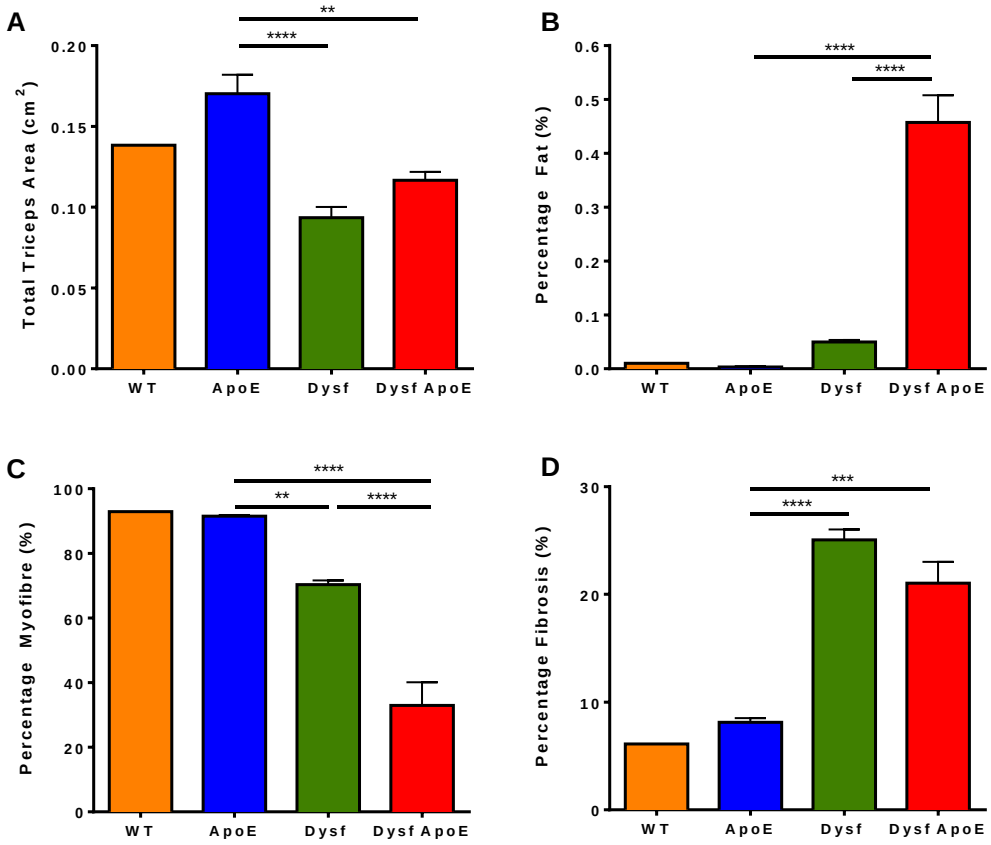

Figure 4.11 Triceps brachii muscle size and composition at 11 months on HFD. (A) Total muscle area, percentage of muscle area composed of (B) fat, (C) healthy myofiber, and (D) collagen. WT (n=1), ApoE (n=3), Dysf (n=8), and Dysf-ApoE (n=5). Mean+SEM, one-way ANOVA, excluding wild-type n=1. **P<0.01 ***P<0.001 ****P<0.0001

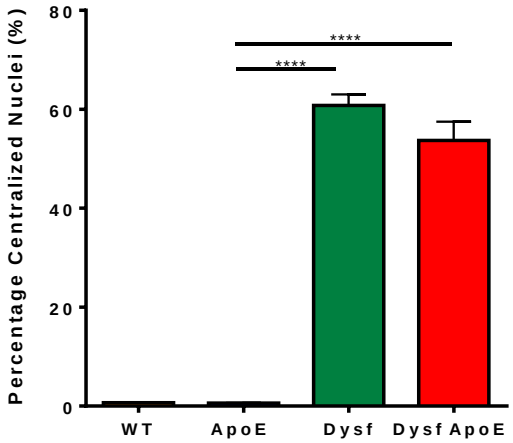

Figure 4.12 Percentage centralized nuclei in triceps brachii at 11 months on HFD. WT (n=1), ApoE (n=3), Dysf (n=8) and Dysf-ApoE (n=5). Mean+SEM, one-way ANOVA excluding WT n=1. ****P<0.0001

Only moderately damaged in comparison to quadriceps femoris and triceps brachii muscles, gastrocnemius also displays changes in size and composition, though only at 11 months of age (Image 4.4). Total gastrocnemius area was similarly reduced in both Dysf-KO and Dysf-ApoE DKO groups while percentage of fat was increased and percentage of healthy myofiber was reduced by 11 months on HFD in the Dysf-ApoE DKO group compared to all other groups (Figure 4.13). Perivascular inflammation was noted in some muscle from both Dysf-KO and Dysf-ApoE DKO mice, including quadriceps femoris and gastrocnemius (Image 4.5) as well as triceps brachii (not shown). In Image 4.5B, vascular leakage of red blood cells into the gastrocnemius muscle tissue can be observed. We also noted sporadic muscle calcification in Dysf-ApoE DKO gastrocnemius muscles at 7 and 11 months of age (Image 4.6).

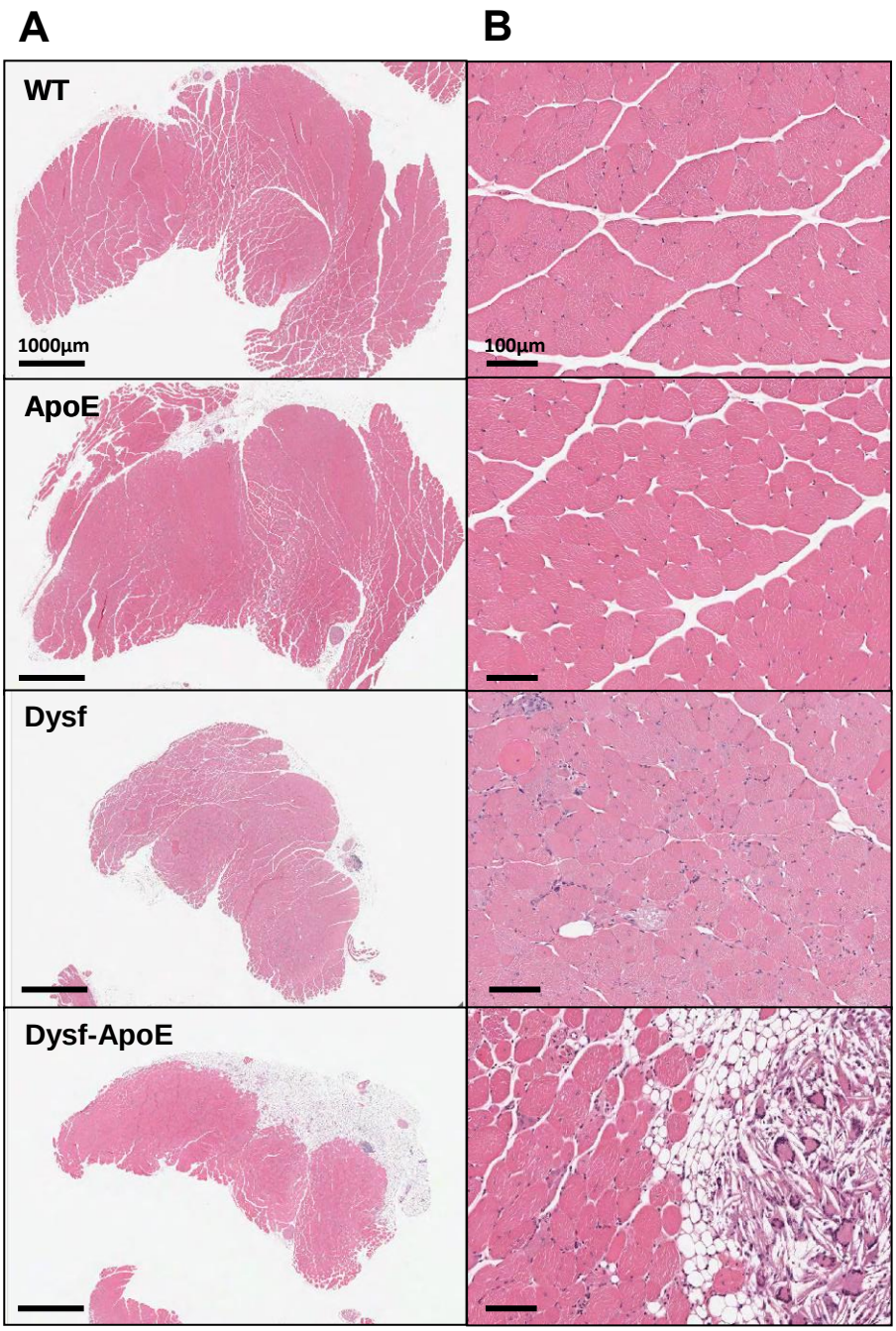

Image 4.4 Representative images of gastrocnemius at 11 months on HFD. (A) 1x zoom, scale bar=1000µm and (B) 8x zoom, scale bar=100µm of wild-type, ApoE-KO, Dysf-KO and Dysf-ApoE DKO H+E stained slides.

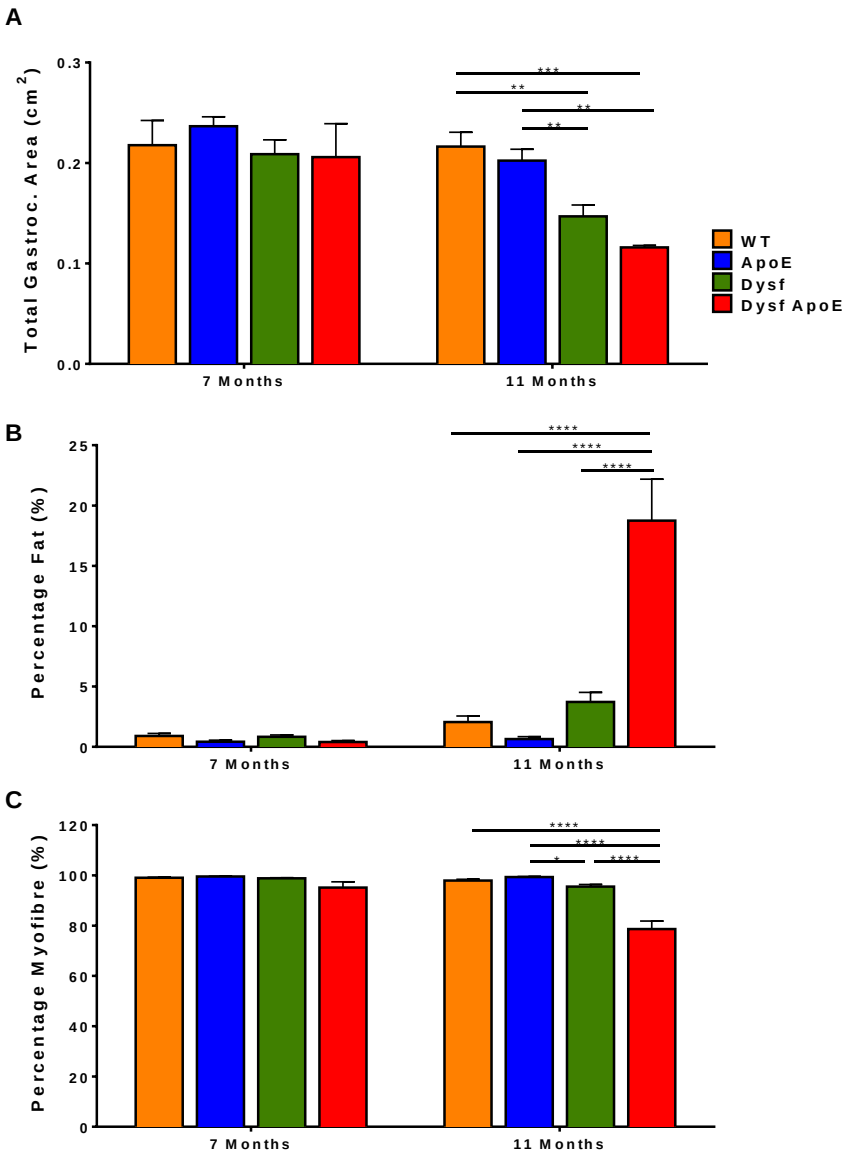

Figure 4.13 Gastrocnemius muscle size and composition at 7 and 11 months on HFD. (A) Total muscle area in cm^2, percentage of muscle area composed of (B) fat and (C) healthy myofiber. WT 7m (n=3), 11m (n=7); ApoE 7m (n=5), 11m (n=10); Dysf 7m (n=4), 11m (n=12); Dysf-ApoE 7m (n=4), 11m (n=4). Mean+SEM, two-way ANOVA. *P<0.05 **P<0.01 ***P<0.001 ****P<0.0001

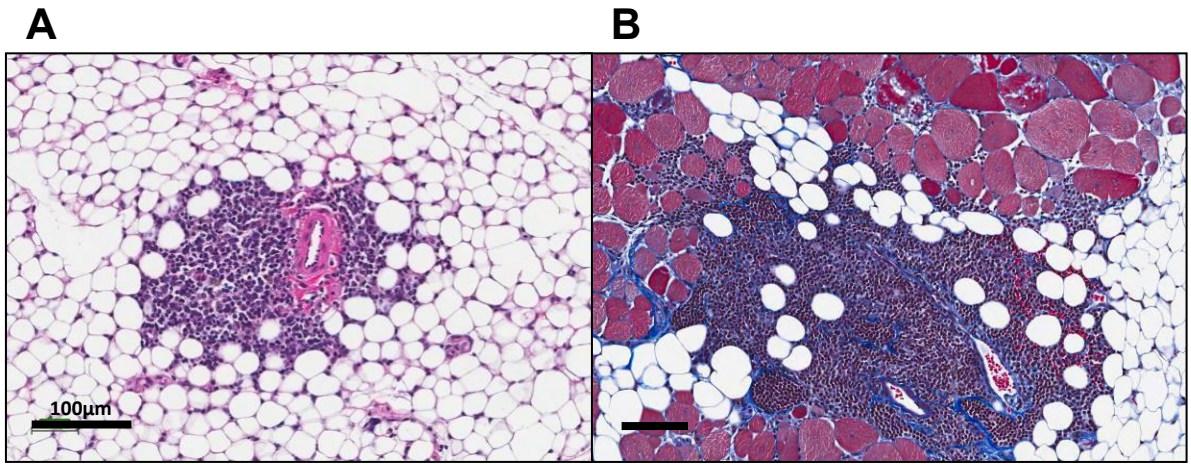

Image 4.5 Examples of vascular leak in Dysf-ApoE DKO mice at 11 months on HFD. (A) 10x zoom of quadriceps femoris stained with H+E and (B) 8x zoom of triceps brachii stained with Masson's trichrome, scale bar=100µm.

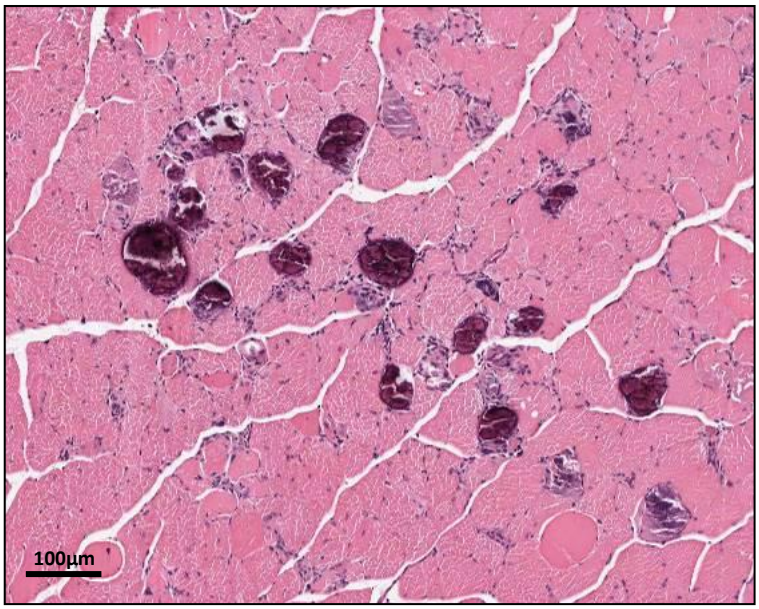

Image 4.6 Example of gastrocnemius calcification in Dysf-ApoE DKO at 7 months on HFD. 4x zoom of H+E stained slide, scale bar=100µm.

Some muscles were not affected by loss of dysferlin, with or without hyperlipidemia. For instance, soleus muscle showed virtually no pathology (Image 4.7). Other than a slight increase in total soleus area in Dysf-KO mice compared to ApoE-KO mice at 11 months of age, there were no other significant differences in muscle size or composition at 7 and 11 months of age on HFD between any groups (Figure 4.14). A similar lack of evident pathology was noted in the diaphragm (Image 4.8).

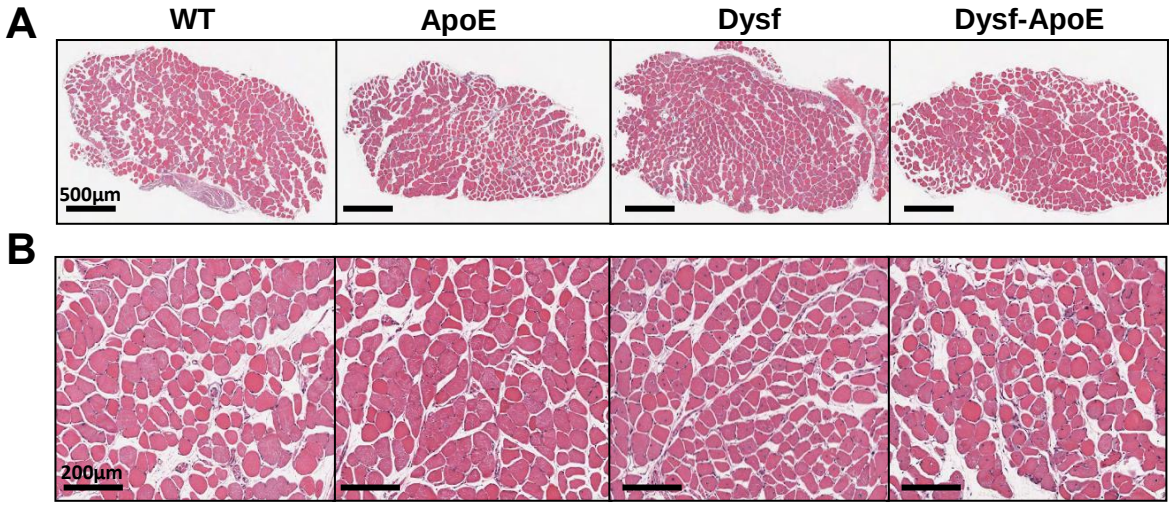

Image 4.7 Representative images of soleus at 11 months on HFD. (A) 2x zoom scale, bar=500µm and (B) 8x zoom, scale bar=200µm of wild-type, ApoE-KO, Dysf-KO and Dysf-ApoE DKO H+E stained slides.

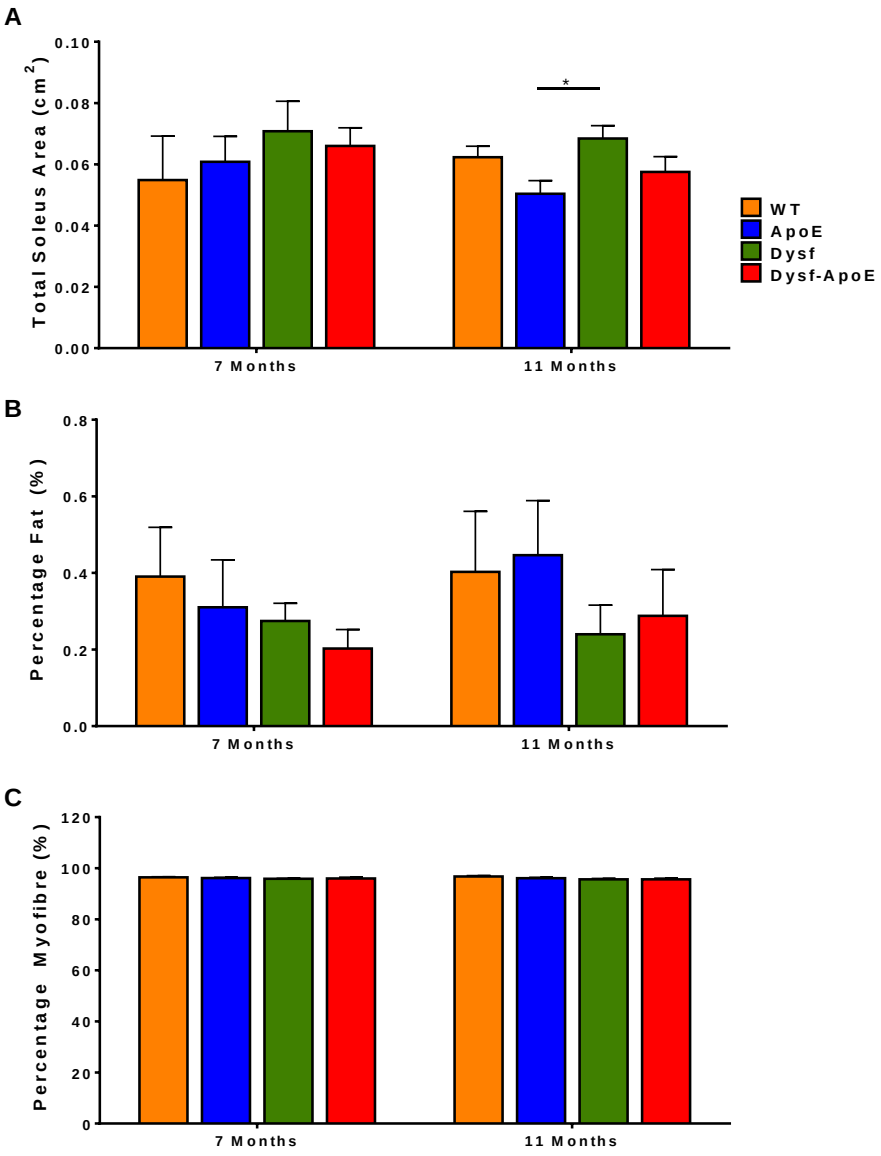

Figure 4.14 Soleus size and composition at 7 and 11 months on HFD. (A) Total soleus area in cm^2, percentage of muscle area composed of (B) fat and (C) healthy myofiber. WT 7m (n=2), 11m (n=8); ApoE 7m (n=6), 11m (n=11); Dysf 7m (n=4), 11m (n=10); and Dysf-ApoE 7m (n=3), 11m (n=4). Mean+SEM, two-way ANOVA. *P<0.05

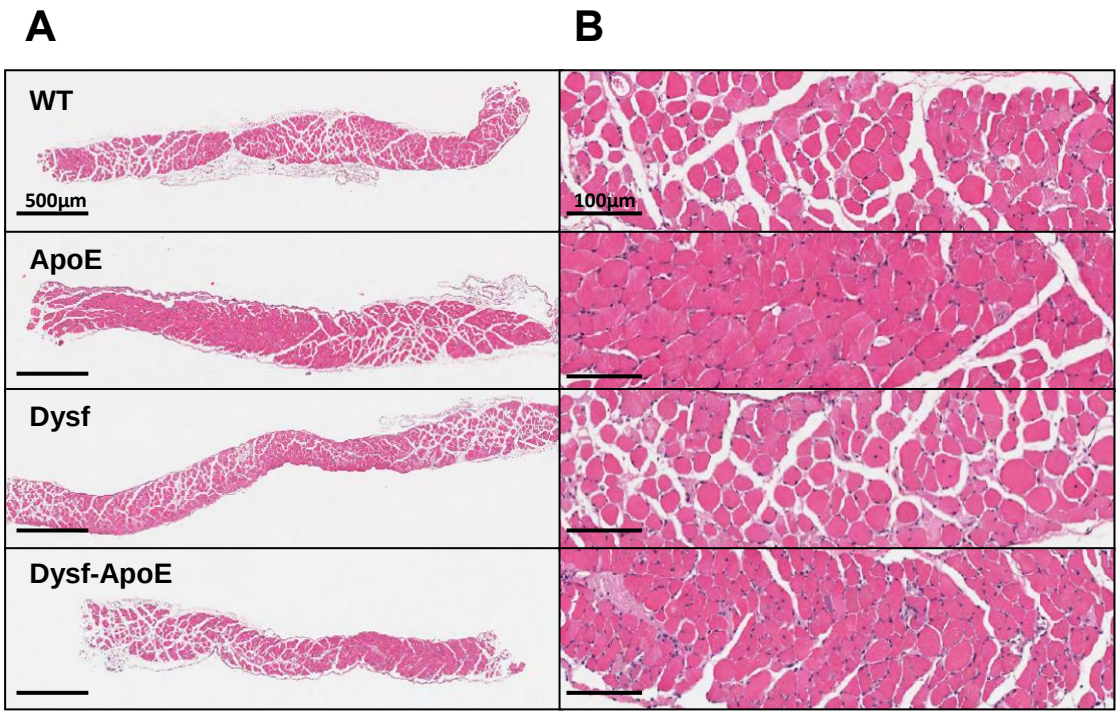

Image 4.8 Representative images of diaphragm at 11 months on HFD. (A) 1.5x zoom, scale bar=500µm and (B) 8x zoom, scale bar=100µm of wild-type, ApoE-KO, Dysf-KO and Dysf-ApoE DKO H+E stained slides.

4.3 Discussion

Dysferlinopathy mouse models have been used to explore the pathogenesis and the therapeutic effects of potential LGMD2B treatments. Unfortunately, currently available models do not fully represent the extent of muscle pathology observed in these patients: animals display very little muscle damage, normal lifespan and mild muscle weakness compared to wild-type mice (Kobayashi, Izawa, Kuwamura, & Yamate, 2012). Our investigation of hyperlipidemia in the context of Dysf-KO mice using double-disease Dysf-ApoE mice has shown that increased

circulating lipid levels worsen dysferlinopathy muscle pathology and can result in complete loss of ambulatory function, which is much more representative of human dysferlinopathy.

The lack of cardiac phenotype in these mice is consistent with dysferlinopathy patients who occasionally develop mild cardiac phenotypes (Nishikawa et al., 2016). Like the majority of LGMD2B patients, animal models of dysferlinopathy do not display significant heart dysfunction, showing normal heart parameters except for a transient, clinically insignificant decrease in ejection fraction observed in A/J mice compared to wild-type at the 10 months timepoint only (Chase, Cox, Burzenski, Foreman, & Shultz, 2009). Therefore, echocardiography of mice at 11 months of age confirmed that neither Dysf-KO nor Dysf-ApoE DKO groups develop any significant heart function pathology.

Few studies have measured gait in Dysf-KO mice and even fewer were able to show any ambulatory impairment (Rayavarapu et al., 2010). Loss of ambulatory function, which has never been observed in Dysf-KO mouse studies, was observed in 40% of Dysf-ApoE DKO animals by 11 months of age on HFD. Furthermore, stride length measurement revealed an impairment of motor function culminating at the 11-month time-point. *Ex vivo* muscle function assessment in soleus and in diaphragm show little change in force, fatigue or recovery, which is consistent with previous dysferlinopathy model studies (Zhao, Xu, Ait-Mou, de Tombe, & Han, 2011) and suggests that remaining muscle function is relatively normal and does not account for loss of ambulatory function observed in Dysf-ApoE DKO mice. Lack of significant effect on *ex vivo* diaphragm and soleus function was rationalized when histological assessment revealed no significant pathology in these muscles, consistent with lack of pathology in the diaphragm and soleus of LGMD2B patients (Mahjneh et al., 2001; Nishikawa et al., 2016).

The dramatic ambulation deficit of Dysf-ApoE DKOs was better explained upon gross and histological examination of the limb muscles. Gross hindlimb measurements revealed significant muscle wasting by 11 months of age. Moreover, histological analysis of quadriceps femoris, triceps brachii and gastrocnemius muscles showed that Dysf-ApoE DKO muscles were severely affected, while only mildly diseased in Dysf-KO mice. The pattern was similar in these affected muscles: 1) equivalent decrease in total muscle size and increase in centralized nuclei for Dysf-KO and Dysf-ApoE DKO groups compared to controls; 2) increase in fat infiltration, necrosis, inflammation, and early fibrosis in Dysf-ApoE DKOs compared to all other groups; and 3) resultant decrease in percentage of viable myofiber area in Dysf-ApoE DKOs. Therefore, hindlimb and forelimb muscle atrophy and loss of viable myofiber area likely account for loss of ambulation and reduced step length in HFD-fed Dysf-ApoE DKO mice by 11 months of age. In addition, signs of muscle damage in Dysf-ApoE DKOs, such as increased fat infiltration and necrosis, could be observed in affected muscles as early as 7 months of age. Other important histological features were observed, such as vascular leak and muscle calcification. Perivascular inflammation and vascular leak were observed only in Dysf-KO and Dysf-ApoE DKO muscle, suggesting that loss of dysferlin may be affecting vascular integrity and permeability. Muscle calcification was observed sporadically in Dysf-ApoE DKO gastrocnemius muscle and is likely induced by muscle injury, which has been observed in other settings of induced or congenital muscle damage (Bonucci & Sadun, 1972; Coulton, Morgan, Partridge, & Sloper, 1988; Selle & Urist, 1961).

Chapter 5: Dysferlin-LDLR Double-Knockout Model

5.1 Introduction

To confirm and further investigate the aggravating effect of hyperlipidemia on dysferlinopathy pathology, we sought to investigate loss of LDLR expression in the context of Dysf-KO mice since ApoE has additional anti-inflammatory and antioxidant functions (Ali, Middleton, Pure, & Rader, 2005; Baitsch et al., 2011; Raffai, Loeb, & Weisgraber, 2005). In fact, studies that rescue of macrophage-specific ApoE expression in ApoE-null mice led to atherosclerosis regression (Tenger & Zhou, 2003). Therefore, we wanted to confirm that the effect observed in the Dysf-ApoE DKO model was due to elevated plasma lipids and impaired vascular function, not specifically due to the loss of ApoE. Compared to ApoE-KO, LDLR-deficient mice display mild hyperlipidemia, rich in LDL, and develop atherosclerotic lesion only when on HFD (Ishibashi et al., 1993), which is much more representative of human hyperlipidemia. Since loss of LDLR function is a common cause of FH (Soutar & Naoumova, 2007) and LDLR-KO mice exhibit a more humanized lipid profile, it was proposed as a more suitable and human-relevant model of hyperlipidemia for our study.

The generation of Dysf-LDLR DKO mice was devised to answer some important questions raised from our previous model: 1) Does all hyperlipidemia worsen muscle pathology in dysferlinopathy, or was the effect seen in Dysf-ApoE DKO due specifically to the loss of ApoE expression? 2) Will the mildness of the LDLR-KO model, as compared to the ApoE-KO model, affect the rate of progression and severity of MD pathology exacerbation? 3) Will a lipid profile which more closely resembles human hyperlipidemia better mimic human LGMD2B and be more useful in therapeutic trials? Although we sought new insights and confirmation of our double

disease effect, our results show that there is a much more complex relationship between hyperlipidemia and dysferlinopathy than previously expected.

5.2 Results

5.2.1 Genotyping and Breeding

Genotyping of Dysf-LDLR mice proved to be a challenge since both Dysf-KO and LDLR-KO insertions included a neomycin cassette and the PCR procedure developed for LDLR-KO mice, recommended from Jackson Laboratory, targeted the identification of the neomycin cassette for genotyping. Therefore, dysferlin insertions led to false positives in the LDLR-KO PCR. A new LDLR-KO protocol was devised (Figure 5.1A) which divided the process into two parts: 1) identify the presence of wild-type LDLR using one primer targeted within the wild-type LDLR gene and the other outside in the non-coding region and 2) identify the presence of a LDLR-mutant insertion using one primer within the neomycin cassette and the other in the non-coding region. This method enabled successful differentiation between wild-type, LDLR heterozygote and LDLR-KO in the presence of Dysf-KO insertions, as seen in Figure 5.1B.

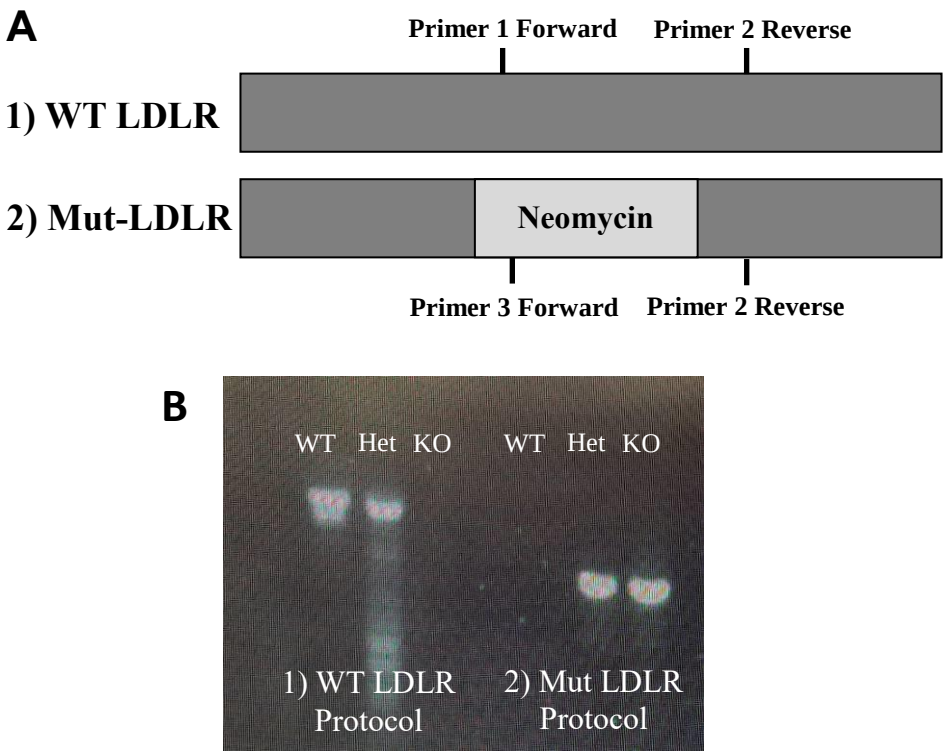

Figure 5.1 Low-density-lipoprotein receptor genotyping strategy and results. (A) Schematic of LDLR double PCR strategy: 1) primers for wild-type allele and 2) primers for mutant insertion. (B) Image of LDLR PCR gel showing wild-type, heterozygote and KO bands using 1) wild-type protocol and 2) mutant insertion protocol.

The original breeding set up of Dysf +/- LDLR +/- littermate crosses produced only two Dysf-LDLR DKO mice that survived to 4 weeks of age after 146 total offspring. Although a Chi squared test did not find a significant difference between observed and predicted animal numbers (1/16 for each experimental group), the rate of Dysf-LDLR DKO generation using this breeding scheme was low and produced no viable offspring (Figure 5.2). One DKO mouse was culled at weaning due to malocclusion and was only identified as a Dysf-LDLR DKO after genotyping was performed. The second DKO was found to be a maloccluded runt before weaning but was kept

until genotyping was completed. When its genotype was discovered, the mouse was immediately sacrificed and tissues were harvested at 5 weeks of age. Photographs (Image 5.1), as well as a video (not shown), were shown to UBC veterinarian Dr. Ian Welch, who described the animal's behaviour as follows:

> The mouse is more "cow hocked" (stifle is abducted) then most mice are. While the mouse demonstrates the ability to extend its hips and stifle at the edge of the cage it does not fully extend its legs during normal gait. It is a little hard to see from the video but it looks like the mouse has a bilateral symmetrical "hip hike". This is similar to what you see dog with advanced hip disease because instead of fully extending the leg the animal swings the leg out to the side. This mouse does not demonstrate evidence of pain and the gait abnormality is not due to an inflammatory disease but rather a degenerative skeletal mouse disease as would be expected.

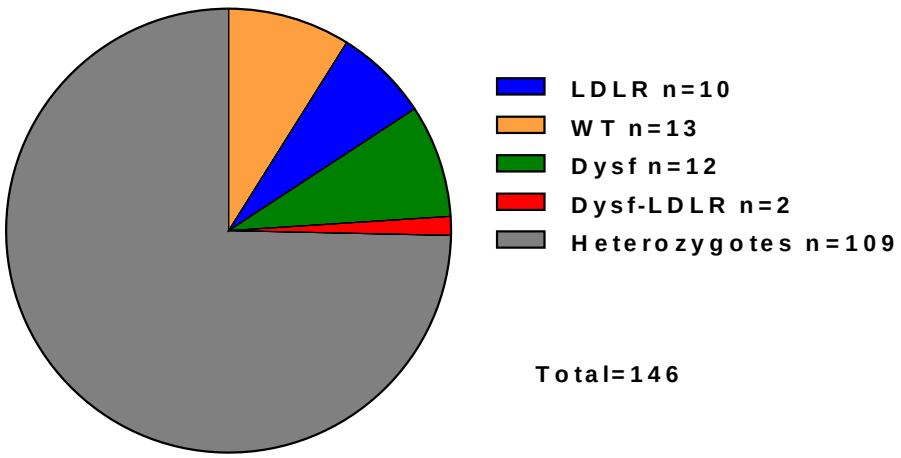

Figure 5.2 Pie chart of animal numbers by genotype in Dysf-LDLR project. Chi squared test based on 1/16th Mendelian expected distribution in experimental groups.

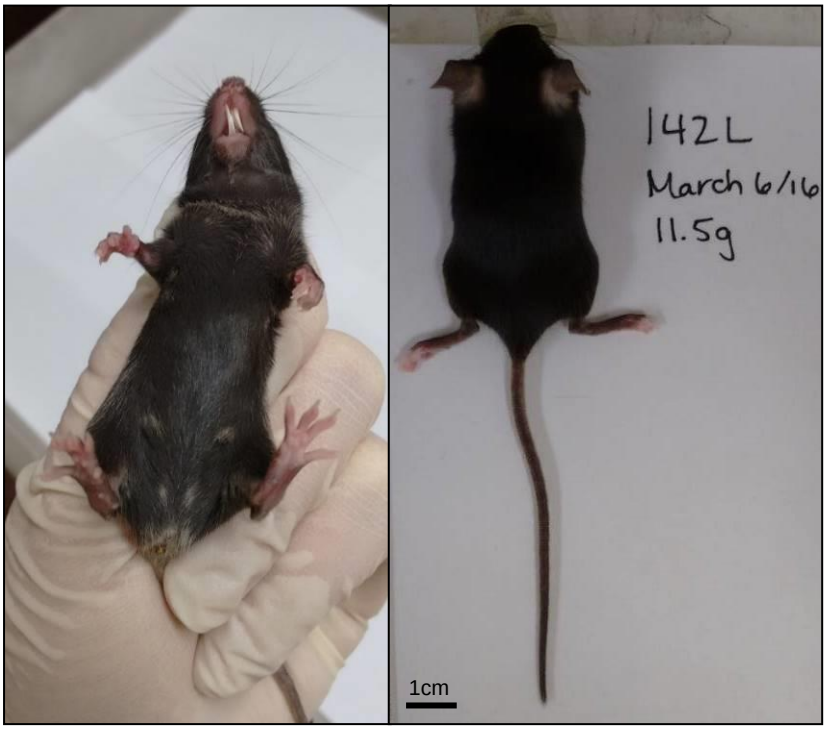

Image 5.1 Photographs of Dysf-LDLR DKO. Taken when discovered at 3 week of age (left) and immediately before sacrifice with animal number, date of sacrifice and animal weight (right), scale bar=1cm.

Since this breeding scheme resulted in such low DKO output, we switched to a "forced" breeding protocol by crossing Dysf -/- LDLR +/- littermates, which should have led to a 1/4 DKO rate, per Mendelian inheritance. However, after 27 offspring from this cross, no Dysf-LDLR DKOs were produced. Therefore, whether due to embryonic lethality or early pup mortality, there seems to be a low production of Dysf-LDLR DKOs and when discovered, they suffer from severe malocclusion and failure to thrive.

5.2.2 Skeletal Muscle Histology

Although we do not have 5-week-old controls with which to compare the skeletal muscle size and composition, there is no evidence of muscle damage, centralized nuclei, fat infiltration, inflammation or collagen deposition in the Dysf-LDLR DKO mouse, as seen in Image 5.2 of quadriceps femoris and triceps brachii. Similar muscle integrity was found in all muscles collected: TA, EDL, soleus, gastrocnemius, biceps brachii and diaphragm (Appendix Image C.1).

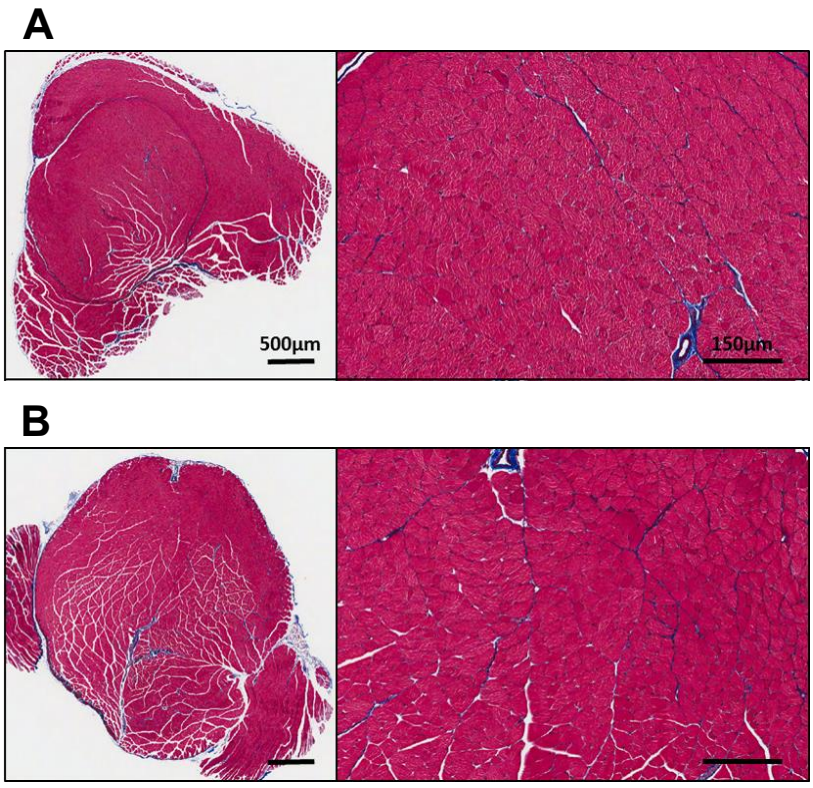

Image 5.2 Representative images of quadriceps femoris and triceps brachii of Dysf-LDLR DKO at 5 weeks of age. (A) Quadriceps femoris and (B) triceps brachii at 2x zoom (left, scale bar=500µm) and 8x zoom (right, scale bar=150µm) of Masson's trichrome stained slides, collagen deposition in blue.

5.3 Discussion

The effect of the loss of LDLR expression in dysferlin-deficient mice that we observed was not anticipated and cannot be adequately explained. Breeding of Dysf-LDLR DKO led to very few DKOs who survived to weaning, all of which displayed severe malocclusion and failure to thrive. Even the implementation of a higher output breeding scheme did not increase DKO numbers. One DKO was characterized before being sacrificed at 5 weeks of age and was found to have abnormal gait properties. However, analysis of its muscle tissue revealed no observable pathology. Whether the low Dysf-LDLR DKO animal numbers are due to embryonic lethality, infanticide or decreased pup viability is not clear. Further analysis of the harvested 5-week-old Dysf-LDLR DKO mouse may some reveal developmental abnormalities. In addition, characterization of Dysf-/-LDLR+/- mice may display an intermediate phenotype, since LDLR heterozygotes have moderately increased plasma cholesterol (I. J. Goldberg et al., 2008), while avoiding viability issues.

Although no effect on muscle histology could be seen, low DKO numbers and animal abnormalities indicate some unknown interaction between dysferlin and LDLR. A potential mechanism for such low yield and reduced viability of Dysf-LDLR DKO is LDLR's role in osteogenesis. Studies have shown that LDLR-deficiency is associated with impaired osteoclast differentiation and function leading to increased bone mass (Okayasu et al., 2012). The disruption of normal bone recycling may be affecting embryonic development or pup viability and may explain the gait abnormalities observed in the viable DKO, while leaving the muscle unaffected. Investigation of Dysf-LDLR DKO development *in utero* and analysis of bone properties in the 5-week old DKO skeleton can be done to assess presence and development of skeletal abnormalities.

Alternatively, lack of LDLR may be affecting the formation of neuromuscular junctions and impairing distal limb development in the context of dysferlin-deficiency. Several studies have shown that a LDLR-related protein, *Lrp4*, is crucial to for neuromuscular junction assembly and *Lrp4* mutant mice do not survive after birth due to severe pre- and post-synaptic abnormalities (Weatherbee, Anderson, & Niswander, 2006; Yumoto, Kim, & Burden, 2012). Perhaps dysferlin-deficient mice are more susceptible to neuromuscular synapse disruption; however, loss of neuromuscular junction activity and subsequent muscle denervation would have led to dramatic limb and muscle defects, as seen in *Lrp4*-mutant mice (Weatherbee, Anderson, & Niswander, 2006), which were not observed in our model. Thus, the mechanism behind the Dysf-LDLR DKO phenotype and lethality we observed is not yet known.

Chapter 6: Mdx-ApoE Double-Knockout Model

6.1 Introduction

In this final project, we aim to assess the effect of hyperlipidemia in DMD using the *mdx* mouse model. The most common hereditary disease affecting children, DMD is memorable not only for its prevalence but also for its severity, leading to loss of walking ability in the majority of boys by 12 years of age (Emery, Muntoni, & Quinlivan, 2015). The huge disparity between the severe muscle pathology seen in DMD patients and the mild damage observed in mouse models makes evaluation of treatment efficacy in preclinical trials extremely challenging. In addition, the *mdx* model cannot be used to investigate prolongation of walking or disease progression in long-term studies since, after the robust muscle regeneration at 8 weeks of age, little muscle damage can be observed (Coulton, Morgan, Partridge, & Sloper, 1988), animals retain their muscle strength and motor function (Coulton, Curtin, Morgan, & Partridge, 1988) and lifespan is only mildly reduced (Chamberlain, Metzger, Reyes, Townsend, & Faulkner, 2007). Development of an aggravated *mdx* model has been explored in the *mdx-utrn* mouse which has simultaneous loss of dystrophin and utrophin expression, resulting in significantly reduced lifespan (approximately 3 months), development of breathing difficulties and mobility impairment (A. Deconinck et al., 1997; Grady et al., 1997). However, the *mdx-utrn* model shows similar histological muscle pathology to the *mdx* mouse and is accompanied by a slew of other systemic and neuromuscular deficits such as impaired bone healing, articular cartilage degeneration and intervertebral disc damage, not typically observed in DMD (Isaac et al., 2013). The lack of muscle histopathology and dramatically shortened lifespan make *mdx-utrn* mouse colonies difficult to maintain and unsuitable for long-term disease progression and therapeutic trial studies (McDonald, Hebert,

Kunz, Ralles, & McLoon, 2015). Therefore, investigation of hyperlipidemic effects on *mdx* pathology was undertaken to explore whether impaired vascular function would have similar effects in dystrophin-deficient MD, as was observed in the dysferlinopathy model, and whether this model can more closely represent the DMD phenotype.

6.2 Results

6.2.1 Ambulatory Function

Although earlier sacrifice time-points were chosen for this project, by 7 months of age we did not observe complete loss of ambulatory function in any animal from any group. At 3 and 6 months of age, stride lengths of all chow- and HFD-fed groups were measured and exercise intolerance and difficulty breathing were observed in Mdx and Mdx-ApoE DKO groups. At 3 months of age on HFD, there was a significant reduction in step length for Mdx and Mdx-ApoE DKO mice compared to controls, with no significant difference between dystrophin-deficient groups (Figure 6.1A). By 6 months of age on HFD, only the Mdx-ApoE DKO group showed a significant decrease in stride length compared to wild-type and ApoE-KO groups (Figure 6.1A). Similar 3- and 6- month results were found in chow-fed groups (Figure 6.1B).

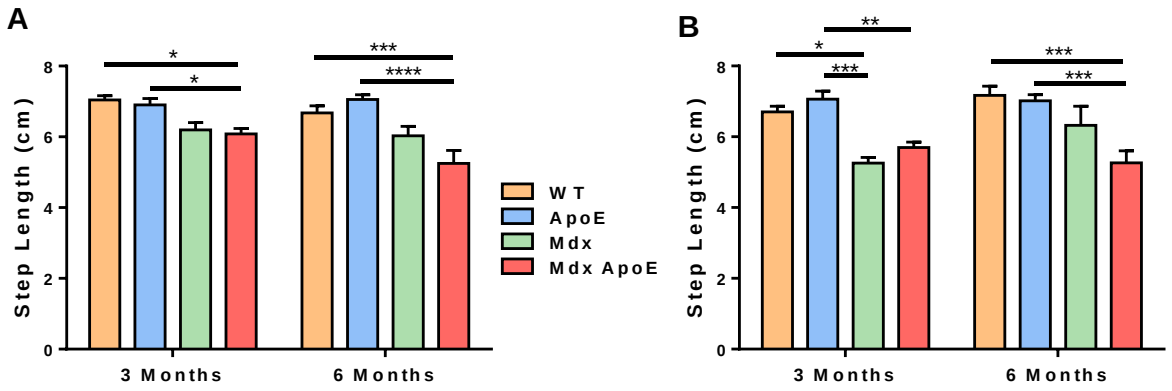

Figure 6.1 Step length at 3 and 6 months on HFD and on chow. (A) HFD- and (B) chow-fed average step lengths in cm. HFD: WT 3m (n=6), 6m (n=6); ApoE 3m (n=9), 6m (n=7); Mdx 3m (n=10), 6m (n=5); and Mdx-ApoE 3m (n=13), 6m (n=10). Chow: WT 3m (n=3), 6m (n=3); ApoE 3m (n=5), 6m (n=4); Mdx 3m (n=6), 6m (n=3); and Mdx-ApoE 3m (n=10), 6m (n=9). Mean+SEM, two-way ANOVA. *P<0.05 **P<0.01 ***P<0.001 ****P<0.0001

6.2.2 *In Vivo* Heart Function

Using echocardiogram, parameters of heart function such as cardiac output, fractional shortening, ejection fraction, stroke volume, left ventricular diameter and volume in diastole and systole were measured. At 3 and 6 months of age, there was no significant change in heart function parameters between HFD-fed groups, except for left ventricular systolic volume between Mdx and Mdx-ApoE DKO groups at 6 months on HFD (Figure 6.2) and no change was found in any heart parameters at 3 and 6 months of age in chow fed groups (Figure 6.3).

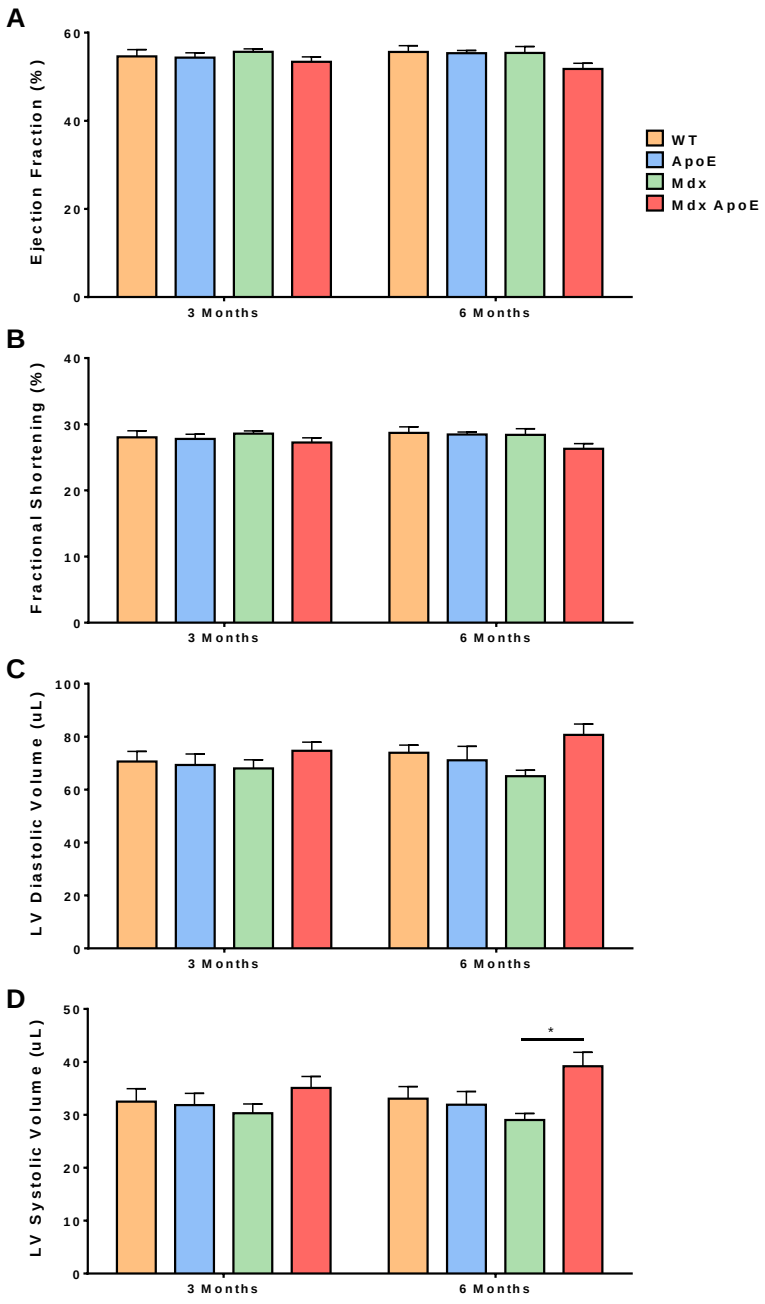

Figure 6.2 *In vivo* heart function parameters at 3 and 6 months on HFD. (A) Percent ejection fraction, (B) percent fractional shortening, (C) left ventricular diastolic volume in μL, and (D) left ventricular systolic volume in μL. WT 3m (n=10), 6m (n=6); ApoE 3m (n=10), 6m (n=7); Mdx

3m (n=12), 6m (n=6); and Mdx-ApoE 3m (n=15), 6m (n=11). Mean+SEM, two-way ANOVA. *P<0.05

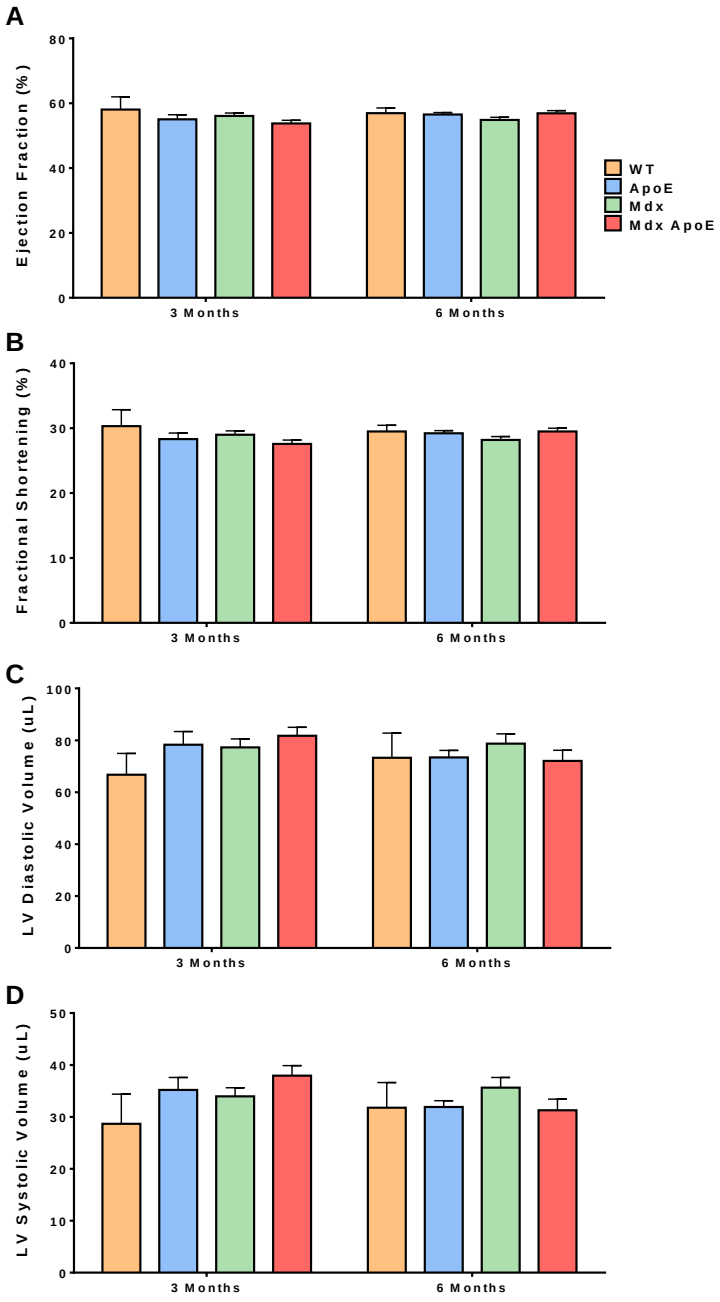

Figure 6.3 *In vivo* heart function parameters at 3 and 6 months on chow. (A) Percent ejection fraction, (B) percent fractional shortening, (C) left ventricular diastolic volume in µL, and (D) left

ventricular systolic volume in µL. WT 3m (n=3), 6m (n=3); ApoE 3m (n=4), 6m (n=4); Mdx 3m (n=6), 6m (n=6); and Mdx-ApoE 3m (n=9), 6m (n=11), 6m (n=11). Mean+SEM, two-way ANOVA.

6.2.3 *Ex Vivo* Skeletal Muscle Function

Function of skeletal muscle as assessed by myography was performed on a single mouse per genotype at 4 months of age on HFD as a pilot study of Mdx-ApoE soleus and diaphragm function *ex vivo*. In the diaphragm, there was little difference in force-velocity curves or force recovery between groups (Figure 6.4A and 6.4C). During repeat stimulation, the Mdx-ApoE DKO diaphragm seems to fatigue less than Mdx and ApoE-KO groups, with wild-type showing the most severe loss of relative force after 35 stimulations (Figure 6.4B). Soleus in ApoE-KO and Mdx-ApoE DKO mice showed lower velocity at a given load compared to wild-type and Mdx muscles (Figure 6.5A); however, fatigue and recovery curves were not strikingly different between groups (Figure 6.5B and 6.5C).

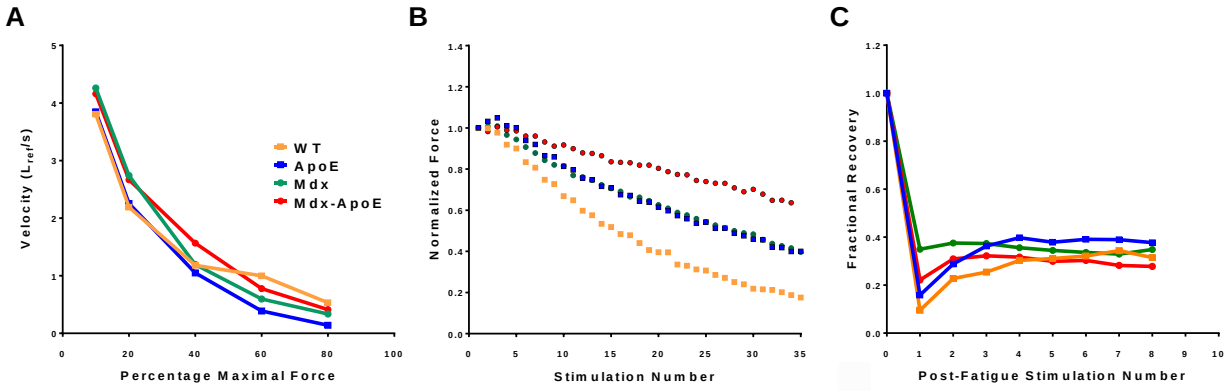

Figure 6.4 Pilot study of diaphragm *ex vivo* muscle function at 5 months on HFD. (A) Force-velocity curve normalized to muscle length in reference length per second, (B) muscle force fatigue over 35 stimulations expressed as fraction of pre-fatigue muscle force, and (C) fractional force

recovery over 8 stimulations post-fatigue expressed as fraction of pre-fatigue muscle force, n=1 for each group.

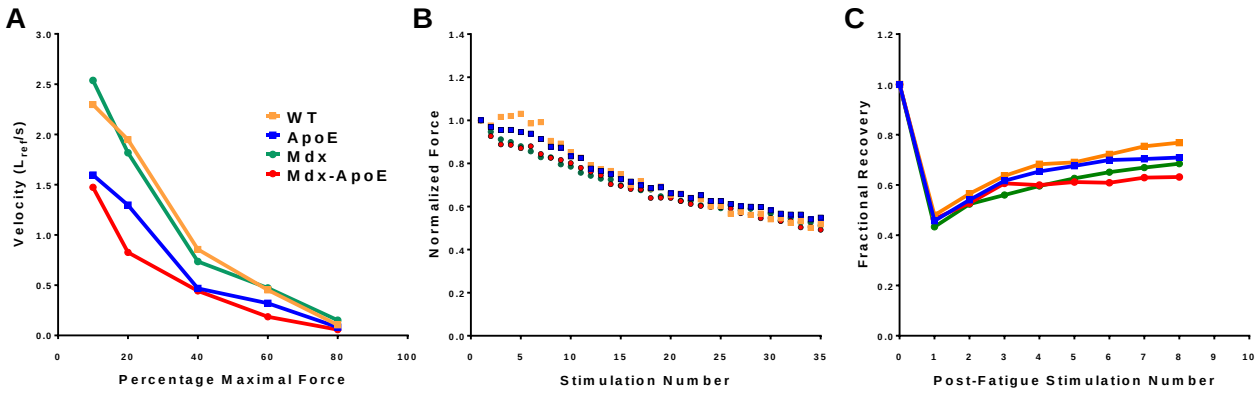

Figure 6.5 Pilot study of soleus *ex vivo* muscle function at 5 months on HFD. (A) Force-velocity curve normalized to muscle length in reference length per second, (B) muscle force fatigue over 35 stimulations expressed as fraction of pre-fatigue muscle force, and (C) fractional force recovery over 8 stimulations post-fatigue expressed as fraction of pre-fatigue muscle force, n=1 for each group.

6.2.4 Gross Hindlimb Size and Skin Lesion Scores

Gross skeletal muscle size was found to be increased in dystrophin-deficient mice (Image 6.1). There was a significant increase in hindlimb size in Mdx and Mdx-ApoE DKO groups compared to wild-type and ApoE-KO controls at 4 months of age on HFD and similar results were seen at 7 months on chow (Figure 6.6A and 6.6B). However, by 7 months of age on HFD, only Mdx-ApoE DKO mice had significantly increased hindlimb size compared to wild-type (Figure

6.6A). Skin lesions were not observed in any group, likely due to the 4- and 7-month time-points on HFD being too early to develop significant skin lesions or xanthomas.

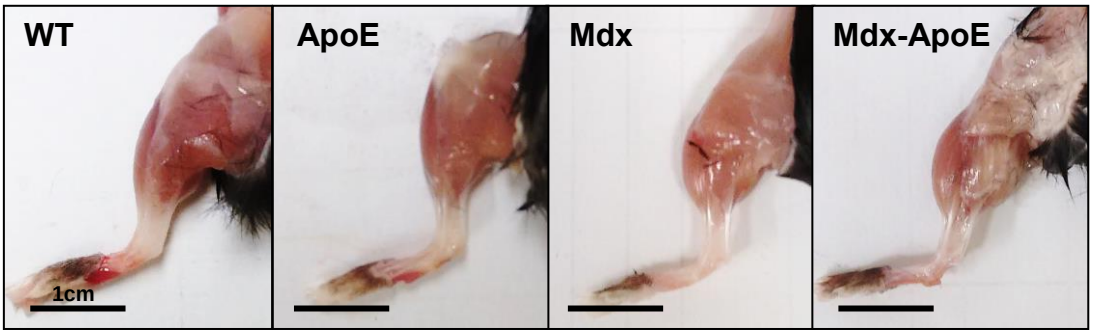

Image 6.1 Representative images of hindlimb at 7 months on HFD. Scale bar=1cm.

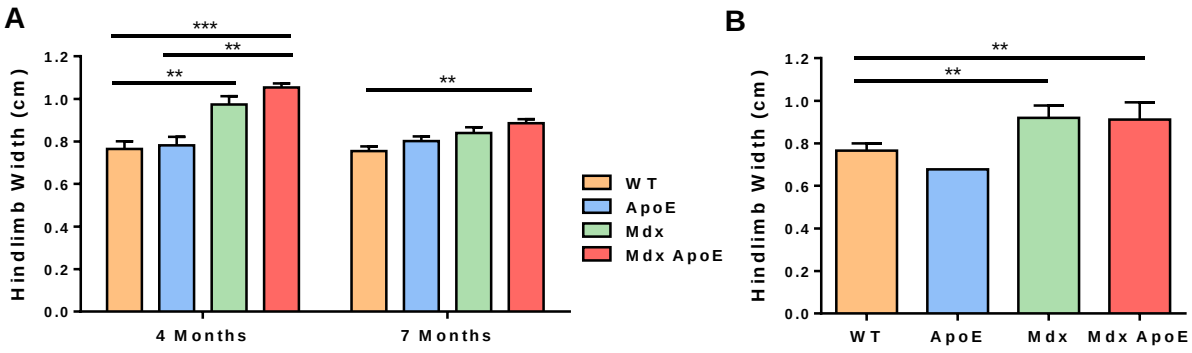

Figure 6.6 Hindlimb size at 4 and 7 months on HFD and at 7 months on chow. Hindlimb width in cm (A) on HFD at 4 and 7 months and (B) on chow at 7 months. HFD: WT 4m (n=4), 7m (n=6); ApoE 4m (n=2), 7m (n=8); Mdx 4m (n=7), 7m (n=7); and Mdx-ApoE 4m (n=5), 7m (n=10). Chow: WT (n=3), ApoE (n=1), Mdx (n=10), and Mdx-ApoE (n=11). Mean+SEM, (A) two-way ANOVA and (B) one-way ANOVA, excluding ApoE n=1 on chow. **P<0.01 ***P<0.001

6.2.5 Skeletal Muscle Histology

Histological analysis of skeletal muscle revealed exacerbation of muscle damage in Mdx-ApoE DKO mice compared to Mdx and controls in some, but not all, skeletal muscles: i.e. triceps brachii, gastrocnemius, and quadriceps femoris. The triceps brachii was severely affected in the Mdx-ApoE DKO mice as seen in Image 6.2. Triceps brachii muscle of Mdx-ApoE DKO mice showed an initial increase in total area at 4 months on HFD, which was not present by 7 months of age (Figure 6.7A). Increased collagen was observed in both dystrophin-deficient groups as early as 4 months of age (Figure 6.7D). However, by 7 months of age there was increased fibrofatty infiltration, inflammation and necrosis in Mdx-ApoE DKO muscle led to significant alteration in muscle composition compared to all other groups: increased fat, increased collagen and decreased viable muscle area (Figure 6.7).

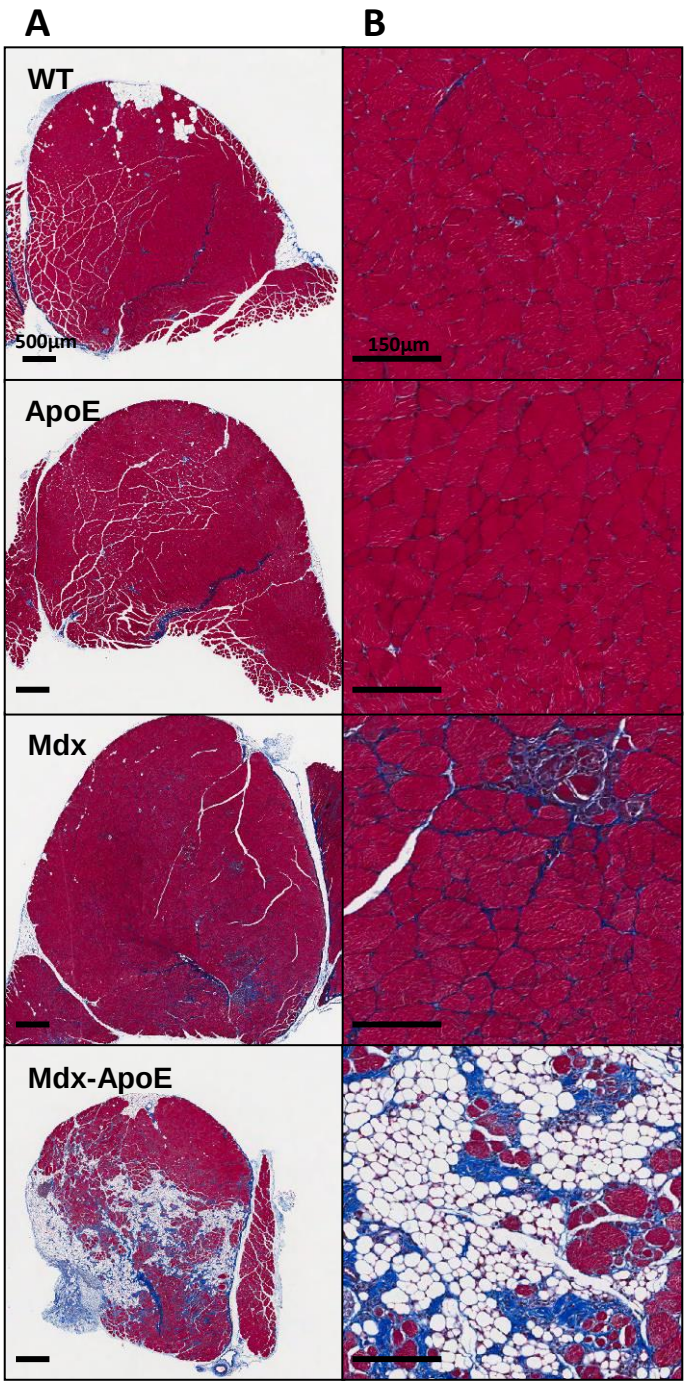

Image 6.3 Representative images of triceps brachii at 7 months on HFD. (A) 2x zoom scale, bar=500µm and (B) 8x zoom, scale bar=150µm of wild-type, ApoE-KO, Mdx and Mdx-ApoE DKO Masson's trichrome stained slides, collagen deposition in blue.

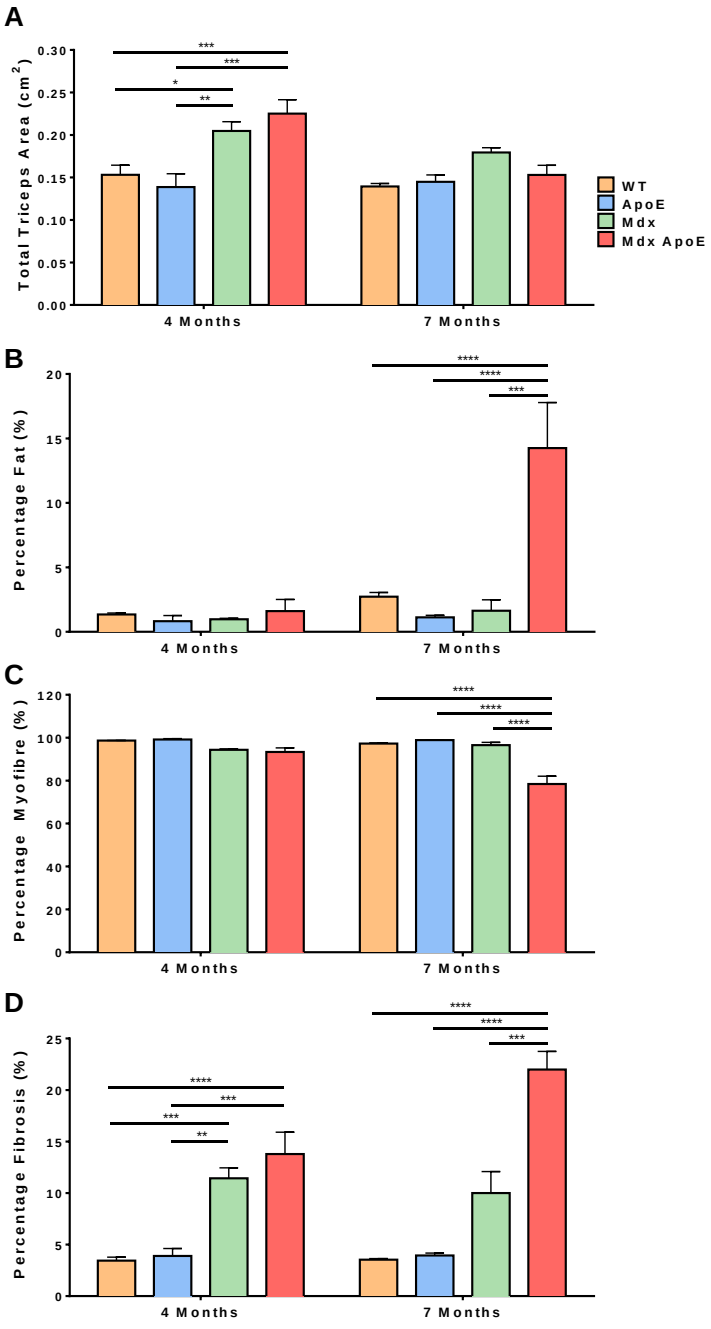

Figure 6.7 Triceps brachii muscle size and composition at 4 and 7 months on HFD. (A) Total muscle area in cm^2, percentage of muscle area composed of (B) fat, (C) healthy myofiber, and (D) collagen. WT 4m (n=4), 7m (n=6); ApoE 4m (n=3), 7m (n=7); Mdx 4m (n=7), 7m (n=2); and

Mdx-ApoE 4m (n=6), 7m (n=6). Mean+SEM, two-way ANOVA. *P<0.05 **P<0.01 ***P<0.001 ****P<0.0001

Gastrocnemius was the most severely affected by concurrent MD and hyperlipidemia in the Mdx-ApoE DKO model (Image 6.4). A significant decrease in total gastrocnemius size was observed in Mdx-ApoE DKO mice compared to wild-type and ApoE-KO groups by 7 months of age on HFD, although not at 4 months (Figure 6.8A). Muscle composition in Mdx-ApoE DKOs was also greatly altered by 7 months of age compared to all other groups: increased fat and collagen content as well as decreased healthy myofiber area (Figure 6.8). At the 7-month time-point, the Mdx group also display a mild increase in fibrosis compared to wild-type and ApoE-KO controls (Figure 6.8C). As early as 4 months of age, collagen deposition was found to be significantly increased in Mdx-ApoE DKO gastrocnemius muscle compared to all other groups (Figure 6.8C).

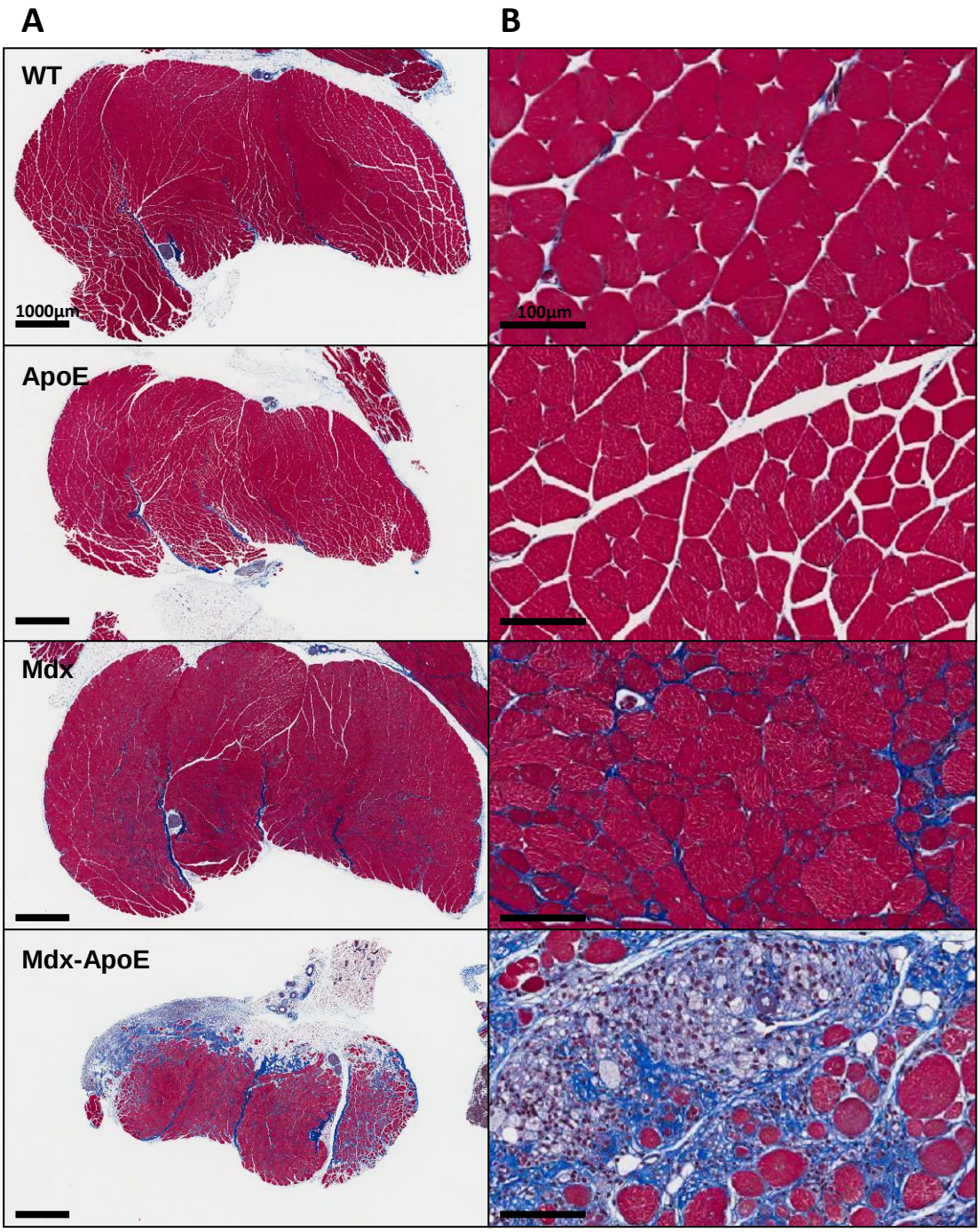

Image 6.4 Representative images of gastrocnemius at 7 months on HFD. (A) 2x zoom, scale bar=1000µm and (B) 8x zoom, scale bar=100µm of wild-type, ApoE-KO, Mdx and Mdx-ApoE DKO Masson's trichrome stained slides, collagen deposition in blue.

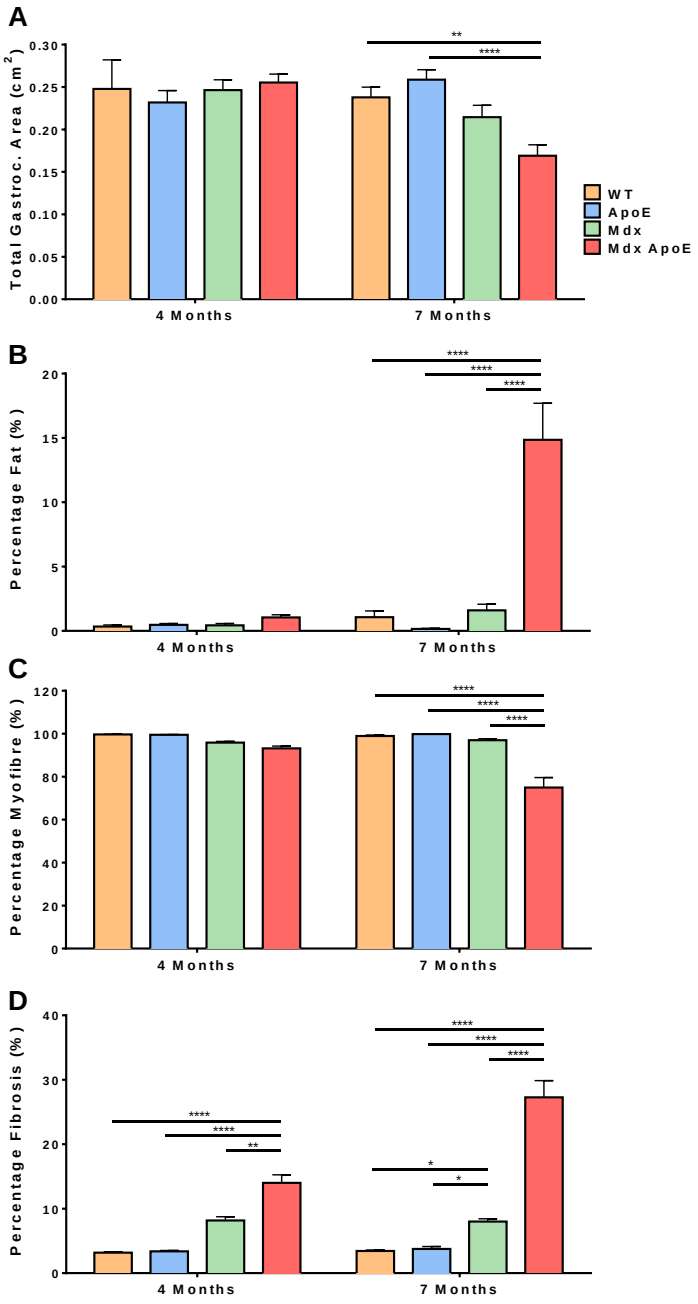

Figure 6.8 Gastrocnemius muscle size and composition at 4 and 7 months on HFD. (A) Total muscle area in cm^2, percentage of muscle area composed of (B) fat, (C) healthy myofiber, and (D) collagen. WT 4m (n=3), 7m (n=9); ApoE 4m (n=3), 7m (n=8); Mdx 4m (n=7), 7m (n=6); and

Mdx-ApoE 4m (n=6), 7m (n=6). Mean+SEM, two-way ANOVA. *P<0.05 **P<0.01 ***P<0.001 ****P<0.0001

On the other hand, the rectus femoris of the quadriceps muscle was not significantly worsened in the Mdx-ApoE DKO model (Image 6.5). Both Mdx and Mdx-ApoE groups showed an increase in total rectus femoris size at 4 months of age, while only Mdx-ApoE DKO quadriceps had significant increased total area by 7 months (Figure 6.9A). Similarly, both Mdx and Mdx-ApoE DKO groups showed significant fibrosis in the quadriceps, at both 4- and 7-months of age (Figure 6.9D). Surprisingly, Mdx mice had small, but significant increase fat infiltration (<4%) compared to all other groups at 7 months (Figure 6.9B), although no significant change in healthy myofiber percentage was observed in any group (Figure 6.9C). Percentage centralized nuclei at 7 months of age on HFD was also calculated in the rectus femoris of quadriceps and found to be similarly increased in both Mdx and Mdx-ApoE DKO groups (Figure 6.10).

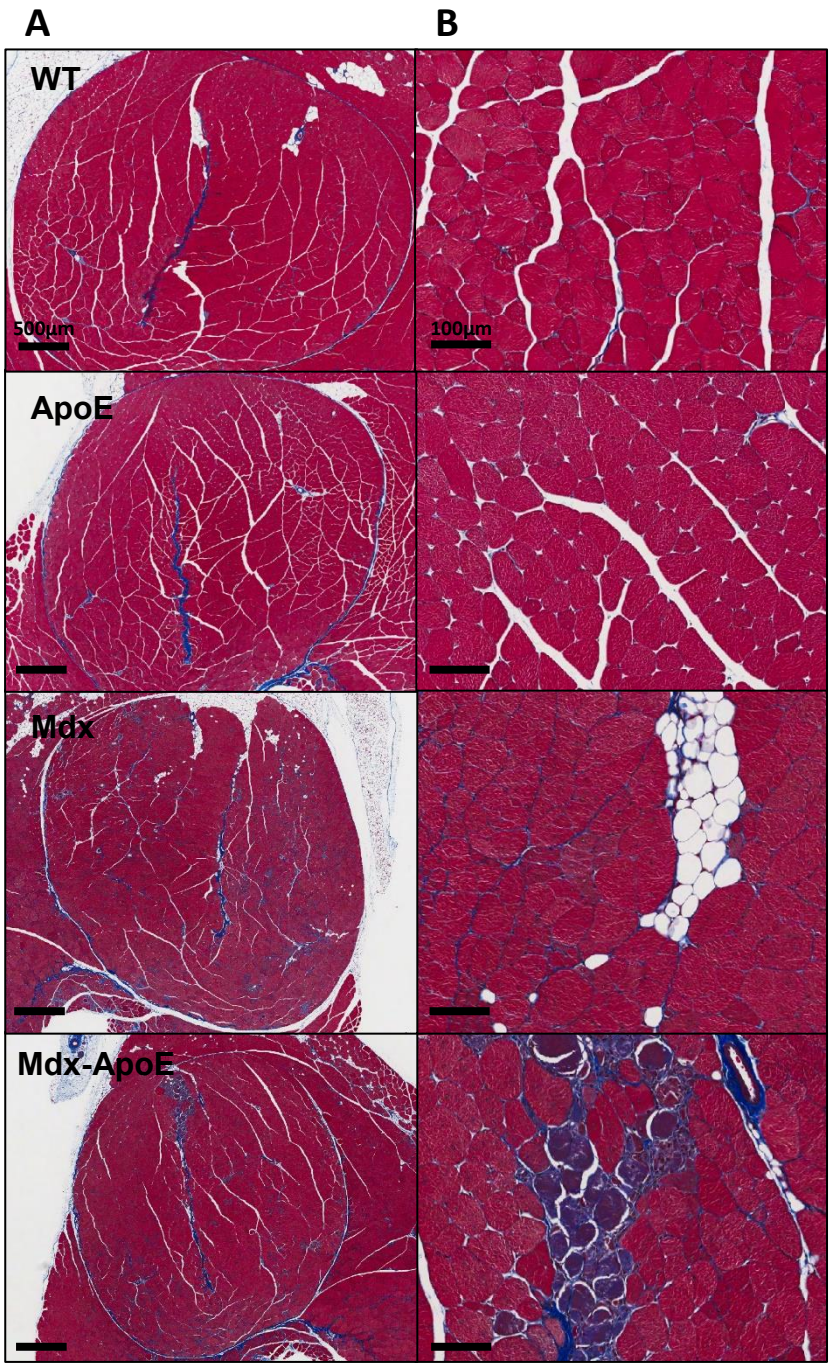

Image 6.5 Representative images of quadriceps femoris at 7 months on HFD. (A) 2x zoom, scale bar=500µm and (B) 8x zoom, scale bar=100µm of wild-type, ApoE-KO, Mdx and Mdx-ApoE DKO Masson's trichrome stained slides, collagen deposition in blue.

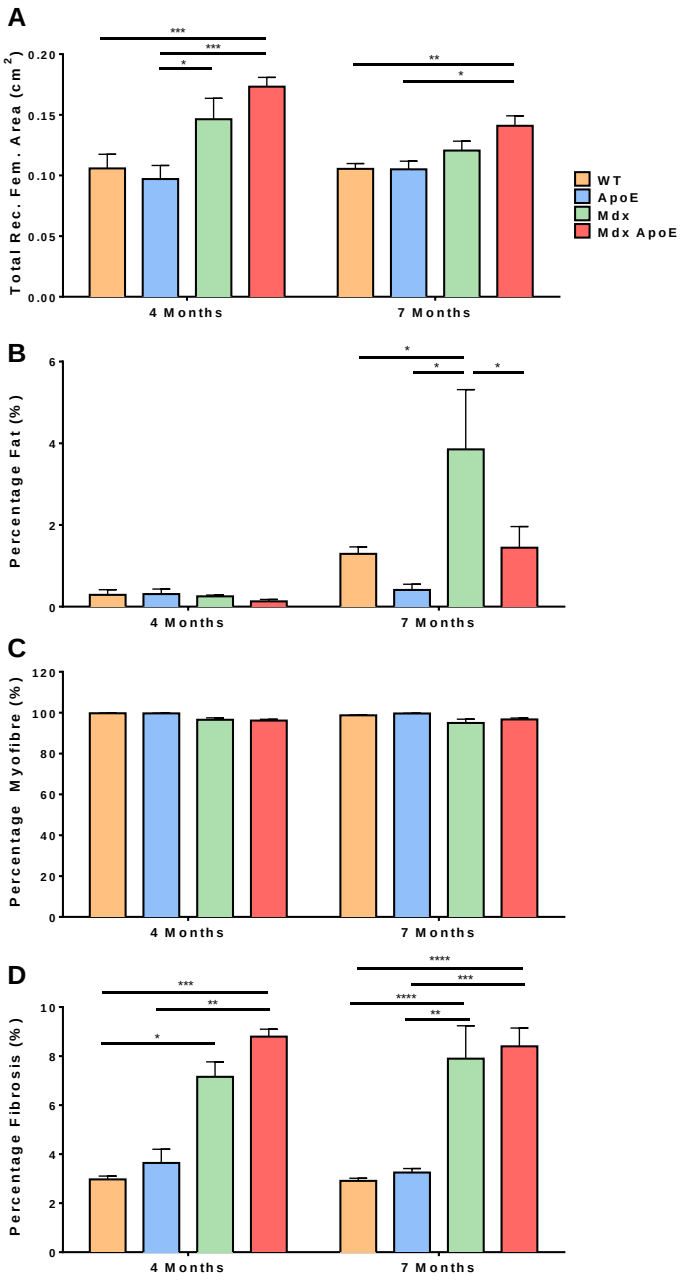

Figure 6.9 Quadriceps femoris muscle size and composition at 4 and 7 months on HFD. (A) Total rectus femoris area in cm^2, percentage of rectus femoris area composed of (B) fat, (C) healthy myofiber, and (D) collagen. WT 4m (n=4), 7m (n=9); ApoE 4m (n=4), 7m (n=4); Mdx 4m (n=4),

7m (n=7); and Mdx-ApoE 4m (n=4), 7m (n=11). Mean+SEM, two-way ANOVA. *P<0.05 **P<0.01 ***P<0.001 ****P<0.0001

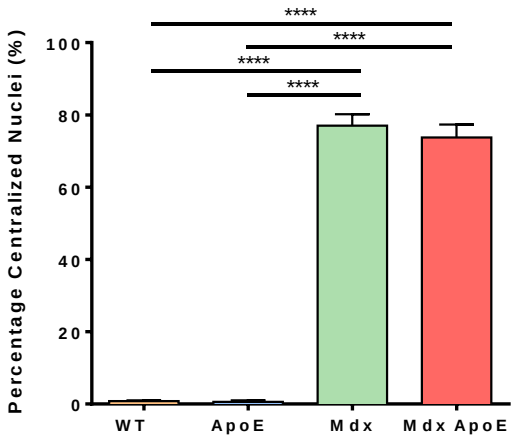

Figure 6.10 Percentage centralized nuclei in quadriceps femoris at 7 months on HFD. WT (n=5), ApoE (n=4), Mdx (n=4), and Mdx-ApoE (n=5). Mean+SEM, one-way ANOVA. ****P<0.0001

The diaphragm muscle was severely damage in both Mdx and Mdx-ApoE DKO groups at 7 months on HFD (Image 6.6). There was a similar increase fibrosis and decreased healthy myofiber area in both dystrophin-deficient groups compared to wild-type and ApoE-KO groups, which was not worsened in Mdx-ApoE DKO mice (Figure 6.11). Interestingly, only the Mdx group seems to have a significant increase in fat infiltration in the diaphragm (Figure 6.11B).

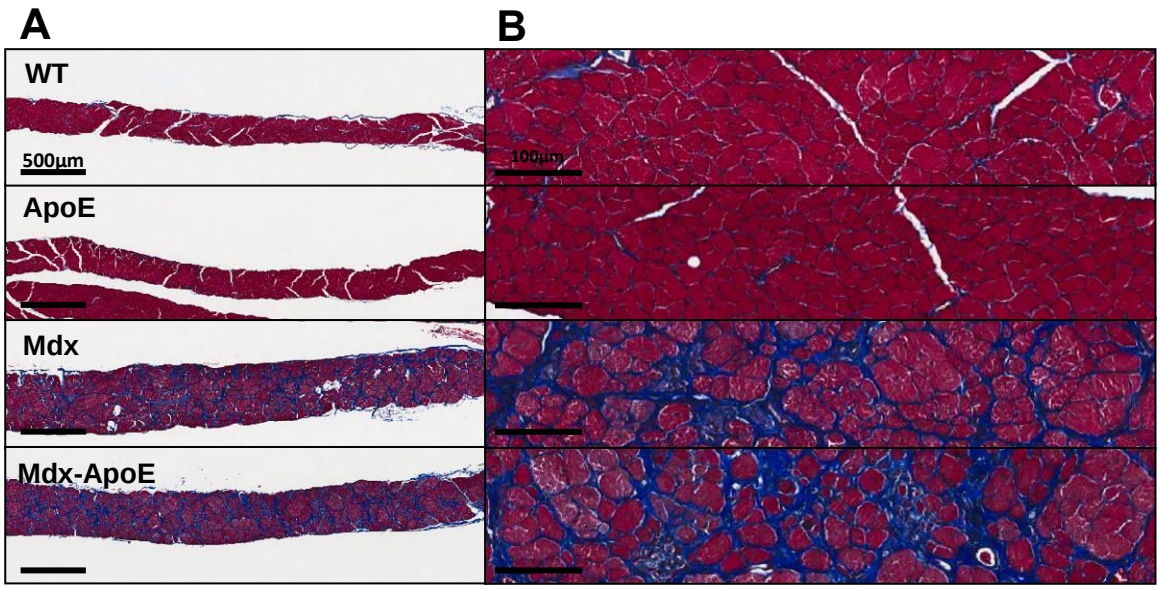

Image 6.6 Representative images of diaphragm at 7 months on HFD. (A) 2x zoom, scale bar=500µm and (B) 8x zoom, scale bar=100µm of wild-type, ApoE-KO, Mdx and Mdx-ApoE DKO Masson's trichrome stained slides, collagen deposition in blue.

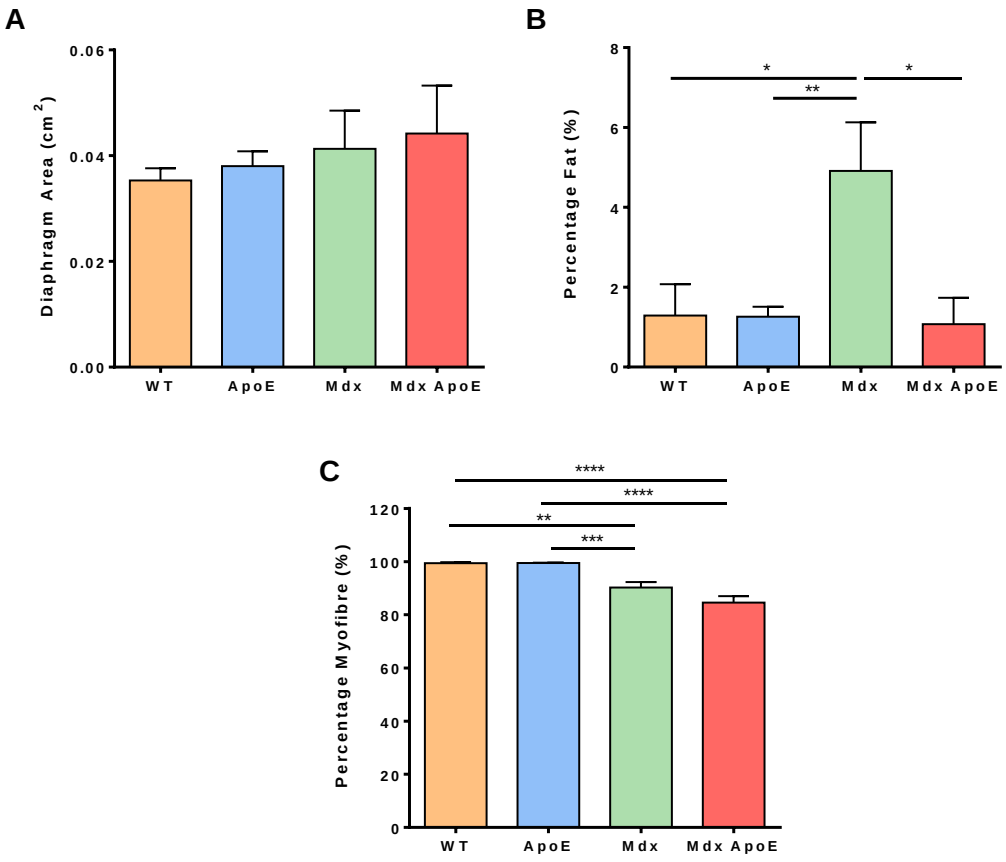

Figure 6.11 Diaphragm muscle size and composition at 7 months on HFD. (A) Total muscle area in cm^2, percentage of muscle area composed of (B) fat and (C) healthy myofiber. WT (n=6), ApoE (n=8), Mdx (n=3), and Mdx-ApoE (n=5). Mean+SEM, one-way ANOVA. *P<0.05 **P<0.01 ***P<0.001 ****P<0.0001

Some other interesting pathological features were observed via skeletal muscle histology. Vascular leak was noted in many Mdx-ApoE DKOs, leading to inflammatory cells and red blood cells infiltrating muscle tissue, as seen in Image 6.7 of Mdx-ApoE DKO gastrocnemius muscle. Also, significant areas of muscle calcification were observed in Mdx and Mdx-ApoE DKO mice and, in rare cases, ectopic bone formation in Mdx-ApoE DKO mice, confirmed via Alizarin red

staining (Image 6.8). In addition, intracellular vesicles were seen within myofibers of Mdx-ApoE DKO mice on HFD (Image 6.9). Although the content of these vesicles is unknown, PAS staining did not reveal significant glycogen deposition and ORO stain showed some intracellular lipid cellular (not shown).

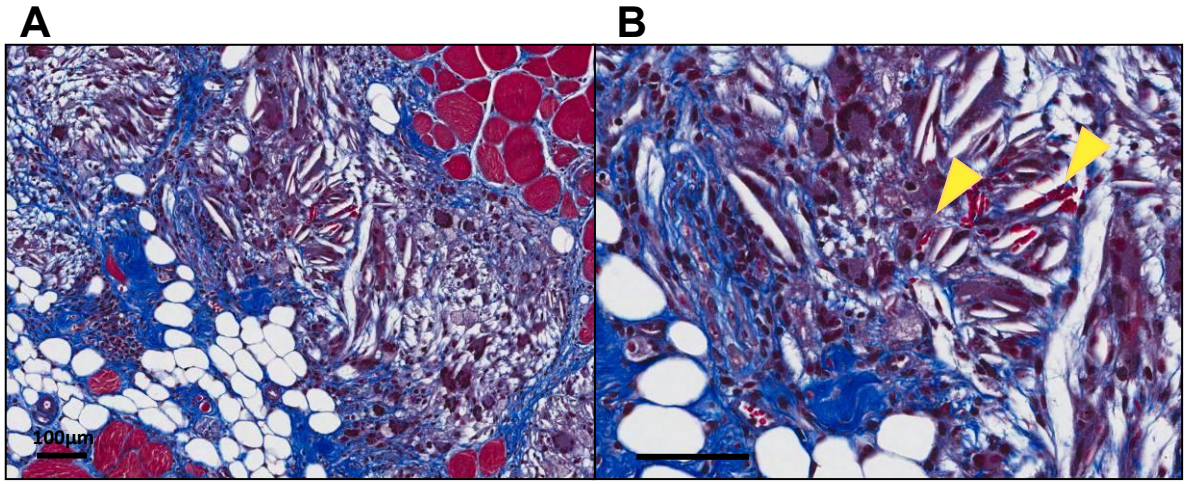

Image 6.7 Examples of vascular leak in Mdx-ApoE DKO at 7 months on HFD. (A) 4x and (B) 10x zoom of gastrocnemius Masson's trichrome stained slides (arrows indicate red blood cells), scale bars=100µm.

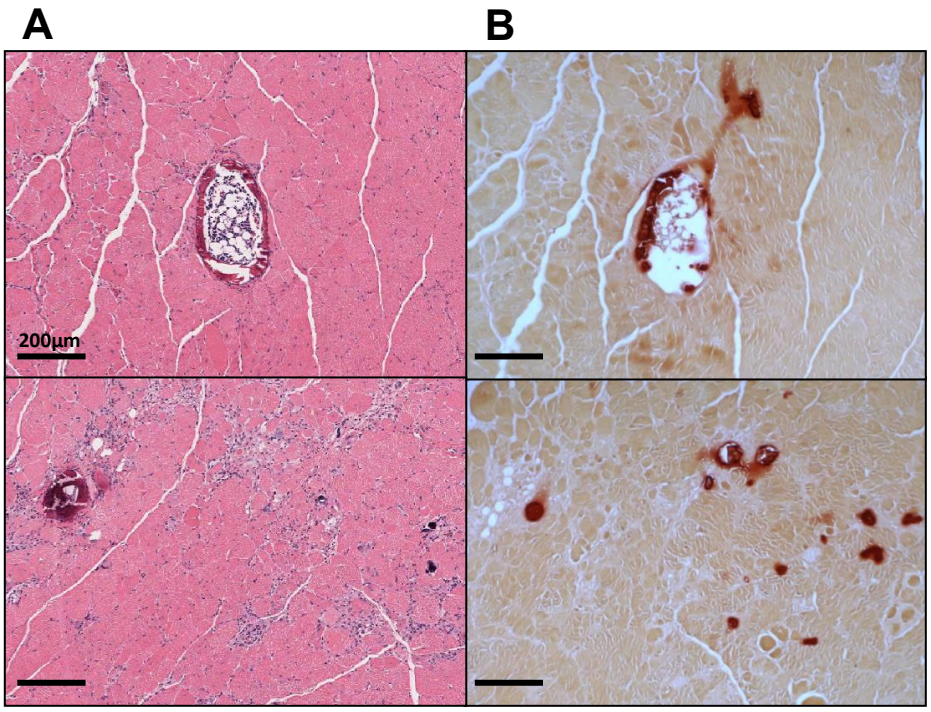

Image 6.8 Examples of ectopic bone and calcification in gastrocnemius of Mdx-ApoE DKO at 4 months on HFD. 4x zoom of (A) H+E and (B) Alizarin red stained serial sections of ectopic bone (top) and calcification (bottom), scale bar=200µm.

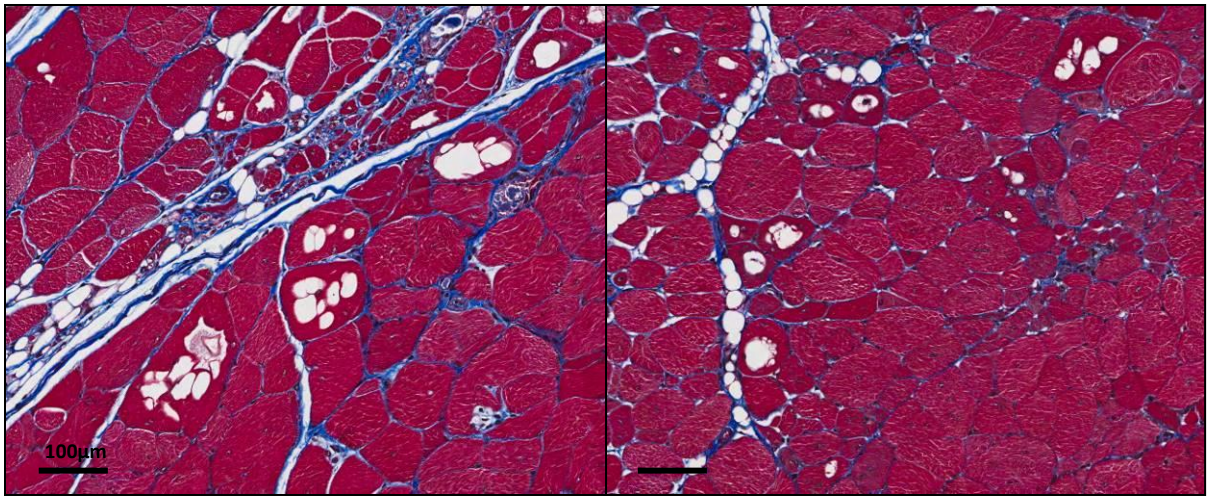

Image 6.9 Examples of intracellular vesicles in Mdx-ApoE DKO mice at 7 months of age on HFD. 8x zoom of quadriceps femoris Masson's trichrome stained slide, scale bar=100µm.

6.2.6 Aortic Atherosclerosis

Quantification of atherosclerotic plaque deposition using Sudan IV staining of the aorta revealed significantly increased plaque coverage in ApoE-KO and Mdx-ApoE DKO mice (Image 6.10). At 4 months of age on HFD, both hyperlipidemic groups had increased plaque in the aortic arch compared to wild-type and Mdx groups, with significantly less plaque in Mdx-ApoE DKO mice compared to ApoE-KO mice (Figure 6.12A). By 7 months of age on HFD, plaque coverage was significantly higher in all aortic segments of ApoE-KO and Mdx-ApoE DKO groups compared to controls, while only the thoracic segment of the aorta showed a significant decrease in plaque deposition in the Mdx-ApoE-KO group compared to ApoE-KO mice (Figure 6.12B). In chow-fed groups, there was only an increase in plaque coverage of ApoE-KO aortic arches compared to all other groups (Figure 6.12C). Analysis of ORO stained aortic root sections (Image 6.11) showed a significant increase in plaque percentage in ApoE-KO and Mdx-ApoE DKO at 4- and 7-months on HFD compared to wild-type and Mdx groups, without significant difference between hyperlipidemic groups (Figure 6.13).

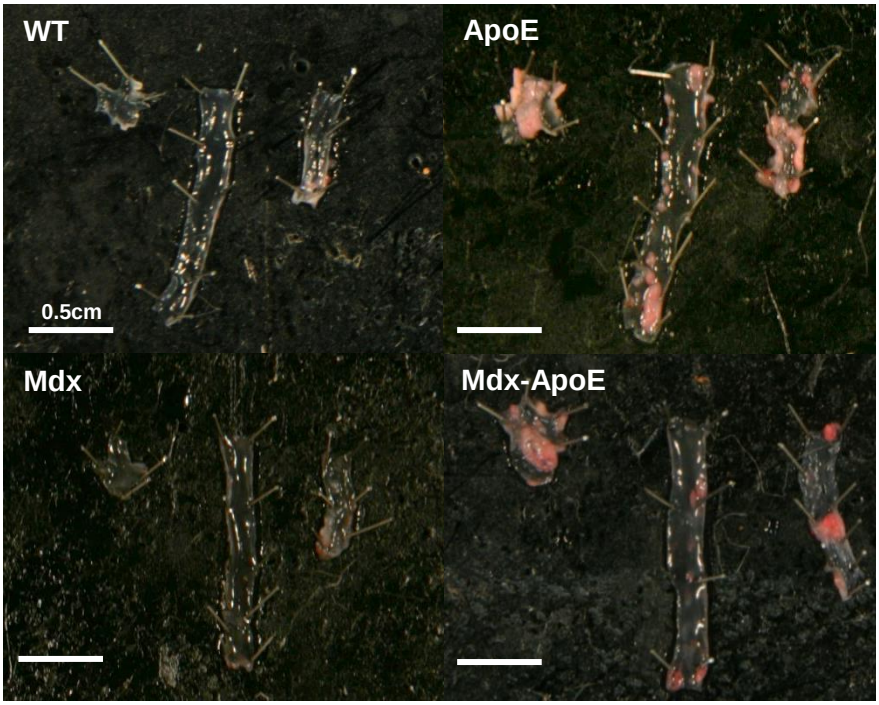

Image 6.10 Representative images of atherosclerotic plaque in aortic segments at 7 months of age on HFD. Sudan IV stained arch, thoracic and abdominal sections of the aorta (from left to right), scale bar=0.5cm.

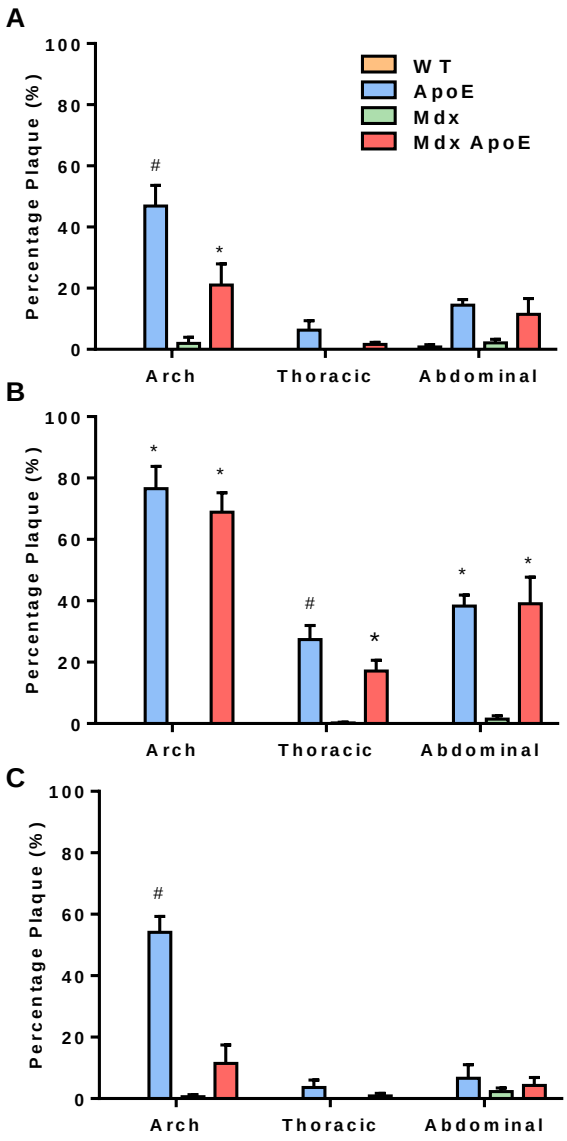

Figure 6.12 Atherosclerotic plaque coverage in aortic segments on HFD and chow. Percentage of aortic area covered in plaque by segment at (A) 4- and (B) 7-months on HFD; and (C) 7-months on chow. HFD: WT 4m (n=3), 7m (n=5); ApoE 4m (n=4), 7m (n=5); Mdx 4m (n=5), 7m (n=4); and Mdx-ApoE 4m (n=5), 7m (n=5). Chow 7m: WT (n=3), ApoE 7m (n=5), Mdx 7m (n=4) and Mdx-ApoE 7m (n=4). Mean+SEM, two-way ANOVA. *P<0.05 compared to wild-type and Mdx; #P<0.05 compared to all other groups.

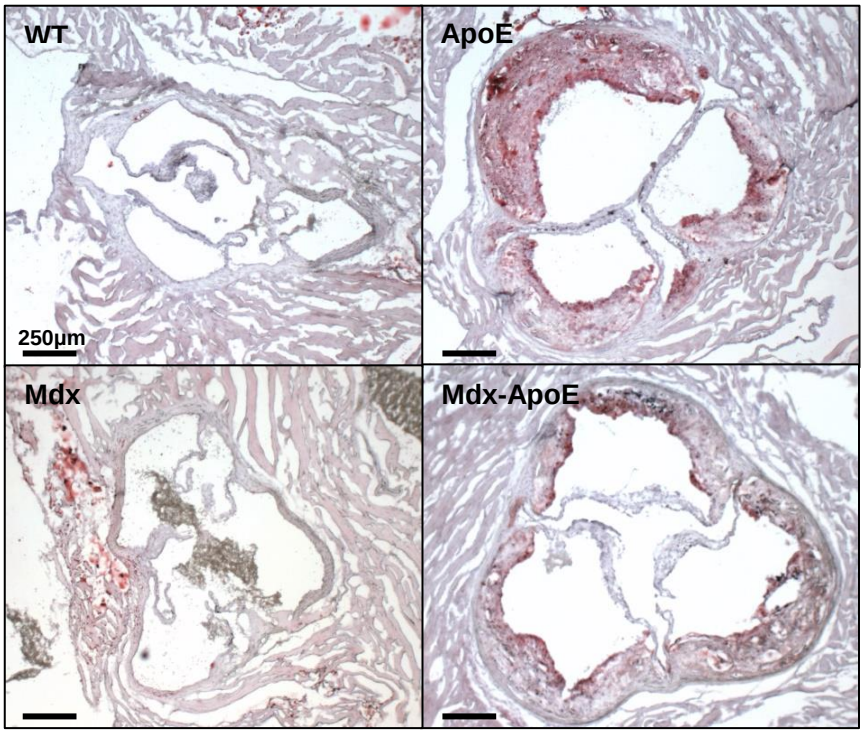

Image 6.11 Representative images of aortic root plaque at 7 months of age on HFD. ORO stained slides, scale bar=250µm.

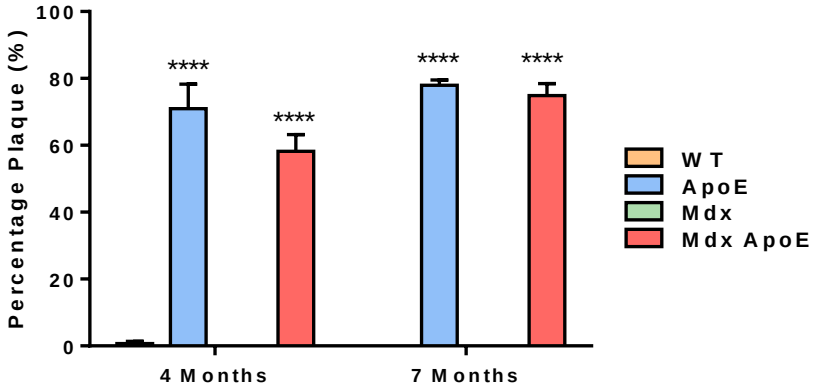

Figure 6.13 Atherosclerotic plaque coverage in aortic root at 4 and 7 months on HFD. Percentage of aortic root wall area taken up by plaque. WT 4m (n=4), 7m (n=7); ApoE 4m (n=4),

7m (n=7); Mdx 4m (n=2), 7m (n=3); and Mdx-ApoE 4m (n=6), 7m (n=6). Mean+SEM, two-way ANOVA. ****P<0.0001 compared to wild-type and Mdx.

6.2.7 Plasma Analysis

Measurement of plasma CK levels was performed on plasma collected via facial bleeding from chow-fed experimental groups at 5 months of age. As expected, levels of CK were significantly elevated in Mdx and Mdx-ApoE DKO groups compared to wild-type (Figure 6.14). Large variability was seen in wild-type plasma CK levels, but not in the Mdx and Mdx-ApoE DKO groups.

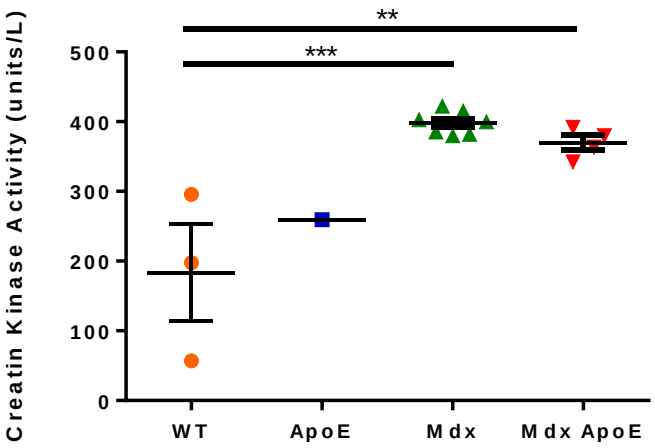

Figure 6.14 Plasma creatine kinase activity at 5 months of age on chow. Expressed as units per liter (units/L) in plasma collected via facial bleeding. Each point represents one mouse. WT (n=3), ApoE (n=1), Mdx (n=7), and Mdx-ApoE (n=4). Mean±SEM, one-way ANOVA excluding ApoE n=1. **P<0.01 ***P<0.001

6.3 Discussion

As a model of DMD, *mdx* mice fail to exhibit the severity of muscle damage and motor function impairment observed in DMD patients. Several studies have observed minor muscle phenotypes in *mdx* such as centralized nuclei, mild fibrosis and necrosis associated with a slight reduction in muscle force and normal ambulatory function (Collins & Morgan, 2003). Therefore, development of more representative models for use in drug screening is particularly important since DMD is severely debilitating and relatively common. Our investigation of the effects of hyperlipidemia in the *mdx* mouse model of DMD showed worsened pathology in some skeletal muscles by 7 months of age on HFD. However, we did not observe any exacerbation of muscle *ex vivo* function or overall ambulatory function in Mdx-ApoE groups compared to Mdx mice.

None of the animals in this project lost the ability to walk and when step-length was measured, both Mdx and Mdx-ApoE groups were similarly reduced compared to controls 3 months of age while only Mdx-ApoE DKO had significantly smaller step length compared to wild-type and ApoE-KO by 6 months. This is consistent with studies of *mdx5*^{cv} mice that have shown a decrease in stride length similar to the results shown in this study: approximately 7cm in wild-type to 5-6cm in *mdx* groups (Beastrom et al., 2011). Several studies examining *mdx* skeletal muscle *ex vivo* parameters (such as tension, specific force and fatigability) have shown little or no weakness in soleus, TA, EDL and diaphragm muscles (J. E. Anderson, Bressler, & Ovalle, 1988; Coulton, Curtin, Morgan, & Partridge, 1988; Cox et al., 1993; Dupont-Versteegden, McCarter, & Katz, 1985; Quinlan, Johnson, McKee, & Lyden, 1992). Our pilot study of muscle function in one animal from each experimental group at 5 months of age did not show any drastic difference in soleus and diaphragm force-velocity relationship or force fatigue/recovery parameters.

Significant hindlimb muscle hypertrophy was observed in Mdx and Mdx-ApoE DKO mice at 4 months of age and Mdx-ApoE DKO mice at 7 months of age, consistent with pseudohypertrophy observed in DMD calves. A dramatic exacerbation of MD pathology was observed upon histological examination of certain skeletal muscles. For instance, triceps brachii and gastrocnemius muscles from the Mdx-ApoE DKO group had increased myofiber damage, muscle fibrosis, and fat infiltration compared to all other groups. Despite this dramatic effect in gastrocnemius and triceps brachii, muscle damage in the quadriceps femoris and diaphragm muscles was not further exacerbated by hyperlipidemia in Mdx-ApoE DKO mice. Although significant muscle damage was observed, only a small yet similar increase in plasma CK was found in Mdx and Mdx-ApoE DKO groups. Other studies looking at CK levels in *mdx* mice found much higher and more variable plasma CK measurements (between 400-20,000 units/L) (Coulter, et al. 1988). However, levels of plasma CK have been shown to decrease with the progression of the disease and are significantly lower in *mdx* mice by 23 weeks of age (Glesby, Rosenmann, Nylen, & Wrogemann, 1988). Cardiac function was also assessed and, in accordance with several other studies, our Mdx group did not develop DCM nor display any functionally significant changes in heart function by 6 months of age (Fayssoil et al., 2013; Quinlan et al., 2004). In addition, hyperlipidemia was found to have no effect on the development of DCM in our Mdx-ApoE DKO mice, besides an increase in left ventricular systolic volume at 6 months of age. Future aging studies of these mice can be conducted to assess cardiac function decline and allow us to determine whether hyperlipidemia accelerates or aggravates this DMD phenotype at later time-points.

Consistent with a previous study which showed that dystrophin-deficiency resulted in reduced atherosclerotic plaque development in a similar ApoE-null *mdx* mouse model (Shami et

al., 2015), our analysis of Mdx-ApoE DKO aortas showed a significant reduction in aortic plaque coverage in the arch compared to ApoE-KO mice at 4-months on HFD and 7-months on chow. However, by 7-months of age on HFD, there is only a slight decrease in thoracic aorta plaque coverage in the Mdx-ApoE DKO compared to ApoE-KO. It is possible, as hypothesized in the previous ApoE-null *mdx* study (Shami et al., 2015), that the atheroprotective effect of dystrophin-deficiency may be due to increased VSMCs infiltration – leading to more stable plaques – as well as decreased presence of T cells, which are known to contribute to atherogenesis.

In all, this double-disease model has shown that hyperlipidemia and vascular disease can worsen the pathology of some muscles in *mdx* mice. Although significant muscle damage was only observable via analysis of muscle histology, showing little change in ambulation, this model still better represents the muscle phenotype observed in human DMD patients: dramatic muscle degeneration and persistent fibrosis, fat infiltration, necrosis and inflammation. This exacerbated phenotype may provide a larger window for improvement when screening potential therapeutics while still being suitable for long-term studies.

Chapter 7: Conclusion

Even after decades of research, there is still a need for effective MD therapeutics and representative models with which to assess their efficacy. Our Dysf-ApoE DKO and Mdx-ApoE DKO double-disease models of MD and hyperlipidemia exhibit significantly worsened MD pathology in some muscles and more closely mimic the human phenotype. These models may be more useful in therapeutic screening due to their obvious histological abnormalities and measurable ambulatory decline. Impairment of vascular function in these models led to exacerbated skeletal muscle necrosis, increased fat infiltration, increased inflammation and decreased healthy myofiber area in affected muscles. Despite the exacerbation observed in the Dysf-ApoE DKO model, the generation of another dysferlinopathy double-disease model using the milder, more humanized LDLR-KO model of hyperlipidemia was unsuccessful. Dysf-LDLR DKO breeding resulted in very few DKO mice, none of which were viable, and although they displayed stunted growth and abnormal gait, muscle histology did not reveal any striking pathology. Beyond the potential use of these double-disease mice as more representative models of their respective MD and their potential use in drug screening, our results also reveal vascular contributions to MD pathophysiology and point towards the exploration of lipid-lowering and vascular-targeted medications for the treatment of MD.

7.1 Potential Mechanisms of MD Exacerbation

The precise mechanism through which hyperlipidemia worsens the muscle pathology in MD has not been fully explored. After observing such localized and severe necrosis and fibrofatty infiltration in the muscle, it was posited that perhaps thrombosis and occlusion of muscle vascular

supply subsequent to severe atherosclerosis was causing the increased muscle damage observed in Dysf-ApoE and Mdx-ApoE DKO models. However, no apparent muscle pathology was observed in any ApoE-KO mice at any time-point, even when quantification of atherosclerotic plaque coverage was found to be equally, if not more, severe in ApoE-null mice compared to DKO models. Therefore, the exact method whereby increased circulating cholesterol and lipids exacerbates muscle pathology is likely more complex than just the ischemic effects of advanced atherosclerosis. One possible mechanism is through hyperlipidemia's effect on endothelial function and vascular leak. The level of vascular leak in dysferlin- and dystrophin-deficient vessels has not been thoroughly explored, although one study looking at multiple sclerosis brain vessels found significant overexpression of dysferlin in areas of increased vascular leak and inflammatory cell extravasation in multiple sclerosis (Hochmeiseter et al., 2006). To the contrary, we have observed inflammatory cell and red blood cell leakage from skeletal muscle blood vessels in all MD groups, suggesting that there is a disruption of endothelial barrier function subsequent to loss of dystrophin and dysferlin expression in the vasculature. Therefore, the increased immune cell infiltration of muscle tissue observed in double-disease models may be facilitating immune cell response to damaged muscle tissue and triggering remodeling and fibrofatty replacement of damaged areas. In addition, dysferlin- and dystrophin-deficient myofibers may be more susceptible to oxidative stress and free radical-mediated injury, which is known to be increased in the context of hyperlipidemia (Rando, Disatnik, Yu, & Franco, 1988; Terrill et al., 2013; Tidball & Wehling-Henricks, 2007; Whitehead, Yeung, & Allen, 2006).

Since generation of another dysferlin-deficient double-disease model using the LDLR-KO failed to confirm the results observed with the ApoE-KO, there were concerns that the muscle

pathology exacerbation seen in Dysf-ApoE DKO mice was specific to ApoE-deficiency and loss of ApoE biological functions outside of cholesterol and lipid homeostasis. Still, compared to previously mentioned studies looking at MD mouse models on regular chow, our HFD-fed Dysf-KO and Mdx mice displayed worsened muscle damage, even without disrupting cholesterol clearance. This suggests that a lipid-rich diet may be enough to aggravate muscle pathology. In fact, other studies have shown that long-term HFD administration can affect muscle metabolism (Gomez-Perez, Capllonch-Amer, Gianotti, Llado, & Proenza, 2012; Lindholm et al., 2013) and incite myofiber type switch from slow oxidative type 1 to fast glycolytic type 2 (Denies et al., 2014; Ljubicic et al., 2011), which may be adding further stress to susceptible MD myofibers.

7.2 Implications for MD treatment

Our results suggest that lipid-lowering therapeutics and nutritional interventions are worth investigating in MD. Though lipid levels are higher in some forms of MD, hyperlipidemia and vascular dysfunction have been largely overlooked as a potential contributing factors and pathological features of the disease and medical intervention has largely focused on correcting skeletal muscle, cardiac and respiratory pathologies. Plus, the rare but severe muscle side effects of many lipid-lowering therapies were thought to make them unsuitable in these patients (Hodel, 2002). Nevertheless, in the *mdx* model of DMD, statin treatment (i.e. simvastatin) was shown to significantly improve muscle function and fibrosis with no evidence of rhabdomyolysis (Whitehead, Kim, Bible, Adams, & Froehner, 2015). However, this improvement was accomplished without a significant change in plasma cholesterol, suggesting that the beneficial

effects of simvastatin treatment were due to its antioxidant "pleiotropic" effects and not necessarily through total cholesterol lowering.

Other vascular targeted therapies – including angiotensin converting enzyme inhibitors (ACEIs), angiotensin receptor blockers (ARBs), phosphodiesterase 5 (PDE5) inhibitors, VEGF administration and NO-donating drugs – have been explored in DMD (Ennen, Verma, & Asakura, 2013), however little research has explored their effect in dysferlinopathies. Although many of these drugs were found to improve cardiac function, mainly by enhancing vasodilation and lowering blood pressure (Spurney et al., 2011), few showed significant improvement of skeletal muscle pathology. Of note, the PDE5 inhibitor tadalafil ameliorated functional ischemia in *mdx* mouse muscle leading to decreased muscle damage and improved muscle force (Asai et al., 2007). Treatment of *mdx* mice with sildenafil, another PDE5 inhibitor, showed significantly reduced diaphragm fibrosis (Percival et al., 2012) and reversal of cardiomyopathy (Adamo et al., 2010), while BMD and DMD patients displayed reduced muscle ischemia (M. D. Nelson et al., 2014) without significant effect on the cardiac function (Leung et al., 2014; Witting et al., 2014). Similarly, VEGF administration was able to reduce muscle ischemia in *mdx* mice via increased vascular density, leading to improved muscle strength, reduced myofiber necrosis and increased activation of satellite cells (Deasy et al., 2009; Messina et al., 2007). In addition, treatment with NO-donating drugs has been shown to reduce fat deposition and fibrosis in *mdx* skeletal muscle (Cordani, Pisa, Pozzi, Sciorati, & Clementi, 2014). Therefore, it seems lipid-lowering and vascular-targeted therapies for treatment of dysferlinopathy and dystrophinopathy patients may be worth exploring.

7.3 Improved Models of MD

So far, the Dysf-ApoE DKO model is one of the first model of dysferlinopathy to show dramatic impairment of *in vivo* muscle function and complete loss of walking ability (Kobayashi, Izawa, Kuwamura, & Yamate, 2012). The Dysf-ApoE DKO model mimics the muscle pattern observed in LGMD2B, where mainly the proximal limb muscles (such as quadriceps femoris and triceps brachii) are affected in the early stages with progression towards the more distal limb muscles over time (such as gastrocnemius and TA). Although difficult to harvest and quantify due to the level of muscle wasting, Dysf-ApoE DKOs also displayed significant wasting and fat replacement of the pelvic girdle muscles such as the psoas major. Similarly, the Mdx-ApoE DKO model mimics DMD pathology more closely than Mdx mice, developing the most severe pathology in the gastrocnemius and diaphragm muscles (Kornegay et al., 2012).

Since Dysf-KO mice display little to no change in muscle strength and ambulation, drug trials in the mouse model cannot assess prolongation of walking ability, a major outcome of most MD clinical trials, and rely on histopathological assessment of muscle damage. Therefore, the ability of step length measurement to detect observable impairment of ambulatory function in Dysf-ApoE DKOs offers a non-invasive technique for tracking of disease progression without significantly affecting muscle integrity – unlike voluntary running wheels which can induce muscle necrosis (Biondi et al., 2013). Another advantage to the use of our double-disease models in therapeutic screening is the accelerated time-line of muscle pathology: significant degeneration and fibrofatty replacement can be detected in some muscles as early as 4- and 7-months of age for Mdx-ApoE and Dysf-ApoE DKOs, respectively. This makes these models ideal for both short-

and long-term studies and, since the muscle pathology as assessed by histology can be quite severe at the later stages, this creates a large window for therapeutic improvement.

7.4 Limitations of Double-Disease Models

Use of animal models in any study of human disease and therapeutic screening must take into consideration the many critical differences between animal models and human patients. Often, insights gained from animal model research fail to translate to the human disease. Depending on the particular area of research, the translation of preclinical to clinical studies can be tremendously unsuccessful: for instance in cancer research, less than 8% of treatments are effectively translated to the clinic (Mak, Evaniew, & Ghert, 2014). Therefore, all findings observed entirely in animal models should be considered with caution until confirmed in human studies.

Another caveat of this research is the use of genetically modified murine models and their divergence from human disease. Two of our projects utilized the ApoE-KO model of hyperlipidemia, which displays extremely severe hyperlipidemia and atherosclerosis. Although the atherosclerotic lesions in ApoE-KO mice develop through a similar mechanism as those seen in humans (Nakashima, Plump, Raines, Breslow, & Ross, 1994), the marked increase in circulating VLDL and chylomicrons remnants over LDL is not representative of the human lipid profile (R. H. Nelson, 2013). In addition, ApoE can be found in macrophages and has other functions beyond cholesterol transport, such as its "antioxidant, antiproliferative (smooth muscle cells, lymphocytes), anti-inflammatory, antiplatelet, and NO-generating properties" (Zadelaar et al., 2007). Therefore, loss of ApoE expression may have led to unknown systemic effects and these other changes may also have affected MD progression. Also, development of significant skin

lesions occurred occasionally in ApoE-KO and Dysf-ApoE DKO groups and were sometimes so severe that the animals had to be sacrificed prematurely. These animals could not be included in this study since severe skin lesions have been shown to impair limb movement and activate immune response in mouse models of atherosclerosis which may influence ambulatory decline and muscle pathology (Ishibashi, Goldstein, Brown, Herz, & Burns, 1994; Zabalawi et al., 2007). Since LDLR has few known functions outside of lipoprotein clearance, it was proposed as superior hyperlipidemia model; however, generation of Dysf-LDLR was not successful.

There are also some obvious differences between our murine models and human patients. The Mdx-ApoE DKO differs from human DMD patients in that complete loss of walking ability and cardiac dysfunction were not observed in the Mdx-ApoE DKO model by 7 months of age on HFD while roughly 90% of DMD patients stop walking by 12 years of age (Emery, Muntoni, & Quinlivan, 2015) and develop significant cardiomyopathy by 18 (Townsend, Yasuda, & Metzger, 2007). It is possible that the 7-month time-point of this study was not sufficient time for skeletal and cardiac muscle damage to incur functional deficits. Investigation of cardiac damage via histology and longer studies of the Mdx-ApoE DKO model could be conducted to track progressive ambulatory and cardiac decline as well as to determine whether hyperlipidemia has any effect on lifespan beyond 7 months of age. Nevertheless, survival to at least 7 and 11 months of age in the Mdx-ApoE and Dysf-ApoE DKO models respectively is advantageous for long-term therapeutic studies.

7.5 Future Directions

The chow-fed animal muscles have not yet been processed for the Dysf-ApoE DKO and Mdx-ApoE DKO. However, evaluation of muscle pathology in all MD groups would be helpful in assessing whether HFD has any effect on Dysf-KO and Mdx mice compared to chow. Although few studies have looked at the effects of dietary lipids in dysferlin-deficient mice, our preliminary analyses suggest that Dysf-KO mice on regular chow exhibit less muscle damage and atrophy than age-matched, HFD-fed Dysf-KO mice. As for dystrophin-deficient mice, one study showed no difference in muscle necrosis when *mdx* mice were fed high-fat milk diet until 42 days old (Mokhtarian, Lefaucheur, Even, & Sebille, 1995), while another study at 6-months of age demonstrated increased running distance and decreased muscle necrosis in *mdx* mice fed HFD: from approximately 3% in chow-fed *mdx* to 1% for *mdx* on HFD (Radley-Crabb, Fiorotto, & Grounds, 2011).

Also, generation of an alternate double-disease model of dysferlinopathy and hyperlipidemia may be worth exploring. Use of Dysf -/- LDLR +/- mice may be useful since LDLR heterozygotes have been shown to display intermediate plasma lipid elevation (I. J. Goldberg et al., 2008) and can be generated more easily than the Dysf-LDLR DKO. Or, the ApoE*3-Leiden (E3L) transgenic mice, which have a copy of the human APOE3 gene from familial dysbetalipoproteinemia, have moderate plasma cholesterol elevation and develop atherosclerotic lesions similar to human pathology (Lutgens et al., 1999). In addition, the E3L mice respond more favorably to lipid-lowering therapies, such as PCSK9 mAb, than ApoE-KO and LDLR-KO models (Ason et al., 2014; Zadelaar et al., 2007). This could facilitate future evaluation of vascular-targeted and lipid-lowering therapies on our double-disease model. If lipid-lowering therapies are

found to be effective at both cholesterol lowering and muscle pathology improvement, it would help confirm that elevated cholesterol and TGs are detrimental to MD muscle health and that these therapies may be beneficial in MD patients.

Exploration of the precise mechanism by which hyperlipidemia and impaired vascular function are affecting the progression of both dystrophin- and dysferlin-deficient MDs is warranted. It may be due to the increased vascular leak we observed which, when combined with the increased oxidative stress and inflammation in hyperlipidemia, leads to increased muscle damage and/or impaired regeneration. A study looking at the extent of vascular leak in our models would help reveal if endothelial barrier function is disrupted in dysferlin- and dystrophin-deficiency. Also, evaluation of exercise- or toxin-induced muscle damage in our DKOs may help elucidate whether our double-disease models shows impaired muscle regeneration in response to external damage. Altogether, our research has indicated that further study of the relationship between MD and hyperlipidemia is critical and will hopefully improve our understanding and treatment of MD in the future.

Bibliography

Aartsma-Rus, A., Fokkema, I., Verschuuren, J., Ginjaar, I., van Deutekom, J., van Ommen, G. J., & den Dunnen, J. T. (2009). Theoretic applicability of antisense-mediated exon skipping for Duchenne muscular dystrophy mutations. *Hum Mutat, 30*(3), 293-299. doi:10.1002/humu.20918

Adamo, C. M., Dai, D.-F., Percival, J. M., Minami, E., Willis, M. S., Patrucco, E., . . . Beavo, J. A. (2010). Sildenafil reverses cardiac dysfunction in the *mdx* mouse model of Duchenne muscular dystrophy. *PNAS, 107*(44), 19079-19083. doi:10.1073/pnas.1013077107

Ali, K., Middleton, M., Pure, E., & Rader, D. J. (2005). Apolipoprotein E suppresses the type I inflammatory response in vivo. *Circ Res, 97*(9), 922-927. doi:10.1161/01.RES.0000187467.67684.43

Anderson, J. E., Bressler, B. H., & Ovalle, W. K. (1988). Functional regeneration in the hindlimb skeletal muscle of the mdx mouse. *J Muscle Res Cell Motil, 9*, 499-515.

Anderson, T. J., Gerhard, M. D., Meredith, I. T., Charbonneau, F., Delagrange, D., Creager, M. A., . . . Ganz, P. (1995). Systemic Nature of Endothelial Dysfunction in Atherosclerosis. *Am J Cardiol, 75*, 71B-74B.

Angelini, C., Peterle, E., Gaiani, A., Bortolussi, L., & Borsato, C. (2001). Dysferlinopathy course and sportive activity: clues for possible treatment. *Acta Myologica, 30*, 127-132.

Aoki, M. (2015). Dysferlinopathy. *GeneReviews NCBI Bookshelf*.

Asai, A., Sahani, N., Kaneki, M., Ouchi, Y., Martyn, J. A., & Yasuhara, S. E. (2007). Primary role of functional ischemia, quantitative evidence for the two-hit mechanism, and phosphodiesterase-5 inhibitor therapy in mouse muscular dystrophy. *PLoS One, 2*(8), e806. doi:10.1371/journal.pone.0000806

Ason, B., van der Hoorn, J. W., Chan, J., Lee, E., Pieterman, E. J., Nguyen, K. K., . . . Jackson, S. (2014). PCSK9 inhibition fails to alter hepatic LDLR, circulating cholesterol, and atherosclerosis in the absence of ApoE. *J Lipid Res, 55*(11), 2370-2379. doi:10.1194/jlr.M053207

Baitsch, D., Bock, H. H., Engel, T., Telgmann, R., Muller-Tidow, C., Varga, G., . . . Nofer, J. R. (2011). Apolipoprotein E induces antiinflammatory phenotype in macrophages. *Arterioscler Thromb Vasc Biol, 31*(5), 1160-1168. doi:10.1161/ATVBAHA.111.222745

Bansal, D., Miyake, K., Vogel, S. S., Groh, S., Chen, C.-C., Williamson, R., . . . Campbell, K. P. (2003). Defective membrane repair in dysferlin-deficient muscular dystrophy. *Nature, 423*, 168-172.

Barthélémy, F., Wein, N., Krahn, M., Lévy, N., & Bartoli, M. (2011). Translational research and therapeutic perspectives in dysferlinopathies. *Mol Med, 17*(9-10), 875-882.

Bashir, R., Britton, S., Strachan, T., Keers, S., Vafiadaki, E., Lako, M., . . . Bushby, K. (1998). A gene related to *Caenorhabditis elegans* spermatogenesis factor *fer-1* is mutated in limb-girdle muscular dystrophy 2B. *Nature Genetics, 20*, 37-42.

Beastrom, N., Lu, H., Macke, A., Canan, B. D., Johnson, E. K., Penton, C. M., . . . Montanaro, F. (2011). *mdx5*^{cv} mice manifest more severe muscle dysfunction and diaphragm force deficits than do *mdx* Mice. *Am J Pathol, 179*(5), 2464-2474. doi:10.1016/j.ajpath.2011.07.009

Bejaoui, K., Hirabayashi, K., Hentati, F., Haines, J. L., Ben Hamida, C., Belal, S., . . . Brown, R. H., Jr. (1995). Linkage of Miyoshi myopathy (distal autosomal recessive muscular dystrophy) locus to chromosome 2p12-14. *Neurology, 45*, 768-772.

Biggar, W. D., Gingras, M., Fehlings, D. L., Harris, V. A., & Steele, C. A. (2001). Deflazacort treatment of Duchenne muscular dystrophy. *J Pediatr, 138*(1), 45-50. doi:10.1067/mpd.2001.109601

Biondi, O., Villemeur, M., Marchand, A., Chretien, F., Bourg, N., Gherardi, R. K., . . . Authier, F. J. (2013). Dual effects of exercise in dysferlinopathy. *Am J Pathol, 182*(6), 2298-2309. doi:10.1016/j.ajpath.2013.02.045

Bittner, R. E., Anderson, L. V. B., Burkhardt, K., Bashir, R., Vafiadaki, E., Ivanova, S., . . . Reis, A. (1999). Dysferlin deletion in SJL mice (SJL-*Dysf*) defines a natural model for limb girdle muscular dystrophy 2B. *Nature Genetics, 23*, 141-142.

Bonetti, P. O. (2002). Endothelial Dysfunction: A Marker of Atherosclerotic Risk. *Arteriosclerosis, Thrombosis, and Vascular Biology, 23*(2), 168-175. doi:10.1161/01.atv.0000051384.43104.fc

Bonucci, E., & Sadun, R. (1972). An Election Microscope Study on Experimental Calcification of Skeletal Muscle. *Clin Orthop Relat Res, 88*, 197-217.

Bostick, B., Shin, J. H., Yue, Y., Wasala, N. B., Lai, Y., & Duan, D. (2012). AAV micro-dystrophin gene therapy alleviates stress-induced cardiac death but not myocardial fibrosis in >21-m-old mdx mice, an end-stage model of Duchenne muscular dystrophy cardiomyopathy. *J Mol Cell Cardiol, 53*(2), 217-222. doi:10.1016/j.yjmcc.2012.05.002

Bouillon, K., Singh-Manoux, A., Jokela, M., Shipley, M. J., Batty, G. D., Brunner, E. J., . . . Kivimaki, M. (2011). Decline in low-density lipoprotein cholesterol concentration: lipid-lowering drugs, diet, or physical activity? Evidence from the Whitehall II study. *Heart, 97*(11), 923-930. doi:10.1136/hrt.2010.216309

Boulanger, C. M., Tanner, F. C., Béa, M.-L., Hahn, A. W. A., Werner, A., & Lüscher, T. F. (1992). Oxided Low Density Lipoproteins Induce mRNA Expression and Release of Endothelin From Human and Porcine Endothelium. *Circ Res, 70*, 1191-1197.

Bulfield, G., Sillers, W. G., Wight, P. A. L., & Moore, K. J. (1984). X chromosome-linked muscular dystrophy (*mdx*) in the mouse. *Proc Natl Acad Sci U S A, 81*, 1189-1192.

Bushby, K., Finkel, R., Birnkrant, D. J., Case, L. E., Clemens, P. R., Cripe, L., . . . Constantin, C. (2010). Diagnosis and management of Duchenne muscular dystrophy, part 1: diagnosis and pharmacological and psychosocial management. *Lancet Neurol, 9*, 77-93. doi:10.1016/S14744422(09)70271-6

Bushby, K., Gardner-Medwin, D., Nicholson, L. V. B., Johnson, M. A., Haggerty, I. D., Cleghorn, N. J., . . . Bhattacharyal, S. S. (1993). The clinical, genetic and dystrophin characteristics of Becker muscular dystrophy. I. Natural history. *J Neurol, 240*(2), 98-104.

Cai, C., Weisleder, N., Ko, J. K., Komazaki, S., Sunada, Y., Nishi, M., . . . Ma, J. (2009). Membrane repair defects in muscular dystrophy are linked to altered interaction between MG53, caveolin-3, and dysferlin. *J Biol Chem, 284*(23), 15894-15902. doi:10.1074/jbc.M109.009589

CDC. (2009). *Table 16. Presence of selected chronic conditions at office visits, by patient age and sex: United States*. Retrieved from http://www.cdc.gov/nchs/data/ahcd/namcs_summary/2009_namcs_web_tables.pdf, September 2016.

CDC. (2014). *CDC National Health Report: Leading Causes of Morbidity and Mortality and Associated Behavioral Risk and Protective Factors - United States, 2005-2013*. Retrieved from https://www.cdc.gov/mmwr/preview/mmwrhtml/su6304a2.htm, September 2016.

Cenacchi, G., Fanin, M., De Giorgi, L. B., & Angelini, C. (2005). Ultrastructural changes in dysferlinopathy support defective membrane repair mechanism. *J Clin Pathol, 58*(2), 190-195. doi:10.1136/jcp.2004.018978

Chamberlain, J. S., Metzger, J., Reyes, M., Townsend, D., & Faulkner, J. A. (2007). Dystrophin-deficient mdx mice display a reduced life span and are susceptible to spontaneous rhabdomyosarcoma. *FASEB J, 21*(9), 2195-2204. doi:10.1096/fj.06-7353com

Chamberlain, J. S., Pearlman, J. A., Muzny, D. M., Gibbs, R. A., Ranier, J. E., Reeves, A. A., & Caskey, C. T. (1988). Expression of the Murine Duchenne Muscular Dystrophy Gene in Muscle and Brain. *Science, 239*(4846), 1416-1418.

Chao, D. S., Gorospe, J. R. M., Brenman, J. E., Rafael, J. A., Peters, M. F., Froehner, S. C., . . . Bredt, D. S. (1996). Selective Loss of Sarcolemmal Nitric Oxide Synthase in Becker Muscular Dystrophy. *J Exp Med, 184*, 609-618.

Chapman, V. M., Miller, D. R., Armstrong, D., & Caskey, C. T. (1989). Recovery of induced mutations for X chromosome-linked muscular dystrophy in mice. *Proc Natl Acad Sci U S A, 86*, 1292-1296.

Chase, T. H., Cox, G. A., Burzenski, L., Foreman, O., & Shultz, L. D. (2009). Dysferlin deficiency and the development of cardiomyopathy in a mouse model of limb-girdle muscular dystrophy 2B. *Am J Pathol, 175*(6), 2299-2308. doi:10.2353/ajpath.2009.080930

Chelly, J., Kaplan, J.-C., Maire, P., Gautron, S., & Kahn, A. (1988). Transcription of the dystrophin gene in human muscle and non-muscle tissues. *Nature, 333*, 858-860.

Chénard, A. A., Bécane, H. M., Tertrain, F., De Kermadec, J.-M., & Weiss, Y. A. (1993). Ventricular arrhythmia in Duchenne muscular dystrophy: prevalence, significance and prognosis. *Neuromuscul Disord, 3*(3), 201-206.

Chiu, Y. H., Hornsey, M. A., Klinge, L., Jorgensen, L. H., Laval, S. H., Charlton, R., . . . Bushby, K. (2009). Attenuated muscle regeneration is a key factor in dysferlin-deficient muscular dystrophy. *Hum Mol Genet, 18*(11), 1976-1989. doi:10.1093/hmg/ddp121

Collins, C. A., & Morgan, J. E. (2003). Duchenne's muscular dystrophy: animal models used to investigate pathogenesis and develop therapeutic strategies. *Int J Ex Path, 84*, 165-172.

Cooper, B. J., Valentine, B. A., Wilson, S., Patterson, D. F., & Concannon, P. W. (1988). Canine muscular dystrophy: confirmation of X-linked inheritance. *J Hered, 79*(6), 405-408.

Cordani, N., Pisa, V., Pozzi, L., Sciorati, C., & Clementi, E. (2014). Nitric oxide controls fat deposition in dystrophic skeletal muscle by regulating fibro-adipogenic precursor differentiation. *Stem Cells, 32*(4), 874-885. doi:10.1002/stem.1587

Coulton, G. R., Curtin, N. A., Morgan, J. E., & Partridge, T. A. (1988). The *mdx* mouse skeletal muscle myopathy: II. Contractile properties. *Neuropath and Appl Neurobio, 14*, 299-314.

Coulton, G. R., Morgan, J. E., Partridge, T. A., & Sloper, J. C. (1988). The *mdx* mouse skeletal muscle myopathy: I. A histological, morphometric and biochemical investigation. *Neuropath Appl Neurobio, 14*, 53-70.

Cox, G. A., Cole, N. M., Matsumura, K., Phelps, S. F., Hauschka, S. D., Campbell, K. P., . . . Chamberlain, J. S. (1993). Overexpression of dystrophin in transgenic *mdx* mice eliminates dystrophic symptoms without toxicity. *Nature, 364*, 725-729.

Cros, D., Harnden, P., Pellissier, J. F., & Serratrice, G. (1989). Muscle hypertrophy in Duchenne muscular dystrophy. A pathological and morphometric study. *J Neurol, 236*(1), 43-47.

Danialou, G., Comtois, A. S., Dudley, R., Karpati, G., Vincent, G., Des Rosiers, C., & Petrof, B. J. (2001). Dystrophin-deficient cardiomyocytes are abnormally vulnerable to mechanical stress-induced contractile failure and injury. *The FASEB Journal*. doi:10.1096/fj.01-0030fje

Daniels, T. F., Killinger, K. M., Michal, J. J., Wright, R. W. J., & Jiang, Z. (2009). Lipoproteins, cholesterol homeostasis and cardiac health. *Int J Biol Sci, 5*(5), 474-488.

Danko, I., Chapman, V., & Wolff, J. A. (1992). The Frequency of Revertants in mdx Mouse Genetic Models for Duchenne Muscular Dystrophy. *Pediatric Research, 32*(1), 128-131.

Davignon, J. (2004). Beneficial cardiovascular pleiotropic effects of statins. *Circulation, 109*(23 Suppl 1), III39-43. doi:10.1161/01.CIR.0000131517.20177.5a

de Kermadec, J.-M., Bécane, H.-M., Chénard, A., Tertrain, F., & Weiss, Y. (1994). Prevalence of left ventricular systolic dysfunction in Duchenne muscular dystrophy An echocardiographic study. *American Heart Journal, 127*(3), 618-623.

De Luna, N., Freixas, A., Gallano, P., Caselles, L., Rojas-Garcia, R., Paradas, C., . . . Gallardo, E. (2007). Dysferlin expression in monocytes: a source of mRNA for mutation analysis. *Neuromuscul Disord, 17*(1), 69-76. doi:10.1016/j.nmd.2006.09.006

de Morree, A., Flix, B., Bagaric, I., Wang, J., van den Boogaard, M., Grand Moursel, L., . . . van der Maarel, S. M. (2013). Dysferlin regulates cell adhesion in human monocytes. *J Biol Chem, 288*(20), 14147-14157. doi:10.1074/jbc.M112.448589

Deasy, B. M., Feduska, J. M., Payne, T. R., Li, Y., Ambrosio, F., & Huard, J. (2009). Effect of VEGF on the regenerative capacity of muscle stem cells in dystrophic skeletal muscle. *Mol Ther, 17*(10), 1788-1798. doi:10.1038/mt.2009.136

Deconinck, A., Rafael, J. A., Skinner, J. A., Brown, S. C., Potter, A. C., Metzinger, L., . . . Davies, K. E. (1997). Utrophin-Dystrophin-Deficient Mice as a Model for Duchenne Muscular Dystrophy. *Cell, 90*, 717-727.

Deconinck, N., & Dan, B. (2007). Pathophysiology of duchenne muscular dystrophy: current hypotheses. *Pediatr Neurol, 36*(1), 1-7. doi:10.1016/j.pediatrneurol.2006.09.016

Demonbreun, A. R., Posey, A. D., Heretis, K., Swaggart, K. A., Earley, J. U., Pytel, P., & McNally, E. M. (2010). Myoferlin is required for insulin-like growth factor response and muscle growth. *FASEB J, 24*(4), 1284-1295.

Denies, M. S., Johnson, J., Maliphol, A. B., Bruno, M., Kim, A., Rizvi, A., . . . Medler, S. (2014). Diet-induced obesity alters skeletal muscle fiber types of male but not female mice. *Physiol Rep, 2*(1), e00204. doi:10.1002/phy2.204

Dimachkie, M. M., & Barohn, R. J. (2014). Distal myopathies. *Neurol Clin, 32*(3), 817-842, x. doi:10.1016/j.ncl.2014.04.004

Doherty, K. R., Cave, A., Davis, D. B., Delmonte, A. J., Posey, A., Earley, J. U., . . . McNally, E. M. (2005). Normal myoblast fusion requires myoferlin. *Development, 132*(24), 5565-5575. doi:10.1242/dev.02155

Dupont-Versteegden, E. E., McCarter, R. J., & Katz, M. S. (1985). Voluntary exercise decreases progression of muscular dystrophy in diaphragm of *mdx* mice. *J Appl Physiol, 77*(4), 1736-1741.

Durbeej, M., & Campbell, K. P. (2002). Muscular dystrophies involving the dystrophin-glycoprotein complex: an overview of current mouse models. *Curr Opin Gen & Devel, 12*, 349-361.

Dye, W. W., Gleason, R. L., Wilson, E., & Humphrey, J. D. (2007). Altered biomechanical properties of carotid arteries in two mouse models of muscular dystrophy. *J Appl Physiol (1985), 103*(2), 664-672. doi:10.1152/japplphysiol.00118.2007

Eagle, M., Baudouin, S. V., Chandler, C., Giddings, D. R., Bullock, R., & Bushby, K. (2002). Survival in Duchenne muscular dystrophy: improvements in life expectancy since 1967 and the impact of home nocturnal ventilation. *Neuromuscul Disord, 12*, 926-929.

Emery, A. E. H. (1991). Population frequencies of inherited neuromuscular diseases - a world survey. *Neuromuscul Disord, 1*(1), 19-29.

Emery, A. E. H. (2002). The muscular dystrophies. *The Lancet, 359*(9307), 687-695. doi:10.1016/s0140-6736(02)07815-7

Emery, A. E. H., Muntoni, F., & Quinlivan, R. C. M. (2015). *Duchenne Muscular Dystrophy* (Fourth Edition ed.).

Ennen, J. P., Verma, M., & Asakura, A. (2013). Vascular-targeted therapies for Duchenne muscular dystrophy. *Skeletal Muscle, 3*(9), 1-12.

Ervasti, J. M., & Campbell, K. P. (1993). A Role for the Dystrophin-Glycoprotein Complex as a Transmembrane Linker between Laminin and Actin. *J Cell Biol, 122*(4), 809-823.

Faulkner, J. A., Brooks, S. V., Dennis, R. G., & Lynch, G. S. (1997). The Functional Status of Dystrophic Muscles and Functional Recovery by Skeletal Muscles Following Myoblast Transfer. *Basic Appl Myol, 7*(3&4), 257-264.

Fayssoil, A., Renault, G., Guerchet, N., Marchiol-Fournigault, C., Fougerousse, F., & Richard, I. (2013). Cardiac Characterization of *mdx* Mice Using High-Resolution Doppler Echocardiography. *J Ultrasound Med, 32*, 757-761.

Galassi, G., Rowland, L. P., Hays, A. P., Hopkins, L. C., & DiMauro, S. (1987). High serum levels of creatine kinase: asymptomatic prelude to distal myopathy. *Muscle Nerve, 10*(4), 346-350.

Gallardo, E., de Luna, N., Diaz-Manera, J., Rojas-Garcia, R., Gonzalez-Quereda, L., Flix, B., . . . Illa, I. (2011). Comparison of dysferlin expression in human skeletal muscle with that in monocytes for the diagnosis of dysferlin myopathy. *PLoS One, 6*(12), e29061. doi:10.1371/journal.pone.0029061

Gallardo, E., Rojas-Garcia, R., de Luna, N., Pou, A., & Brown, R. H. J. (2001). Inflammation in dysferlin myopathy: Immunohistochemical characterization of 13 patients. *Neurology, 57*, 2136-2138.

Gaw, A., Mancini, F. P., & Ishibashi, S. (1995). Rapid genotyping of low density lipoprotein receptor knockout mice using a polymerase chain reaction technique. *Laboratory Animals, 29*, 447-449.

Getz, G. S., & Reardon, C. A. (2009). Apoprotein E as a lipid transport and signaling protein in the blood, liver, and artery wall. *J Lipid Res, 50*, S156-161. doi:10.1194/jlr.R800058-JLR200

Glesby, M. J., Rosenmann, E., Nylen, E. G., & Wrogemann, K. (1988). Serum CK, calcium, magnesium, and oxidative phosphorylation in *mdx* mouse muscular dystrophy. *Muscle Nerve, 11*(8), 852-856.

Glover, L., & Brown, R. H., Jr. (2007). Dysferlin in membrane trafficking and patch repair. *Traffic, 8*(7), 785-794. doi:10.1111/j.1600-0854.2007.00573.x

Goldberg, A. C., & Gidding, S. S. (2016). Knowing the Prevalence of Familial Hypercholesterolemia Matters. *Circulation, 133*(11), 1054-1057. doi:10.1161/CIRCULATIONAHA.116.021673

Goldberg, I. J., Hu, Y., Noh, H. L., Wei, J., Huggins, L. A., Rackmill, M. G., . . . Huang, L. S. (2008). Decreased lipoprotein clearance is responsible for increased cholesterol in LDL receptor knockout mice with streptozotocin-induced diabetes. *Diabetes, 57*(6), 1674-1682. doi:10.2337/db08-0083

Gomez-Perez, Y., Capllonch-Amer, G., Gianotti, M., Llado, I., & Proenza, A. M. (2012). Long-term high-fat-diet feeding induces skeletal muscle mitochondrial biogenesis in rats in a sex-dependent and muscle-type specific manner. *Nutr Metab (Lond), 9*, 15. doi:10.1186/1743-7075-9-15

Gouni-Berthold, I., & Berthold, H. K. (2014). PCSK9 antibodies for the treatment of hypercholesterolemia. *Nutrients, 6*(12), 5517-5533. doi:10.3390/nu6125517

Grady, R. M., Teng, H., Nichol, M. C., Cunningham, J. C., Wilkinson, R. S., & Sanes, J. R. (1997). Skeletal and Cardiac Myopathies in Mice Lacking Utrohpin and Dystrophin - A Model for Duchenne Muscular Dystrophy. *Cell, 90*, 729-738.

Griggs, R. C., Moxley, R. T. r., Mendell, J. R., Fenichel, G. M., Brooke, M. H., Pestronk, A., . . . Group, C. I. o. D. D. (1991). Prednisone in Duchenne Dystrophy: A Randomized, Controlled Trial Defining the Time Course and Dose Response. *Arch Neurol, 48*, 383-388.

Grounds, M. D., Terrill, J. R., Radley-Crabb, H. G., Robertson, T., Papadimitriou, J., Spuler, S., & Shavlakadze, T. (2014). Lipid accumulation in dysferlin-deficient muscles. *Am J Pathol, 184*(6), 1668-1676. doi:10.1016/j.ajpath.2014.02.005

Guglieri, M., Straub, V., Bushby, K., & Lochmuller, H. (2008). Limb-girdle muscular dystrophies. *Curr Opin Neurol, 21*(5), 576-584. doi:10.1097/WCO.0b013e32830efdc2

Han, R., Bansal, D., Miyake, K., Muniz, V. P., Weiss, R. M., McNeil, P. L., & Campbell, K. P. (2007). Dysferlin-mediated membrane repair protects the heart from stress-induced left ventricular injury. *J Clin Invest, 117*(7), 1805-1813. doi:10.1172/JCI30848

Han, R., Kobuke, K., Anderson, M., de Bernabé, D. B.-V., Kobayashi, Y., Yang, B., & Campbell, K. P. (2011). Improved genotyping of the dysferlin-null mouse. *Protocol Exchange*.

Hennessy, D. A., Tanuseputro, P., Tuna, M., Bennett, C., Perez, R., Shields, M., . . . Manuel, D. G. (2016). *Population health impact of statin treatment in Canada*. Retrieved from

Ho, M., Post, C. M., Donahue, L. R., Lidov, H. G., Bronson, R. T., Goolsby, H., . . . Brown, R. H., Jr. (2004). Disruption of muscle membrane and phenotype divergence in two novel mouse models of dysferlin deficiency. *Hum Mol Genet, 13*(18), 1999-2010. doi:10.1093/hmg/ddh212

Hochmeiseter, S., Grundtner, R., Bauer, J., Englehardt, B., Lyck, R., Gordon, G., . . . Lassmann, H. (2006). Dysferlin Is a New Marker for Leaky Brain Blood Vessels in Multiple Sclerosis. *J Am Assoc Neuropath, 65*(9), 855-865.

Hodel, C. (2002). Myopathy and rhadbomyolysis with lipid-lowering drugs. *Toxicology Letters, 128*, 159-168.

Hoffman, E. P., Brown, R. H., Jr., & Kunkel, L. M. (1987). Dystrophin: The Protein Product of the Duchenne Muscular Dystrophy Locus. *Cell, 51*, 919-928.

Hornsey, M. A., Laval, S. H., Barresi, R., Lochmuller, H., & Bushby, K. (2013). Muscular dystrophy in dysferlin-deficient mouse models. *Neuromuscul Disord, 23*(5), 377-387. doi:10.1016/j.nmd.2013.02.004

Hughes, B. P. (1972). Lipid changes in Duchenne muscular dystrophy. *Journal of Neurology, Neurosurgery and Psychiatry, 35*, 658-663.

Ieronimakis, N., Hays, A., Prasad, A., Janebodin, K., Duffield, J. S., & Reyes, M. (2016). PDGFRalpha signalling promotes fibrogenic responses in collagen-producing cells in Duchenne muscular dystrophy. *J Pathol*. doi:10.1002/path.4801

Isaac, C., Wright, A., Usas, A., Li, H., Tang, Y., Mu, X., . . . Huard, J. (2013). Dystrophin and utrophin "double knockout" dystrophic mice exhibit a spectrum of degenerative musculoskeletal abnormalities. *J Orthop Res, 31*(3), 343-349. doi:10.1002/jor.22236

Ishibashi, S., Brown, M. S., Goldstein, J. L., Gerard, R. D., Hammer, R. E., & Herz, J. (1993). Hypercholesterolemia in Low Density Lipoprotein Receptor Knockout Mice and its Reversal by Adenovirus-mediated Gene Delivery. *J Clin Invest, 92*, 883-893.

Ishibashi, S., Goldstein, J. L., Brown, M. S., Herz, J., & Burns, D. K. (1994). Massive Xanthomatosis and Atherosclerosis in Cholesterol-fed Low Density Lipoprotein Receptor-negative Mice. *J Clin Invest, 93*, 1885-1893.

Ito, K., Kimura, S., Ozasa, S., Matsukura, M., Ikezawa, M., Yoshioka, K., . . . Miike, T. (2006). Smooth muscle-specific dystrophin expression improves aberrant vasoregulation in mdx mice. *Hum Mol Genet, 15*(14), 2266-2275. doi:10.1093/hmg/ddl151

Ito, K., Kimura, S., Thomas, G., Ozasa, S., Matsukura, M., Ikezawa, M., . . . Miwa, T. (2005). Dystrophin in Vascular Smooth Muscle Is Important for Duchenne Muscular Dystrophy Therapy. *Molecular Therapy, 11*, 99-99. doi:10.1016/j.ymthe.2005.06.254

Jones, D. A., Round, J. M., Edwards, R. H., Grindwood, S. R., & Tofts, P. S. (1983). Size and composition of the calf and quadriceps muscles in Duchenne muscular dystrophy. A tomographic and histochemical study. *J Neurol Sci, 60*(2), 307-322.

Kobayashi, K., Izawa, T., Kuwamura, M., & Yamate, J. (2010). The distribution and characterization of skeletal muscle lesions in dysferlin-deficient SJL and A/J mice. *Exp Toxicol Pathol, 62*(5), 509-517. doi:10.1016/j.etp.2009.06.009

Kobayashi, K., Izawa, T., Kuwamura, M., & Yamate, J. (2012). Dysferlin and animal models for dysferlinopathy. *J Toxicol Pathol, 25*(2), 135-147. doi:10.1293/tox.25.135

Kornegay, J. N., Childers, M. K., Bogan, D. J., Bogan, J. R., Nghiem, P., Wang, J., . . . Wagner, K. R. (2012). The paradox of muscle hypertrophy in muscular dystrophy. *Phys Med Rehabil Clin N Am, 23*(1), 149-172, xii. doi:10.1016/j.pmr.2011.11.014

Kubes, P., Suzuki, M., & Granger, D. H. (1991). Nitric oxide: an endogenous modulator of leukocyte adhesion. *Proc Natl Acad Sci U S A, 88*(11), 4651-4655.

Kuru, S., Yasuma, F., Wakayama, T., Kimura, S., Konagay, M., Aoki, M., . . . Takahashi, T. (2004). A patient with limb girdle muscular dystrophy type 2B (LGMD2B) manifesting cardiomyopathy. *Rinsho Shinkeigaku, 44*(6), 375-378.

Kwiterovich, P. O. (2000). The Metabolic Pathways of High-Density Lipoprotein, Low-Density Lipoprotein, and Triglycerides: A Current Review. *Am J Cardiol, 85*(suppl), 5L-10L.

Lek, A., Evesson, F. J., Sutton, R. B., North, K. N., & Cooper, S. T. (2012). Ferlins: regulators of vesicle fusion for auditory neurotransmission, receptor trafficking and membrane repair. *Traffic, 13*(2), 185-194. doi:10.1111/j.1600-0854.2011.01267.x

Lerman, A., & Burnett, J. C. J. (1992). Intact and altered endothelium in regulation of vasomotion. *Circ, 86*(6), 12-19.

Leung, D. G., Herzka, D. A., Thompson, W. R., He, B., Bibat, G., Tennekoon, G., . . . Wagner, K. R. (2014). Sildenafil Does Not Improve Cardiomyopathy in Duchenne and Becker Muscular Dystrophy. *Ann Neurol, 76*(4), 541-549. doi:10.1002/ana.24214

Li, X., Kypreos, K., Zanni, E. E., & Zannis, V. (2003). Domains of apoE Required for Binding to apoE Receptor 2 and to Phospholipids: Implications for the Function of apoE in the Brain. *Biochem, 42*, 10406-10417.

Lindholm, C. R., Ertel, R. L., Bauwens, J. D., Schmuck, E. G., Mulligan, J. D., & Saupe, K. W. (2013). A high-fat diet decreases AMPK activity in multiple tissues in the absence of hyperglycemia or systemic inflammation in rats. *J Physiol Biochem, 69*(2), 165-175. doi:10.1007/s13105-012-0199-2

Liu, J., Aoki, M., Illa, I., Wu, C., Fardeau, M., Angelini, C., . . . Brown, R. H., Jr. (1998). Dysferlin, a novel skeletal muscle gene, is mutated in Miyoshi myopathy and limb girdle muscular dystrophy. *Nature Genetics, 20*, 31-36.

Ljubicic, V., Miura, P., Burt, M., Boudreault, L., Khogali, S., Lunde, J. A., . . . Jasmin, B. J. (2011). Chronic AMPK activation evokes the slow, oxidative myogenic program and triggers beneficial adaptations in mdx mouse skeletal muscle. *Hum Mol Genet, 20*(17), 3478-3493. doi:10.1093/hmg/ddr265

Lostal, W., Bartoli, M., Bourg, N., Roudaut, C., Bentaib, A., Miyake, K., . . . Richard, I. (2010). Efficient recovery of dysferlin deficiency by dual adeno-associated vector-mediated gene transfer. *Hum Mol Genet, 19*(10), 1897-1907. doi:10.1093/hmg/ddq065

Loufrani, L., Dubroca, C., You, D., Li, Z., Levy, B., Paulin, D., & Henrion, D. (2004). Absence of dystrophin in mice reduces NO-dependent vascular function and vascular density: total recovery after a treatment with the aminoglycoside gentamicin. *Arterioscler Thromb Vasc Biol, 24*(4), 671-676. doi:10.1161/01.ATV.0000118683.99628.42

Loufrani, L., Levy, B. I., & Henrion, D. (2002). Defect in Microvascular Adaptation to Chronic Changes in Blood Flow in Mice Lacking the Gene Encoding for Dystrophin. *Circulation Research, 91*(12), 1183-1189. doi:10.1161/01.res.0000047505.11002.81

Loufrani, L., Matrougui, K., Gorny, D., Duriez, M., Blanc, I., Lévy, B. I., & Henrion, D. (2001). Flow (Shear Stress)-Induced Endothelium-Dependent Dilation Is Altered in Mice Lacking the Gene Encoding for Dystrophin. *Circulation, 103*, 864-870.

Lutgens, E., Daemen, M., Kockx, M., Doevendans, P., Hofker, M., Havekes, L., . . . de Muinck, E. D. (1999). Atherosclerosis in APOE*3-Leiden Transgenic Mice - From Proliferative to Atheromatous Stage. *Circ, 99*, 276-283.

Lynch, G. S., Hinkle, R. T., Chamberlain, J. S., Brooks, S. V., & Faulkner, J. A. (2001). Force and power output of fast and slow skeletal muscles from mdx mice 6-28 months old. *Journal of Physiology, 535*(2), 591-600.

Ma, Y., Wang, W., Zhang, J., Lu, Y., Wu, W., Yan, H., & Wang, Y. (2012). Hyperlipidemia and atherosclerotic lesion development in Ldlr-deficient mice on a long-term high-fat diet. *PLoS One, 7*(4), e35835. doi:10.1371/journal.pone.0035835

Mahjneh, I., Marconi, G., Bushby, K., Anderson, L. V. B., Tolvanene-Mahjneh, H., & Somer, H. (2001). Dysferlinopathy (LGMD2B): a 23-year follow-up study of 10 patients homozygous for the same frameshifting dysferlin mutations. *Neuromuscul Disord, 11*, 20-26.

Mahley, R. W. (1988). Apolipoprotein E Cholesterol Tranport Protein with Expanding Role in Cell Biology. *Science, 240*(4852), 622-630.

Mak, I. W. Y., Evaniew, N., & Ghert, M. (2014). Lost in translation: animal models and clinical trials in cancer treatment. *Am J Transl Res, 6*(2), 114-118.

Manzur, A. Y., Kuntzer, T., Pike, M., & Swan, A. (2008). Glucocorticoid corticosteroids for Duchenne muscular dystrophy. *Cochrane Database Syst Rev*(1), Cd003725. doi:10.1002/14651858.CD003725.pub3

Markham, L. W., Spicer, R. L., Khoury, P. R., Wong, B. L., Mathews, K. D., & Cripe, L. H. (2005). Steroid therapy and cardiac function in Duchenne muscular dystrophy. *Pediatr Cardiol, 26*(6), 768-771.

Matsumura, T., Saito, T., Fujimura, H., Shinno, S., & Sakoda, S. (2011). A longitudinal cause-of-death analysis of patients with Duchenne muscular dystrophy. *Rinsho Shinkeigaku, 51*(10), 743-750.

Mavrogeni, S., Bratis, K., Papavasiliou, A., Skouteli, E., Karanasios, E., Georgakopoulos, D., . . . Papadopoulos, G. (2013). CMR detects subclinical cardiomyopathy in mother-carriers of Duchenne and Becker muscular dystrophy. *JACC Cardiovasc Imaging, 6*(4), 526-528. doi:10.1016/j.jcmg.2012.09.017

McDonald, A. A., Hebert, S. L., Kunz, M. D., Ralles, S. J., & McLoon, L. K. (2015). Disease course in mdx:utrophin+/- mice: comparison of three mouse models of Duchenne muscular dystrophy. *Physiol Rep, 3*(4). doi:10.14814/phy2.12391

McNally, E. M., Ly, C. T., Rosenmann, H., Rosenbaum, S. M., Jiang, W., Anderson, L. V. B., & Argov, Z. (2000). Splicing Mutation in Dysferlin Produced Limb-Girdle Muscular Dystrophy With Inflammation. *Am J Med Gen, 91*, 305-312.

Mehlem, A., Hagberg, C. E., Muhl, L., Eriksson, U., & Falkevall, A. (2013). Imaging of neutral lipids by oil red O for analyzing the metabolic status in health and disease. *Nat Protoc, 8*(6), 1149-1154. doi:10.1038/nprot.2013.055

Mehler, M. F. (2000). Brain dystrophin, neurogenetics and mental retardation. *Brain Research Rev, 32*, 277-307.

Melacini, P., Fanin, M., Angelini, A., Pegararo, E., Livi, U., Danieli, G. A., . . . Angelini, C. (1998). Case Report: Cardiac transplantation in a Duchenne muscular dystrophy carrier. *Neuromuscul Disord, 8*, 585-590.

Mendell, J. R., Goemans, N., Lowes, L. P., Alfano, L. N., Berry, K., Shao, J., . . . Telethon Foundation, D. M. D. I. N. (2016). Longitudinal effect of eteplirsen versus historical control on ambulation in Duchenne muscular dystrophy. *Ann Neurol, 79*(2), 257-271. doi:10.1002/ana.24555

Mendell, J. R., Moxley, R. T. r., Brooke, M. H., Fenichel, G. M., Miller, J. P., King, W., . . . Gilder, B. (1989). Randomized, double-blind six-month trial of prednisone in Duchenne's muscular dystrophy. *N Engl J Med, 320*(24), 1592-1597.

Mendell, J. R., Rodino-Klapac, L. R., Sahenk, Z., Roush, K., Bird, L., Lowes, L. P., . . . Eteplirsen Study, G. (2013). Eteplirsen for the treatment of Duchenne muscular dystrophy. *Ann Neurol, 74*(5), 637-647. doi:10.1002/ana.23982

Messina, S., Mazzeo, A., Bitto, A., Aguennouz, M., Migliorato, A., De Pasquale, M. G., . . . Vita, G. (2007). VEGF overexpression via adeno-associated virus gene transfer promotes skeletal muscle regeneration and enhances muscle function in mdx mice. *FASEB J, 21*(13), 3737-3746. doi:10.1096/fj.07-8459com

Meyers, T. A., & Townsend, D. (2015). Early right ventricular fibrosis and reduction in biventricular cardiac reserve in the dystrophin-deficient mdx heart. *Am J Physiol Heart Circ Physiol, 308*(4), H303-315. doi:10.1152/ajpheart.00485.2014

Miike, T., Sugino, S., Ohtani, Y., Taku, K., & Yoshioka, K. (1987). Vascular endothelial cell injury and platelet embolism in Duchenne muscular dystrophy at the preclinical stage. *J Neurolog Sci, 82*, 67-80.

Mokhtarian, A., Lefaucheur, J. P., Even, P. C., & Sebille, A. (1995). Effects of treadmill exercise and high-fat feeding on muscle degeneration in *mdx* mice at the time of weaning. *Clin Sci, 89*, 447-452.

Moore, K. J., & Tabas, I. (2011). Macrophages in the pathogenesis of atherosclerosis. *Cell, 145*(3), 341-355. doi:10.1016/j.cell.2011.04.005

Moorwood, C., Liu, M., Tian, Z., & Barton, E. R. (2013). Isometric and eccentric force generation assessment of skeletal muscles isolated from murine models of muscular dystrophies. *J Vis Exp*(71), e50036. doi:10.3791/50036

Mozaffarian, D., Benjamin, E. J., Go, A. S., Arnett, D. K., Blaha, M. J., Cushman, M., . . . Stroke Statistics, S. (2015). Heart disease and stroke statistics--2015 update: a report from the American Heart Association. *Circulation, 131*(4), e29-322. doi:10.1161/CIR.0000000000000152

Muller, J., Vayssiere, N., Royuela, M., Leger, M. E., Muller, A., Bacou, F., . . . Mornet, D. (2001). Comparative evolution of muscular dystrophin in diaphragm, gastrocnemius and masseter muscles from old male mdx mice. *J Muscle Res Cell Motil, 22*(2), 133-139.

Nagaraju, K., Rawat, R., Veszelovszky, E., Thapliyal, R., Kesari, A., Sparks, S., . . . Hoffman, E. P. (2008). Dysferlin deficiency enhances monocyte phagocytosis: a model for the inflammatory onset of limb-girdle muscular dystrophy 2B. *Am J Pathol, 172*(3), 774-785. doi:10.2353/ajpath.2008.070327

Nakashima, Y., Plump, A. S., Raines, E. W., Breslow, J. L., & Ross, R. (1994). ApoE-Deficient Mice Develop Lesions of All Phases of Atherosclerosis Throughout the Arterial Tree. *Arterioscler Thromb Vasc Biol, 14*, 133-140.

Nelson, M. D., Rader, F., Tang, X., Tavyev, J., Nelson, S. F., Miceli, M. C., . . . Victor, R. G. (2014). PDE5 inhibition alleviates functional muscle ischemia in boys with Duchenne muscular dystrophy. *Neurol, 82*, 2085-2091.

Nelson, R. H. (2013). Hyperlipidemia as a risk factor for cardiovascular disease. *Prim Care, 40*(1), 195-211. doi:10.1016/j.pop.2012.11.003

NINDS. (2011). Muscular dystrophy: Hope through research. Retrieved from http://www.ninds.nih.gov/disorders/md/detail_md.htm, October 2016.

Nishikawa, A., Mori-Yoshimura, M., Segawa, K., Hayashi, Y. K., Takahashi, T., Saito, Y., . . . Murata, M. (2016). Respiratory and cardiac function in japanese patients with dysferlinopathy. *Muscle Nerve, 53*(3), 394-401. doi:10.1002/mus.24741

Okayasu, M., Nakayachi, M., Hayashida, C., Ito, J., Kaneda, T., Masuhara, M., . . . Hakeda, Y. (2012). Low-density lipoprotein receptor deficiency causes impaired osteoclastogenesis and increased bone mass in mice because of defect in osteoclastic cell-cell fusion. *J Biol Chem, 287*(23), 19229-19241. doi:10.1074/jbc.M111.323600

Papa, R., Madia, F., Bartolomeo, D., Trucco, F., Pedemonte, M., Traverso, M., . . . Fiorillo, C. (2016). Genetic and Early Clinical Manifestations of Females Heterozygous for Duchenne/Becker Muscular Dystrophy. *Pediatr Neurol, 55*, 58-63. doi:10.1016/j.pediatrneurol.2015.11.004

Passamanno, L., Taglia, A., Palladino, A., Viggiano, E., D'Ambrosio, P., Scutifero, M., . . . Politano, L. (2012). Improvement of survival in Duchnenne Muscular Dystrophy: retrospective analysis of 835 patients. *Acta Myologica, XXXI*, 121-125.

Percival, J. M., Whitehead, N. P., Adams, M. E., Adamo, C. M., Beavo, J. A., & Froehner, S. C. (2012). Sildenafil reduces respiratory muscle weakness and fibrosis in the *mdx* mouse model of Duchenne muscular dystrophy. *J Pathol, 228*(1), 77-87. doi:10.1002/path.4054

Petrof, B. J., Shrager, J. B., Stedman, H. H., Kelly, A. M., & Sweeney, H. L. (1993). Dystrophin protects the sarcolemma from stresses developed during muscle contraction. *Proc Natl Acad Sci U S A, 90*, 3710-3714.

Phan, B. A., Dayspring, T. D., & Toth, P. P. (2012). Ezetimibe therapy: mechanism of action and clinical update. *Vasc Health Risk Manag, 8*, 415-427. doi:10.2147/VHRM.S33664

Politano, L., Nigro, V., Nigro, G., Petretta, V. R., Passamanno, L., Papparella, S., . . . Comi, L. I. (1996). Development of Cardiomyopathy in Female Carriers of Duchenne and Becker Muscular Dystrophies. *JAMA, 275*(17), 1335-1338.

Quinlan, J. G., Hahn, H. S., Wong, B. L., Lorenz, J. N., Wenisch, A. S., & Levin, L. S. (2004). Evolution of the mdx mouse cardiomyopathy: physiological and morphological findings. *Neuromuscul Disord, 14*(8-9), 491-496. doi:10.1016/j.nmd.2004.04.007

Quinlan, J. G., Johnson, S. R., McKee, M. K., & Lyden, S. P. (1992). Twitch and tetanus in mdx mouse muscle. *Muscle Nerve, 1992*(15), 7.

Radley-Crabb, H. G., Fiorotto, M. L., & Grounds, M. D. (2011). The different impact of a high fat diet on dystrophic mdx and control C57Bl/10 mice. *PLoS Curr, 3*, RRN1276. doi:10.1371/currents.RRN1276

Radomski, M. W., Palmer, R. M. J., & Moncada, S. (1987). The anti-aggregating properties of vascular endothelium: interactions between prostacyclin and nitric oxide. *Br J Pharmacol, 92*, 639-646.

Raffai, R. L., Loeb, S. M., & Weisgraber, K. H. (2005). Apolipoprotein E promotes the regression of atherosclerosis independently of lowering plasma cholesterol levels. *Arterioscler Thromb Vasc Biol, 25*(2), 436-441. doi:10.1161/01.ATV.0000152613.83243.12

Rando, T. A., Disatnik, M.-H., Yu, Y., & Franco, A. (1988). Muscle cells from *mdx* mice have an increased susceptibility to oxidative stress. *Neuromuscul Disord, 8*, 14-21.

Rauch, U., Shami, A., Zhang, F., Carmignac, V., Durbeej, M., & Hultgardh-Nilsson, A. (2012). Increased neointimal thickening in dystrophin-deficient mdx mice. *PLoS One, 7*(1), e29904. doi:10.1371/journal.pone.0029904

Rawat, R., Cohen, T. V., Ampong, B., Francia, D., Henriques-Pons, A., Hoffman, E. P., & Nagaraju, K. (2010). Inflammasome up-regulation and activation in dysferlin-deficient skeletal muscle. *Am J Pathol, 176*(6), 2891-2900. doi:10.2353/ajpath.2010.090058

Rayavarapu, S., Van der Meulen, J. H., Gordish-Dressman, H., Hoffman, E. P., Nagaraju, K., & Knoblach, S. M. (2010). Characterization of dysferlin deficient SJL/J mice to assess preclinical drug efficacy: fasudil exacerbates muscle disease phenotype. *PLoS One, 5*(9), e12981. doi:10.1371/journal.pone.0012981

Reddy, K. G., Nair, R. N., Sheehan, H. M., & Hodgson, J. M. (1994). Evidence that selective endothelial dysfunction may occur in the absence of angiographic or ultrasound atherosclerosis in patients with risk factors for atherosclerosis. *Journal of the American College of Cardiology, 23*(4), 833-843. doi:10.1016/0735-1097(94)90627-0

Robinson, J. G., Farnier, M., Krempf, M., Bergeron, J., Luc, G., Averna, M., . . . Investigators, O. L. T. (2015). Efficacy and safety of alirocumab in reducing lipids and cardiovascular events. *N Engl J Med, 372*(16), 1489-1499. doi:10.1056/NEJMoa1501031

Roche, J. A., Ru, L. W., & Bloch, R. J. (2012). Distinct effects of contraction-induced injury in vivo on four different murine models of dysferlinopathy. *J Biomed Biotechnol, 2012*, 134031. doi:10.1155/2012/134031

Rosales, X. Q., Gastier-Foster, J. M., Lewis, S., Vinod, M., Thrush, D. L., Astbury, C., . . . Mendell, J. R. (2010). Novel diagnostic features of dysferlinopathies. *Muscle Nerve, 42*(1), 14-21. doi:10.1002/mus.21650

Rosenson, R. S. (2016). Patient education: High cholesterol and lipids (hyperlipidemia). *UpToDate.*

Rybakova, I. N., Patel, J. R., & Ervasti, J. M. (2000). The Dystrophin Complex Forms a Mechanically Strong Link Between the Sarcolemma and Costameric Actin. *J Cell Biol, 150*(5), 1209-1214.

Saito, T., Yamamoto, Y., Matsumura, T., Fujimura, H., & Shinno, S. (2009). Serum levels of vascular endothelial growth factor elevated in patients with muscular dystrophy. *Brain Dev, 31*(8), 612-617. doi:10.1016/j.braindev.2008.09.008

Sander, M., Chavoshan, B., Harris, S. A., Iannaccone, S. T., Stull, J. T., Thomas, G. D., & Victor, R. G. (2000). Functional muscle ischemia in neuronal nitric oxide synthase-deficient skeletal muscle of children with Duchenne muscular dystrophy. *Proc Natl Acad Sci U S A, 97*(25), 13818-13823. doi:10.1073/pnas.250379497

Schade van Westrum, S. M., Hoogerwaard, E. M., Dekker, L., Standaar, T. S., Bakker, E., Ippel, P. F., . . . van der Kooi, A. J. (2011). Cardiac abnormalities in a follow-up study on carriers of Duchenne and Becker muscular dystrophy. *Neurology, 77*, 62-66.

Schram, G., Fournier, A., Leduc, H., Dahdah, N., Therien, J., Vanasse, M., & Khairy, P. (2013). All-cause mortality and cardiovascular outcomes with prophylactic steroid therapy in Duchenne muscular dystrophy. *J Am Coll Cardiol, 61*(9), 948-954. doi:10.1016/j.jacc.2012.12.008

Sehayek, E., Shefer, S., Nguyen, L. B., Ono, J. G., Merkel, M., & Breslow, J. L. (2000). Apolipoprotein E regulates dietary cholesterol absorption and biliary cholesterol excretion: studies in C57BL/6 apolipoprotein E knockout mice. *Proc Natl Acad Sci U S A, 97*(7), 3433-3437. doi:10.1073/pnas.050016197

Selle, R. W., & Urist, M. R. (1961). Calcium Deposits and New Bone Formation in Muscle in Rabbits. *J Surg Res, 1*(2), 132-141.

Seror, P., Krahn, M., Laforet, P., Leturcq, F., & Maisonobe, T. (2008). Complete fatty degeneration of lumbar erector spinae muscles caused by a primary dysferlinopathy. *Muscle Nerve, 37*(3), 410-414. doi:10.1002/mus.20910

Shami, A., Knutsson, A., Duner, P., Rauch, U., Bengtsson, E., Tengryd, C., . . . Hultgardh-Nilsson, A. (2015). Dystrophin deficiency reduces atherosclerotic plaque development in ApoE-null mice. *Sci Rep, 5*, 13904. doi:10.1038/srep13904

Sharma, A., Yu, C., Leung, C., Trane, A., Lau, M., Utokaparch, S., . . . Bernatchez, P. (2010). A new role for the muscle repair protein dysferlin in endothelial cell adhesion and angiogenesis. *Arterioscler Thromb Vasc Biol, 30*(11), 2196-2204. doi:10.1161/ATVBAHA.110.208108

Shin, J. H., Hakim, C. H., Zhang, K., & Duan, D. (2011). Genotyping mdx, mdx3cv, and mdx4cv mice by primer competition polymerase chain reaction. *Muscle Nerve, 43*(2), 283-286. doi:10.1002/mus.21873

Sicinski, P., Geng, Y., Ryder-Cook, A. S., Barnard, E. A., Darlison, M. G., & Barnard, P. J. (1989). The Molecular Basis of Muscular Dystrophy in the *mdx* Mouse: A Point Mutation. *Science, 244*(4912), 1578-1580.

Soutar, A. K., & Naoumova, R. P. (2007). Mechanisms of disease: genetic causes of familial hypercholesterolemia. *Nat Clin Pract Cardiovasc Med, 4*(4), 214-225. doi:10.1038/ncpcardio0836

Spurney, C. F., Sali, A., Guerron, A. D., Iantorno, M., Yu, Q., Gordish-Dressman, H., . . . Nagaraju, K. (2011). Losartan decreases cardiac muscle fibrosis and improves cardiac function in dystrophin-deficient mdx mice. *J Cardiovasc Pharmacol Ther, 16*(1), 87-95. doi:10.1177/1074248410381757

Srivastava, N. K., Pradhan, S., Mittal, B., & Gowda, G. A. (2010). High resolution NMR based analysis of serum lipids in Duchenne muscular dystrophy patients and its possible diagnostic significance. *NMR Biomed, 23*(1), 13-22. doi:10.1002/nbm.1419

Staels, B., Dallongeville, J., Auwerx, J., Schoonjans, K., Leitersdorf, E., & Fruchart, J.-C. (1998). Mechanism of Action of Fibrates on Lipid an Lipoprotein Metabolism. *Circulation, 98*, 2088-2093.

Stedman, H. H., Sweeney, H. L., Shrager, J. B., Maguire, H. C., Panettieri, R. A., Petrof, B., . . . Kelly, A. M. (1991). The mdx mouse diaphragm reproduces teh degenerative changes of Duchenne muscular dystrophy. *Nature, 352*, 536-539.

Straub, V., Bittner, R. E., Léger, J. J., & Voit, T. (1992). Direct Visualization of the Dystrophin Network on Skeletal Muscle Fiber Membrane. *J Cell Biol, 119*(5), 1183-1191.

Straub, V., Rafael, J. A., Chamberlain, J. S., & Campbell, K. P. (1997). Animal Models for Muscular Dystrophy Show Different Patterns of Sarcolemmal Disruption. *J Cell Biol, 139*(2), 375-385.

Stromberg, A., Darin, N., Kroksmark, A. K., & Tulinius, M. (2012). S.P.31 What was the age and cause of death in patients with Duchenne muscular dystrophy in Sweden during 2000–2010? *Neuromuscular Disorders, 22*(9-10), 880-881. doi:10.1016/j.nmd.2012.06.256

Tagawa, K., Ogawa, M., Kawabe, K., Yamanaka, G., Matsumura, T., Goto, K., . . . Hayashi, Y. K. (2003). Protein and gene analyses of dysferlinopathy in a large group of Japanese muscular dystrophy patients. *Journal of the Neurological Sciences, 211*(1-2), 23-28. doi:10.1016/s0022-510x(03)00041-8

Tanabe, Y., Esaki, K., & Nomura, T. (1986). Skeletal Muscle Pathology in X Chromosome-linked Muscular Dystrophy (*mdx*) Mouse. *Acta Neuropathol, 69*, 91-95.

Tayeb, M. T. (2010). Deletion mutations in Duchenne muscular dystrophy (DMD) in Western Saudi children. *Saudi J Biol Sci, 17*(3), 237-240. doi:10.1016/j.sjbs.2010.04.008

Temin, P. A., & Islamova, I. B. (1983). Plasma lipids of patients with Duchenne's muscular dystrophy at different stages of the disease. *Zh Nevropatol Psikhiatr Im S S Korsakova, 83*(11), 1632-1636.

Tenger, C., & Zhou, X. (2003). Apolipoprotein E modulates immune activation by acting on the antigen-presenting cell. *Immunology, 109*, 392-397.

Terrill, J. R., Radley-Crabb, H. G., Iwasaki, T., Lemckert, F. A., Arthur, P. G., & Grounds, M. D. (2013). Oxidative stress and pathology in muscular dystrophies: focus on protein thiol oxidation and dysferlinopathies. *FEBS J, 280*(17), 4149-4164. doi:10.1111/febs.12142

Thomas, G., Sander, M., Lau, K. S., Huang, P. L., Stull, J. T., & Victor, R. G. (1998). Impaired metabolic modulation of alpha-adrenergic vasoconstriction in dystrophin-deficient skeletal muscle. *Proc Natl Acad Sci U S A, 95*, 15090-15095.

Thompson, P. D., Clarkson, P. M., Rosenson, R. S., & National Lipid Association Statin Safety Task Force Muscle Safety Expert, P. (2006). An assessment of statin safety by muscle experts. *Am J Cardiol, 97*(8A), 69C-76C. doi:10.1016/j.amjcard.2005.12.013

Tidball, J. G., & Wehling-Henricks, M. (2007). The role of free radicals in the pathophysiology of muscular dystrophy. *J Appl Physiol (1985), 102*(4), 1677-1686. doi:10.1152/japplphysiol.01145.2006

Tomkin, G. H., & Owens, D. (2012). LDL as a Cause of Atherosclerosis. *Open Atheroscl & Thromb Journ, 5*, 13-21.

Townsend, D., Yasuda, S., & Metzger, J. (2007). Cardiomyopathy of Duchenne muscular dystrophy: pathogenesis and prospect of membrane sealants as a new therapeutic approach. *Expert Rev Cardiovasc Ther, 5*(1), 99-109.

Truett, G. E., Heeger, P., Mynatt, R. L., Truett, A. A., Walker, J. A., & Warman, M. L. (2000). Preparation of PCR-Quality Mouse Genomic DNA with Hot Sodium Hydroxide and Tris (HotSHOT). *BioTechniques, 29*(1), 52-54.

Tyler, K. L. (1003). Origins and early descriptions of "Duchenne Muscular Dystrophy". *Muscle Nerve, 28*, 402-422.

Urtasun, M., Saenz, A., Roudaut, C., Poza, J. J., Urtizberea, J. A., Cobo, A. M., . . . Lopez de Munain, A. (1998). Limb-girdle muscular dystrophy in Guipuzcoa (Basque Country, Spain). *Brain, 121*, 1735-1747.

Valentine, B. A., Cooper, B. J., de Lahunta, A., O'Quinnm, R., & Blue, J. T. (1988). Canine X-linked muscular dystrophy - An animal model of Duchenne muscular dystrophy: clinical studies. *J Neurol Sci, 88*, 69-81.

van der Kooi, A. J., Barth, P. G., Busch, H. F. M., de Haan, R., Ginjaar, H. B., van Essen, A. J., . . . de Visser, M. (1996). The clinical spectrum of limb girdle muscular dystrophy: A survey in the Netherlands. *Brain, 119*, 1471-1480.

Walter, M. C., Reilich, P., Thiele, S., Schessi, J., Schreiber, H., Reiners, K., . . . Lochmüller, H. (2013). Treatment of dysferlinopathy with deflazacort a double-blind, placebo-controlled clinical trial. *Orphanet Journal of Rare Diseases, 8*(26), 1-15.

Washington, N. L., & Ward, S. (2006). FER-1 regulates Ca^{2+}-mediated membrane fusion during C. elegans spermatogenesis. *Journal of Cell Science, 119*, 2552-2562. doi:10.1242/jcs

Weatherbee, S. D., Anderson, K. V., & Niswander, L. A. (2006). LDL-receptor-related protein 4 is crucial for formation of the neuromuscular junction. *Development, 133*(24), 4993-5000. doi:10.1242/dev.02696

Weller, A. H., Magliato, S. A., Bell, K. P., & Rosenberg, N. L. (1997). Spontaneous myopathy in the SJL/J mouse: Pathology and strength loss. *Muscle Nerve, 20*, 72-82.

Wenzel, K., Geier, C., Qadri, F., Hubner, N., Schulz, H., Erdmann, B., . . . Ozcelik, C. (2007). Dysfunction of dysferlin-deficient hearts. *J Mol Med (Berl), 85*(11), 1203-1214. doi:10.1007/s00109-007-0253-7

Whitehead, N. P., Kim, M. J., Bible, K. L., Adams, M. E., & Froehner, S. C. (2015). A new therapeutic effect of simvastatin revealed by functional improvement in muscular dystrophy. *PNAS, 112*(41), 12864-12869.

Whitehead, N. P., Yeung, E. W., & Allen, D. G. (2006). Muscle damage in *mdx* (dystrophic) mice: role of calcium and reactive oxygen species. *Clin Exp Pharmacol Physiol, 33*, 657-662.

Wilson, P. W. F., D'Agostino, R. B., Levy, D., Belanger, A. M., Silbershatz, H., & Kannel, W. B. (1998). Prediction of Coronary Heart Disease Using Risk Factor Categories. *Circulation, 97*, 1837-1847.

Witting, N., Kruuse, C., Nyhuss, B., Prahm, K. P., Citirak, G., Lundgaard, S. J., . . . Vissing, J. (2014). Effect of Sildenafil on Skeletal and Cardiac Muscle in Becker Muscular Dystrophy. *Ann Neurol, 76*, 550-557. doi:10.1002/ana.24216

Yumoto, N., Kim, N., & Burden, S. J. (2012). Lrp4 is a retrograde signal for presynaptic differentiation at neuromuscular synapses. *Nature, 489*(7416), 438-442. doi:10.1038/nature11348

Zabalawi, M., Bharadwaj, M., Horton, H., Cline, M., Willingham, M., Thomas, M. J., & Sorci-Thomas, M. G. (2007). Inflammation and skin cholesterol in LDLr-/-, apoA-I-/- mice: link between cholesterol homeostasis and self-tolerance? *J Lipid Res, 48*(1), 52-65. doi:10.1194/jlr.M600370-JLR200

Zadelaar, S., Kleemann, R., Verschuren, L., de Vries-Van der Weij, J., van der Hoorn, J., Princen, H. M., & Kooistra, T. (2007). Mouse models for atherosclerosis and pharmaceutical modifiers. *Arterioscler Thromb Vasc Biol, 27*(8), 1706-1721. doi:10.1161/ATVBAHA.107.142570

Zatz, M., Rapaport, D., Vainzof, M., Passos-Bueno, M. R., Bortolini, E. R., Pavanello, R. C. M., & Peres, C. A. (1991). Serum creatine kinase and pyruvate kinase activities in Duchenne as compared with Becker muscular dystrophy. *Journal of the Neurol Sci, 102*, 190-196.

Zhao, P., Xu, L., Ait-Mou, Y., de Tombe, P. P., & Han, R. (2011). Equal force recovery in dysferlin-deficient and wild-type muscles following saponin exposure. *J Biomed Biotechnol, 2011*, 235216. doi:10.1155/2011/235216

Appendices

Appendix A Supplemental Dysf-ApoE Myography Data

	7 Months				*11 Months*			
Diaphragm	***Wild-type***	***ApoE-KO***	***Dysf-KO***	***DKO***	***Wild-type***	***ApoE-KO***	***Dysf-KO***	***DKO***
Mean F_{max} (SEM)	50.31(2.31)	59.24(9.25)	58.72(10.0)	67.75(15.7)	32.78(4.72)	46.84(7.22)	41.81(7.11)	32.54(4.36)
P_{max}	0.660	0.677	0.650	0.625	0.473	0.550	0.514	0.589
Load at P_{max}	0.305	0.285	0.328	0.281	0.313	0.266	0.246	0.273
Soleus								
Mean F_{max} (SEM)	64.76(34.3)	36.20(3.66)	64.67(8.31)	32.04(2.37)	37.92(4.49)	32.08(6.08)	55.93(8.00)	46.50(6.52)
P_{max}	0.162	0.174	0.182	0.148	0.189	0.141	0.1581	0.215
Load at P_{max}	0.324	0.395	0.348	0.297	0.379	0.387	0.313	0.313

Table A.1 Additional diaphragm and soleus myography data at 7 and 11 months on HFD. Mean absolute maximum force (F_{max}) values in mN, maximum power (P_{max}) in µW and load at P_{max} expressed as fraction of F_{max}. WT 7m (n=2), 11m (n=9); ApoE 7m (n=7), 11m (n=10); Dysf 7m (n=7), 11m (n=12); and Dysf-ApoE 7m (n=4), 11m (n=8).

Appendix B Supplemental Dysf-ApoE Histology

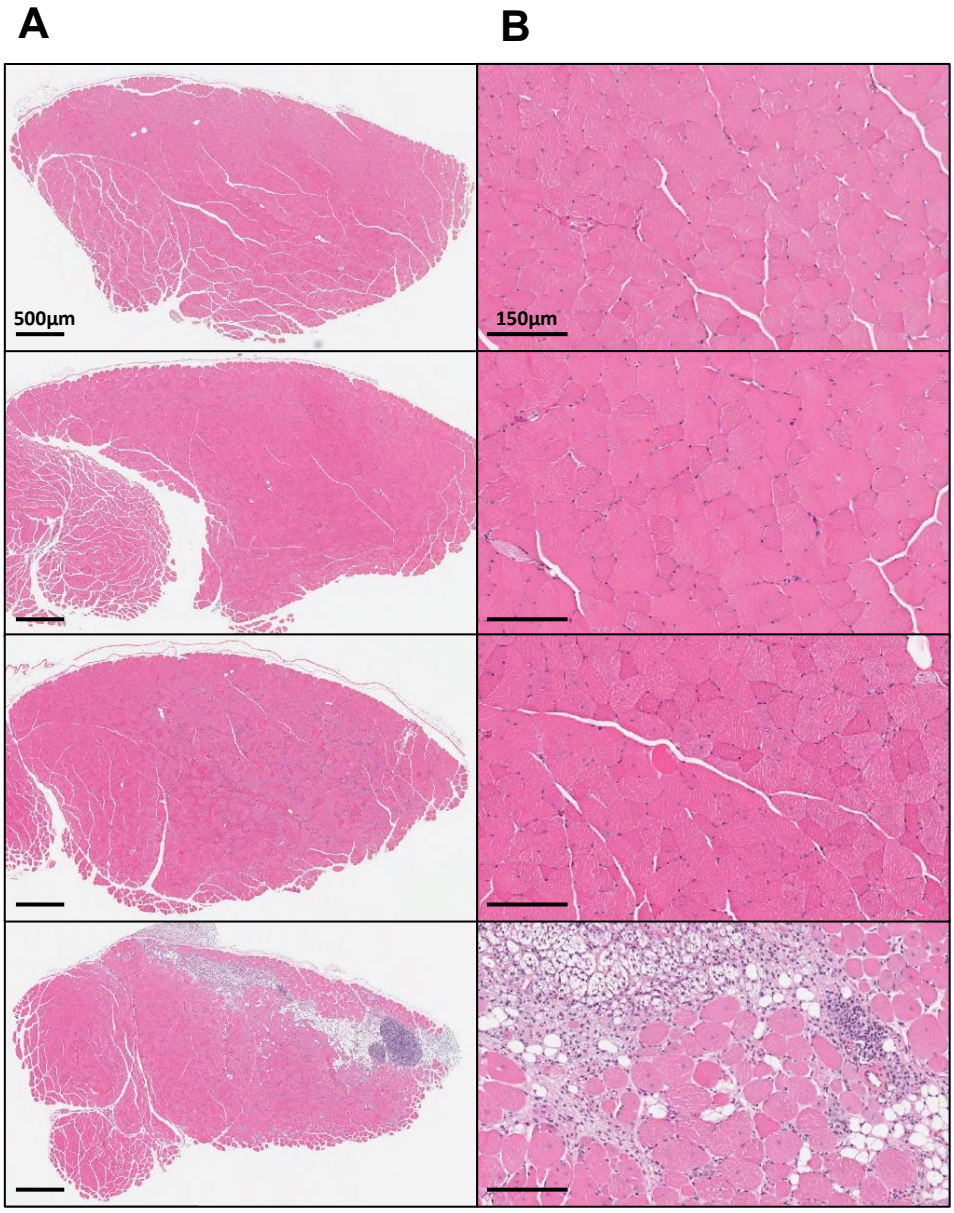

Image B.1 Representative images of TA and EDL muscles at 11 months on HFD. (A) 2x zoom scale bar=500µm and (B) 8x zoom scale bar=150µm of wild-type, ApoE-KO, Dysf-KO and Dysf-ApoE DKO H+E stained slides.

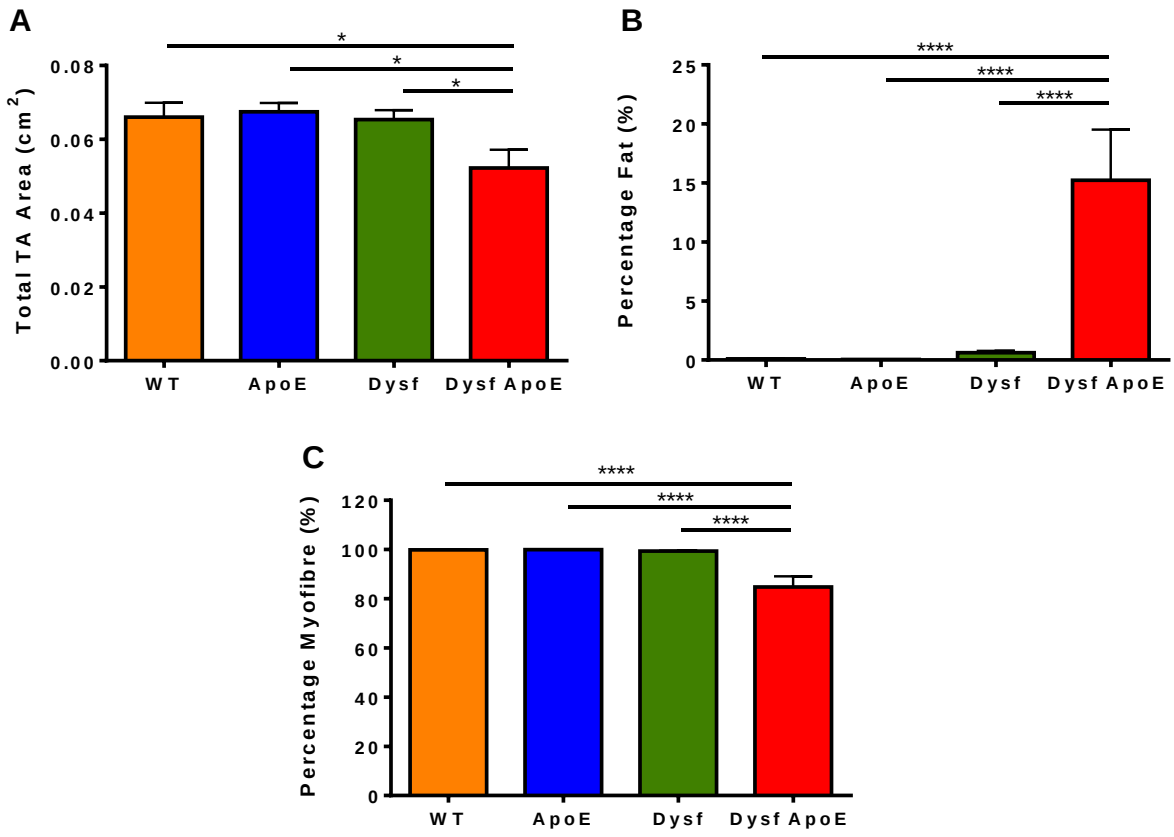

Figure B.1 TA muscle size and composition at 11 months on HFD. (A) Total TA area, (B) percentage of muscle area composed of fat, (C) percentage of muscle composed of healthy myofiber. WT (n=10), ApoE (n=11), Dysf (n=16), and Dysf-ApoE (n=9). Mean+SEM, one-way ANOVA excluding WT n=1. *P<0.05 ***P<0.001 ****P<0.0001

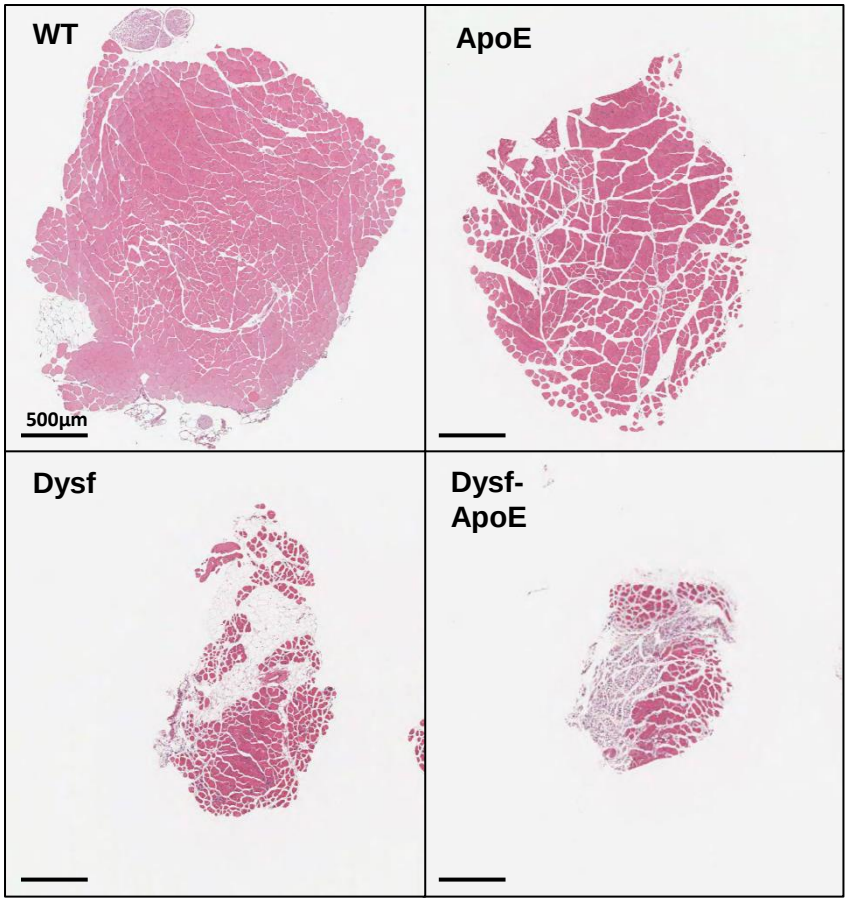

Image B.2 Representative images of psoas major muscle at 11 months on HFD. 2x zoom of wild-type, ApoE-KO, Dysf-KO and Dysf-ApoE DKO H+E stained slides, scale bar=500µm.

Appendix C Supplemental Dysf-LDLR Histology

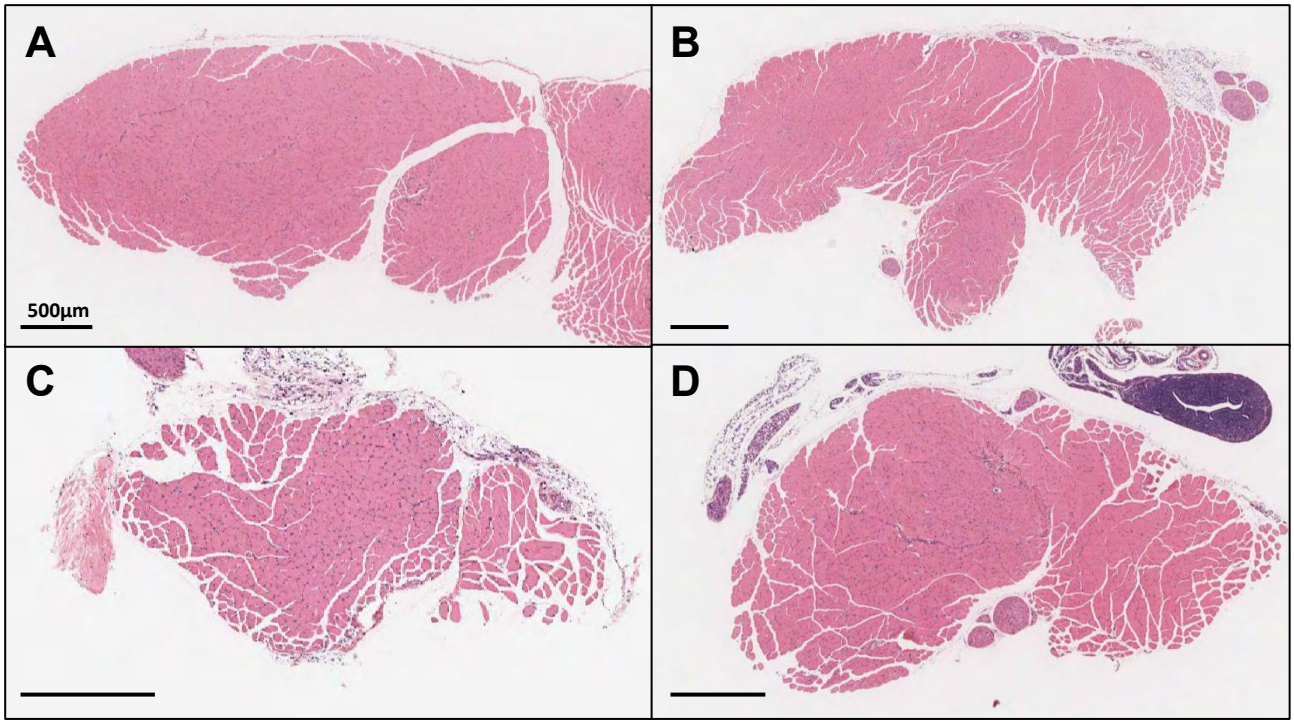

Image C.1 Additional skeletal muscle histology of 5-week old Dysf-LDLR DKO mouse. (A) Tibialis anterior and extensor digitorum longus, (B) gastrocnemius, (C) soleus and (D) psoas major H+E stained slides, scale bar=500µm.